Development of Fiber Optic Sensors using Femtosecond Laser for Refractive Index and Temperature Measurements

by

Farid Ahmed
BSc, University of Dhaka, 2003
MSc, Korea Advanced Institute of Science and Technology, 2007

A Dissertation Submitted in Partial Fulfillment
of the Requirements for the Degree of

DOCTOR OF PHILOSOPHY

in the Department of Mechanical Engineering

Supervisory Committee

Development of Fiber Optic Sensors using Femtosecond Laser for Refractive Index and Temperature Measurements

by

Farid Ahmed
BSc, University of Dhaka, 2003
MSc, Korea Advanced Institute of Science and Technology, 2007

Supervisory Committee

Dr. Martin Byung-Guk Jun
Department of Mechanical Engineering
Supervisor

Dr. Peter Wild
Department of Mechanical Engineering
Departmental Member

Dr. Tao Lu
Department of Electrical Engineering
Outside Member

Abstract

Supervisory Committee
Dr. Martin Byung-Guk Jun
Department of Mechanical Engineering
Supervisor

Dr. Peter Wild
Department of Mechanical Engineering
Departmental Member

Dr. Tao Lu
Department of Electrical Engineering
Outside Member

The development and transition of optical fiber sensors from experimental stage to practical applications largely depends on manufacturing cost and simplicity. To date, in-fiber grating sensors are largely manufactured by ultraviolet lasers despite higher fabrication cost and complexity. Besides, ultraviolet radiation can only write gratings in doped fibers. Therefore, reaping the benefits of existing fibers such as pure silica fiber, photonics crystal fibers etc. cannot be achieved using this technique. In contrast, uses of ultra-fast lasers have the potential to eliminate or minimize those drawbacks. However, extensive fabrication and packaging research is required for ultrafast laser technology to mature and offer grating based sensors fabrication in industrial scale.

This dissertation presents design and fabrication of fiber optic sensors using femtosecond laser for measurement of ambient refractive index and temperature. The femtosecond laser operating at 780 nm with pulse duration of 172 fs and pulse repetition rate of 1 kHz is used to study bulk index modification and fabricate fiber long period and short period gratings. Effective and reliable fabrication of in-fiber gratings requires spatial control of refractive index written in optical fiber. With an aim to better control spatial index modulation in direct ultrafast writing, primary focus of this work is given to write single-shot submicron periodic voids in bulk glass. Femtosecond pulse filamentation in glass is studied to understand the morphology of bulk index change written by ultrashort pulses. Laser writing parameters (such as beam diameter, pulse

energy, scanning speed, depth of focus, etc.) are then further tuned to write pulse filamentation induced refractive index change in optical fibers suitable for fiber grating fabrication. In order to design and tailor grating's spectrum, measurement of in-fiber index is introduced in this work. We propose fiber Bragg grating based Fabry-Perot cavity structure (cavity length, L= 10 mm) to characterize femtosecond pulse filamentation induced refractive index change in the core of standard SMF. In addition, Mach-Zehnder interferometer (MZI) is proposed as an alternative yet effective and low cost tool to measure in-fiber index change. *Comsol simulation* is used to validate the quantification of index change. Measured index change is used in *Optiwave* simulation to design fiber long period gratings in standard telecommunication and pure silica core fibers. To increase fabrication reliability, we introduce inscription of helical long period gratings using a custom made rotary stage. Tapered photonic crystal and microfiber based Mach-Zehnder interferometer is also investigated for ambient refractive index measurement. Miniature fiber Bragg grating written in microfiber Mach-Zehnder interferometer is used in this work for multi-parameter sensing as well as temperature compensated refractive index sensing. Microfiber Bragg gratings buried in materials of higher thermal expansion coefficient is also proposed to significantly enhance temperature sensitivity.

Table of Contents

List of Figures

List of Tables

Acronyms

SMF	Single mode fiber
FBG	Fiber Bragg grating
LPG	Long period grating
HLPG	Helical long period grating
MZI	Mach-Zehnder interferometer
RI	Refractive index
UV	Ultraviolet
IR	Infra-red
PCF	Photonics crystal fiber
MPI	Multi-photon ionization
NA	Numerical aperture
RIP	Refractive index profile
RNF	Refracted near field
MWI	Multi-wavelength interferometry
DIC	Differential interference contrast
CT	Computerized tomography
OPD	Optical path difference
ND	Neutral density
FWHM	Full width at half maximum
PDL	Polarization dependent loss
OPD	Optical path difference
OSA	Optical spectrum analyzer
TEC	Thermal expansion coefficient
RPM	Revolution per minute

Acknowledgements

I gratefully acknowledge the motivation and assistance I received from Dr. Martin Jun as a PhD student at the University of Victoria. To me, Dr. Jun was far more than an academic supervisor; he influenced my life by being very friendly and supportive. I was not only privileged to have the freedom to try new ideas while doing research with him, but also was lucky to be rescued and rectified when having tough time in my PhD pursuit. It was pleasure to work with Dr. Peter Wild and I was fortunate to have his guidance throughout my research work at the University of Victoria. I am also grateful to Dr. Wild group for their friendship, collaboration and equipment support. I would like to extend my gratitude to my committee member, Dr. Tao Lu to let me use his research facilities and valuable comments/suggestion in my dissertation.

The Laboratory for Advanced Multi-scale Manufacturing (LAMM) has been a place where friendship and collaboration are essential part of research work. I am thankful to have such a wide spectrum of friends in the laboratory; diverse skill set and their willingness to help have always been helpful. In particular, I appreciate the support and assistance I received from Yonghyun Cho, Vahid Ahsani, and Akram Saad while working in a team in the LAMM lab.

I would also like to thank my parents and siblings for the support they provided me through my entire life. In particular, I was lucky to have constant love and support from my parents no matter the situation. I must acknowledge my wife and best friend, Fauzia Rupa, without whose love and encouragement, I would not have finished this dissertation.

Chapter 1 – Introduction

The rapid advancement in fiber sensing systems has accelerated the pursuit of developing sensors to overcome the existing shortcomings and push forward to bring innovation in measurement technologies. In-fiber gratings and interferometers are widely used sensors for temperature and refractive index (RI) measurement applications. The commercial success of in-fiber sensors essentially depends on their performance reliability and design/fabrication simplicity. This chapter provides an overview of fiber optic sensors, challenges that are commonly faced in grating based optical sensor fabrication, potential solutions, and an outline of this dissertation.

1.1 Optical sensing technology

A sensor where optical fiber is used as the key sensing element is commonly called fiber optic sensor. One or more optical fibers are used in a generic optical sensor to carry light from source to detector. When a fiber optic sensor is exposed to a quantity (such as temperature, ambient refractive index, strain, pressure, etc.) to be measured, it modifies the fiber and modulates properties of light in it. The change in light properties at the detection end is used to measure that quantity. Depending on sensing head location, fiber optic sensors are classified as intrinsic or extrinsic. In Intrinsic sensing, the environmental change alters the internal properties of the fiber itself and modulates the properties of light at the detection end. Unlike intrinsic sensors, an optical fiber is used in extrinsic optical sensors only as a carrier of modulated light information to the detector to measure a quantity. Based on operating principle, fiber optic sensors may broadly be categorised

as intensity based or phase based. Intensity modulation of light is utilized in intensity based optical sensors to measure a quantity and they offer simple signal processing to achieve absolute and real-time information about a measurand [1]. One example of intensity based refractive index measurement is provided in Appendix A. The intensity based sensors have limited applications due to random variable losses (e.g. losses at connections and splice points, bending of fiber etc.) in the sensing system, which may not happen in the environment. Phase based or interferometric fiber optic sensors have been drawn immense attention due to their miniature size and high sensitivity to temperature, and ambient refractive index sensitivity [2-8]. Several methods can be employed to construct phase based optical sensors such as gratings and interferometers which will be discussed later in details. Femtosecond laser based fabrication of fiber gratings and interferometric sensors along with their applications in ambient refractive index and temperature sensing are studied in this dissertation.

A fiber Bragg grating (FBG) is constructed by inscribing periodic refractive index in the fiber core that results in particular wavelength of light to be reflected towards the source due to its phase matching property. A typical grating has a period of the order of hundreds of nanometers (hence called short period grating). The fabrication of fiber Bragg grating (FBG) using a visible laser was first demonstrated by Kenneth O. Hill in 1978 [9]. Unlike FBGs, long period fiber Bragg gratings (LPG) have grating periods on the order of 100 micrometers to a millimeter and they couple light from a guided core mode into forward propagating cladding modes where it is lost due to absorption and scattering. LPGs, first demonstrated by Vengsarkar et al. in 1996 [10], are fast gaining approval as simple yet versatile devices for multitude of sensing applications. Fiber

interferometric sensors employ interferometry of two beams propagating along different optical paths in a single optical fiber or two different fibers to measure a quantity. Hence, beam splitting and recombining technique is necessary in an interferometric sensor [11]. In optical interferometric sensors, one of the optical paths is available to be exposed to external perturbations. The temporal and spectral information available in interferometric sensors offer direct measurement of a quantity by detecting the changes in intensity, wavelength, phase, frequency, etc. These diversities of sensing indicators have made fiber interferometers to operate over large dynamic range with high sensitivity and accuracy [8].

Fiber optic sensors have shown great potential as practical and commercial measurement systems due to their inherent small size, good ageing characteristics, and immunity to external interferences [12]. In-fiber gratings and interferometers have been demonstrated as efficient tools for wide varieties sensing applications including temperature [13-17], and refractive index sensing [18-24]. Novelty of fiber grating sensors depends on their performance characteristics and their transition from laboratory to field scale deployments depends on fabrication simplicity and scalability. There has been a lot of progress, yet more work needs to be done to promote and develop their uses in specific and advanced applications.

1.2 Fabrication of in-fiber gratings and interferometric sensors

After the invention of photosensitive optical fiber, ultraviolet (UV) laser based fabrication of fiber Bragg grating has been a substantial commercial success [2]. Historically, Bragg gratings were first fabricated using the internal writing [9] and the holographic technique [25]. Both these methods have been largely superseded by the

phase mask techniques [26, 27] which brought reliability in short period grating fabrication. A great varieties of methods have been developed to fabricate long period gratings, including the use of ultraviolet [28-30] and CO_2 laser radiation [31, 32], exposure to electric arcs [33], mechanical pressure [34], and periodic corrugated structure [35, 36]. Out of various existing methods, the fabrication of gratings in photosensitive optical fiber with UV radiation has dominated the grating based optical sensors manufacturing. Refractive index modulation can be written in the core of photosensitive optical fiber by the influence of an electric field following the Pockels effect [37]. According to the Pockels effect, an incident light generates free charge carriers (electrons or holes) by excitation of impurity energy levels at a rate proportional to optical power [37]. The carriers diffuse to the locations where the incident electromagnetic radiation has low intensity leaving behind fixed charges of opposite polarity. The free carriers are then trapped by the impurity ions (like Ge ions in fiber core) leading to recombination and deposition of charge [37]. The overall effect creates an inhomogeneous distribution of space-charge that exists permanently unless any strong radiation or high temperature destroys it. The spatial charge distribution results in an index modulation in the core of a photosensitive fiber [37]. Hill et al. were the first to discover photosensitivity in optical fiber [9], and this technology has been largely used to fabricate fiber Bragg gratings. Later on, it has been demonstrated that germanosilicate glasses when treated with hot hydrogen show increase photosensitivity [38] and this phenomenon was used to write periodic index in germania-silica waveguides [39]. The addition of hydrogen to Ge-doped glass breaks the Si-O-Ge bonds and forms Si-OH bonds and germanium-oxygen deficiency centers. Both of these effects lead to the increase of refractive index. To load a

photosensitive fiber with hydrogen, the fiber is exposed with gaseous hydrogen at high pressure (100- 700 atm) and temperatures ranging from 20 ^{0}C to 100 ^{0}C [40]. After the completion of UV radiation based gratings fabrication in fiber, typically some excess hydrogen remains in the fiber. The post fabrication residual hydrogen enhances local index of refraction, and any further diffusion to retain equilibrium may cause grating instability. Therefore, it is necessary to get rid of excess hydrogen from the fiber before using it in a particular application. Annealing the fiber at high temperature for a short period of time provides better stability for operation at lower temperatures [40].

Since the UV radiation based grating fabrication techniques can be applied only to doped optical fibers, most FBGs and LPGs have been written in photosensitive germanosilicate fibers. Because the index change relaxes below 100 ^{0}C, the gratings fabricated by UV radiation suffer from aging instability especially in long term applications. Besides, doped fibers require extra processing such as hydrogen loading at high pressure to enhance photosensitivity prior to grating fabrication. Inscription of FBGs/LPGs with UV radiation even requires post processing such as short time annealing of the fiber at an elevated temperature. These extra pre- and post-processing steps increase fabrication complexity and heighten manufacturing cost. In contrast, uses of ultra-fast lasers have the potential to eliminate or minimize those drawbacks. Focused femtosecond laser pulses cause permanent refractive index increase in various glasses and these short pulses demonstrated novel techniques to fabricate fiber Bragg gratings [18, 41-44] and long period gratings [3, 45, 46]. High pulse intensity is common for available femtosecond laser systems due to their short pulse duration, which is four to five orders of magnitude less than that of UV excimer lasers [43]. Light intensity is

highly localized at the focal point, and hence a femtosecond laser can induce periodic refractive index modulation in the core of fiber without affecting cladding or polymer coating. A major advantage of femtosecond laser fabrication is that the fabricated gratings have higher temperature resistance; hence they have greater aging characteristic [47]. The superiority of femtosecond laser based fabrication is its capability to inscribe gratings in various types of fiber including pure silica fibers and photonic crystal fibers. Aside from direct inscription of index modulation, diverse infrared (IR) laser based techniques have been reported that include LPG fabrication by drilling micro-holes [48] and filling of air-holes [49] in photonics crystal fibers (PCF).

Fabrication of interferometric fiber optic sensors depends on their types. For instance, a Fabry-Perot interferometer is made of two parallel mirrors separated by a certain distance and the interference happens from the super-positions of reflected and transmitted beams at two parallel surfaces [8, 50, 51]. So, these sensors can be designed and fabricated by creating reflectors either inside or outside of optical fibers [50, 52]. The formation of Fabry-Perot cavity is demonstrated by various techniques including micromachining [53, 54], use of two FBGs [55], chemical etching [56], and thin-film deposition [57]. Fabrication of Mach-Zehnder interferometers depends on involved mechanism used in splitting of incident light and recombining of light at the detection end. Construction of MZIs using a pair of LPGs has been reported for both temperature [58] and ambient refractive index measurements [59]. Besides, MZI based fiber optic sensors have also been demonstrated using core offset by fusion splicing [60], splicing of different fiber types [61], using double cladding fibers [62], micro-cavities [17], and use of a twin-core fiber [63].

1.3 Significance of the problem

Application dependent design and reliable fabrication of fiber optic sensors are ultimate challenges to overcome in fiber sensing technology. This section focusses on the common limitations of existing methods used for fiber optic sensor fabrication. As stated in the previous section, the widely used technique: UV laser based writing is limited by few drawbacks. UV laser method requires a phase mask for creating light interference pattern necessary to write in-fiber index modulation [26, 27]. The phase masks are highly expensive, hence the use of masks increases the fabrication cost of the gratings. This technique requires pre and post processing steps such as hydrogen loading to increase photosensitivity and annealing at high temperature for short time to get rid of access hydrogen from the fiber [64]. Therefore, UV laser fabricated gratings are not suitable where greater ageing characteristics and ability to survive in chemically contaminated environment is required. In long-term and high temperature applications, the UV gratings are in particular vulnerable due to natural hydrogen loading and subsequent disappearance of in-fiber periodic indices. In addition, gratings can only be inscribed in photosensitive fiber using UV radiation which excludes the use of many existing optical fibers such as pure silica fibers or photonic crystal fibers that have great inherent characteristics suitable for many sensing applications.

Use of ultrashort pulsed infrared lasers for in-fiber grating fabrication eliminates or lessens many of the adverse effects observed in UV laser based grating fabrication. Direct and fast writing of permanent index modulation in optical fibers is easily achievable in ultrafast laser inscription [3, 41, 42, 44, 65, 66]. Also, ultrafast laser offers gratings fabrication in numerous fiber types including dopant free fibers [67], doped and pure

silica core fibers [46], and photonic crystal fibers [48]. However, it is challenging to achieve controlled and confined in-fiber index modification in ultrafast inscription which is the key to reliable grating fabrication with minimum insertion loss. Detailed study of ultrashort pulse induced index modification and understanding of laser bulk damage morphology is vital. In addition, consistency in fiber alignment with respect to beam focal point is crucial for grating fabrication in ultrafast writing. Therefore, to develop an ultrafast inscription technique that is forgiving to minor fiber misalignment is critically important.

Inscription of adequate periodic RI in the core of an optical fiber is important in fabrication of optical grating devices such as FBGs and LPGs. Hence, the quantification of laser induced in-fiber index modulation is essential to design and reliably fabricate grating devices in optical fibers. There are few techniques (details provided in chapter 3) available to measure fiber index profile such as Refracted near-field (RNF) method [68], and multi-wavelength interferometry [69]. They are either expensive and/or require a complex reconstruction method. Therefore, it is necessary to have an on-site simple and cost effective techniques to measure laser induced index medication prior to grating fabrication.

1.4 Novel contribution

Ultrashort pulse filamentation induced bulk index modification is employed in this study to improve and diversify in-fiber gratings fabrication. Pulse filamentation offers controlled delivery of pulse energy in the bulk glass and write in-fiber refractive index modulation. Quantification of in-fiber refractive index change is necessary to design fiber gratings. Even though there are several methods available to measure index profile in an

optical fiber, they are either expensive or require a complex reconstruction procedure. We propose fiber Bragg grating based Fabry-Perot cavity structure (cavity length, L= 10 mm) to characterize femtosecond pulse filamentation induced refractive index change in the core of SMFs. In addition, Mach-Zehnder interferometer (MZI) is proposed to be an alternative yet effective and low cost tool to measure in-fiber index change. Femtosecond laser based fabrication of long period gratings in both standard telecommunication fiber and pure silica fiber is demonstrated for ambient index measurement. Highly sensitive tapered PCF and microfiber based MZIs are also presented as alternative approaches for ambient sensing. To demonstrate ambient temperature measurement with enhanced sensitivity, fabrication of miniature Bragg grating in microfiber and subsequent molding with materials of higher thermal expansion coefficients is reported in this work. For simultaneous refractive index and temperature sensing, and temperature compensated refractive index sensing, an integrated structure of fiber Bragg grating and Mach-Zehnder interferometer is also described in this study.

1.5 Content summary

A brief outline of this dissertation is as follows. Chapter 2 introduces ultrashort pulse filamentation based bulk index modification in transparent dielectric materials. Focusing conditions of femtosecond pulses to control pulse filamentation in bulk glass is studied in this chapter. The filamentary bulk voids discussed in this chapter are later used to write in-fiber index modulation. Chapter 3 of this dissertation presents measurement of in-fiber refractive index change inscribed by femtosecond laser radiation. Fabry-Perot cavity and MZI sensor based quantification of core index change is explored in this chapter. Ultra-

short pulse filamentation induced writing of long period gratings in Ge-doped and pure silica core fibers are investigated in Chapter 4. Inscription of in-fiber helical index modulation is demonstrated in Chapter 5 to write long period grating. Writing of helical index modulation demonstrates higher tolerance in fiber alignment and greater reliability in LPG fabrication. Chapter 6 describes two simple configurations of fiber optic Mach-Zehnder interferometer for enhanced refractive sensing. Chapter 7 includes microfiber based fiber Bragg grating and interferometric sensors for enhanced temperature and multi-parameters measurements. Finally, Chapter 8 provides overall conclusion and future works.

Chapter 2 - Near-field modification of femtosecond laser beam to control single-shot pulse filamentation in glass medium

When intense light is focused in the bulk of a transparent dielectric material, it induces a change in local optical properties. Some recent studies show that ultrashort femtosecond pulses when focused inside fused silica glass can inscribe modified structures in the bulk [70-73]. Permanent index change in standard single mode fiber has also been demonstrated using ultra short pulses [74]. Laser radiation induced increase in refractive index as high as 0.01 to 0.035 has been demonstrated in Ge-doped bulk silica glass [73]. Capability of index modification in bulk glass has stimulated interest to using ultrashort pulsed lasers for fiber optic device fabrication. However, controlled deposition of femtosecond pulse energy is essential to inscribe photonic devices in glass. The ultrashort pulse filamentation property of femtosecond lasers has enhanced the guided delivery of pulse energy for permanent refractive index change in glass materials [75]. This chapter provides a detail study on femtosecond laser pulse filamentation based void inscription in glass and a potential mechanism to control void morphology. Ultrashort laser writing of bulk voids offers a unique means to inscribe higher refractive indices in transparent dielectric medium.

2.1 Introduction

Elevated intensity of laser pulses confined in the vicinity of focal point continues to uncover amazing physical phenomena. Intense femtosecond pulses, in particular, introduce interesting phenomenon like pulse filamentation which has been investigated

extensively by many researchers [76-80]. Controlled femtosecond pulse filamentation offers numerous potential applications including fabrication of optical devices and circuits in transparent medium. Employing the filamentation of ultrashort pulses, we previously demonstrated the capability of femtosecond laser to cut glass plates [75]. Controlled and uniform progress of filament plasma column provides better control to write refractive index in transparent dielectric materials. Tuning of underlying factors that influence pulse filamentation is essential to control the length and width of plasma column in a medium. Couairon has demonstrated an analytical estimation for filament length in air as a function of pulse duration and beam energy [81]. Self-guided filamentary propagation in fused silica over several Rayleigh lengths has been achieved as a result of balance between self-focusing and multi-photon ionization (MPI) [82]. By increasing power density at focal volume and minimizing losses (per unit length of filament) due to MPI, enhanced filamentary pulse propagation can be achieved in a given medium. However, to achieve ultra-high power density remains a challenge due to longitudinal and radial spreading of light at focal volume. In case of focusing in a dense transparent medium, it is harder to uplift peak power because of the dominating effect of optical aberration. Nonlinearity and accompanying optical effects like aberrations in dispersive glass mediums make pulse filamentation a complex process. Thus, it is important to better understand this phenomenon.

Intensity distribution at focal point is one of the major parameters to determine filamentation length of a femtosecond pulse in an optical medium. Along the propagation axis of a filament, the balance between alternative Kerr self-focusing and self-defocusing of self-generated plasmas continue to add up regularly spaced plasma spots until pulse

peak power remains higher than the critical power required for pulse filamentation [78-80, 83]. Figure 2.1 depicts basic mechanism involved in ultrashort pulse filamentation. The energy spent in ionizing the medium weakens the pulse and the self-focusing gradually declines and is eventually overcome by diffraction and plasma defocusing, resulting in the termination of the filament.

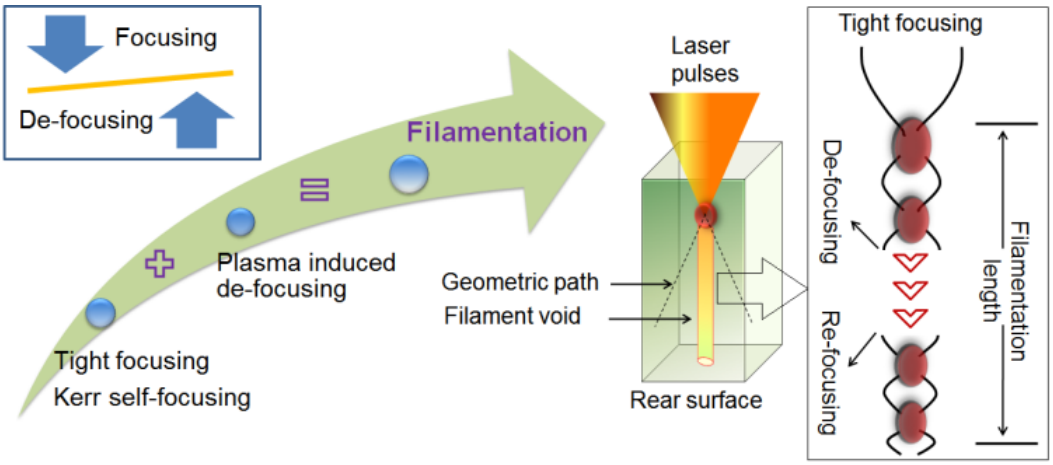

Figure 2.1 Ultrashort pulse filamentation mechanism in transparent dielectric medium

Liu et al. demonstrated that an additional diffraction induced by the plasma accelerates premature termination of filament, although the power is much higher than the critical power [84]. Therefore, it is expected that the intensity distribution at focal point characterizes the primitive plasma volume at focus and thus impacts successive plasma spots and filament length. As shown in Fig. 2.2, for a focused beam, we demonstrate that a glass plate placed next to objective lens at right angle to beam axis increases the effective NA and squeezes the laser energy into a tiny focal volume at an extended depth. Energy confinement in a tiny volume yields a narrow filament ionization column in Corning glass. An ionization column when confined in a narrow channel

undergoes low MPI loss per unit length, compared to a wider ionization column. Minimizing energy leakage in MPI process, the pulses retain peak power greater than the critical filamentation power for an extended length. Long and narrow filamentary void structures are written in corning glass by sustained filament propagation resulted from the balance between alternative Kerr self-focusing and plasma induced defocusing. Although the glass plate is expected to introduce some optical aberration in focal region, the narrow void (height: 700 μm) found in our experiment may result from the elevation of power density in a tiny volume and the reduction of MPI loss per unit length of filament.

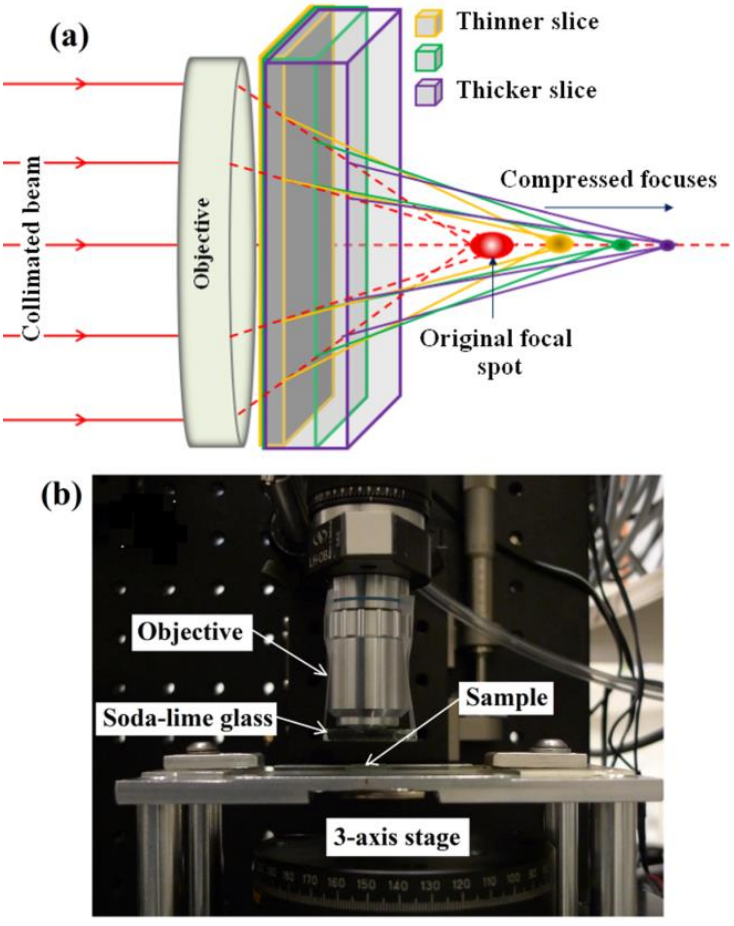

Figure 2.2 (a) Simple illustration of near field compression of focal point before it hits the sample, and (b) experimental setup

2.2 Experiments

A femtosecond laser system operating at 780 nm with pulse duration of 172 fs and pulse repetition rate of 1 kHz was used to carry out the experiments. Focusing was done with an achromatic lens (NA: 0.70) under an incident angle of zero degree onto the sample. As depicted in Fig. 2.2(a), soda-lime glass (Refractive index: 1.52) plate of variable thickness (1 mm ~ 6 mm) was horizontally placed right after the objective lens to gradually tighten the focusing of beam at focal point. The experimental setup is shown in Fig. 2.2(b). The beam was focused beneath the front surface to fabricate single-shot void at rear surface of the sample glass (Corning Eagle^{2000}, thickness: 700 μm). The samples were mounted on a computer controlled 3-axis stage to inscribe voids at suitable depth. Mechanical cleaving of the samples revealed the morphologies of the void structures imprinted on the sample cross sections. The samples were analyzed using an optical microscope (OM) to study filamentary void morphology.

2.3 Result and discussion

2.3.1 Solid immersion to elevate pulse energy

Elevation of peak power turned out to be the primary requirement to enhance filamentation in optical medium. As stated earlier, filamentation is essentially a chain of hot plasma spots along the propagation axis resulted from alternative focusing and defocusing of the pulse until the peak power remains higher than its critical power necessary for filamentation. Critical power for self-focusing is given by

$$P_c = 3.77\lambda^2/8\pi n_2 n_0 \quad (2.1)$$

where λ is the central wavelength of the pulse, n_0 is the linear index of refraction, and n_2 is the coefficient of the Kerr nonlinear index of refraction [85]. The numerical aperture of

an objective lens is defined as $NA = n \sin\alpha_0$, where α_0 is one-half the angular aperture of the objective, and n is the refractive index of the medium between the objective front lens and sample (≈1 for air). An increase of effective NA up to 2.0 has been demonstrated using gallium phosphide solid immersion technique [86]. In our experiment, when the object space between the lens and sample is filled with a high refractive index solid such as soda-lime glass, it works as a solid immersion lens with higher effective NA. Tightly focused laser beam elevates power density in a very tiny focal volume. Figure 2.3 shows cross-sectional images of the evolution of focal volume as the focused beam passes through a dense medium of gradually increasing thickness. Thicker mediums essentially enhance the focusing of objective lens and confine the light in spatially reduced focal volume as shown in Fig. 2.3. Optical aberration effect is evident toward the right hand side of Fig. 2.3, yet focusing seems to get tighter when pulses pass through thicker glass plates. A thicker medium impedes radial spreading of pulses due to stronger focusing and thus elevates power density at focal volume.

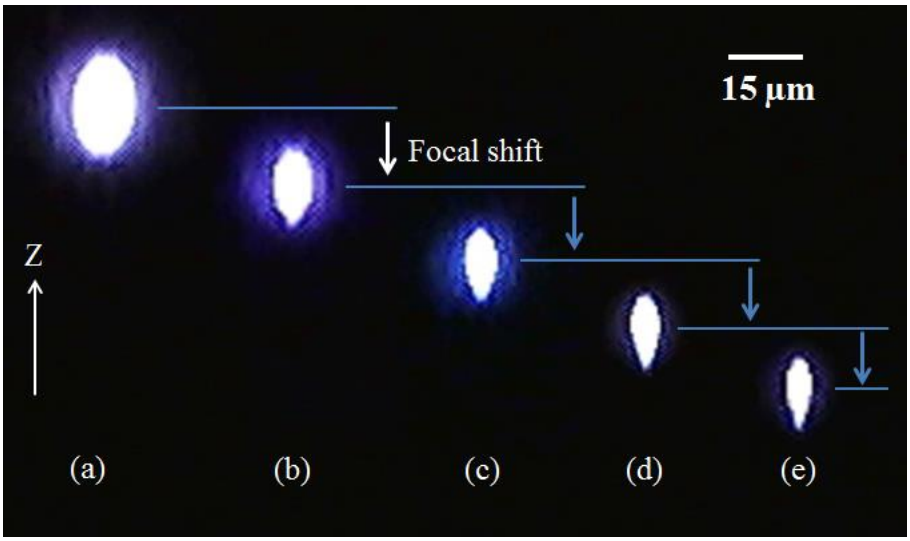

Figure 2.3 Evolution of focal volume when a dense medium (soda-lime glass) is placed after objective of NA 0.4: (a) without any medium, (b) with medium thickness of 3 mm, (c) with

medium thickness of 5 mm, (d) with medium thickness of 6 mm, (e) with medium thickness of 8 mm. Relative to the original focal point (a), the amount of downward linear focal shifts from (b) to (e) are 428.3 µm, 1041 µm, 1401.40 µm, and 2123.90 µm respectively

2.3.2 Pulse filamentation induced void morphologies

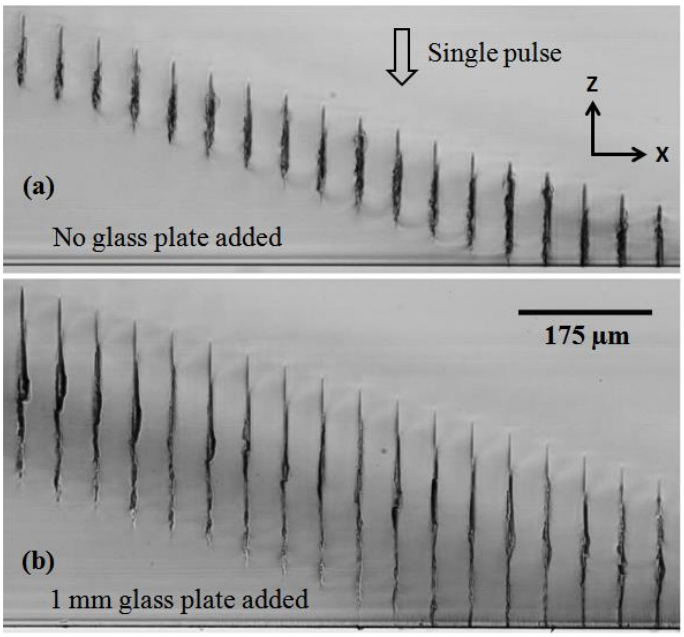

Figure 2.4 Single-shot filamentary damage morphology in Corning Eagle^{2000} glass when no glass is placed after the objective lens (a), and when 1 mm soda-lime glass is added after the objective lens (b)

Figure 2.4 shows the single-shot voids written with average pulse energy of 40 µJ in Corning glass at scanning speed of 10 mm/sec. Filament length is longer when the pulses are focused deeper inside the sample glass. Thus, for a focused beam, we consider that a bulk transparent medium (1~ 6 mm thick soda-lime glass) located just after objective lens, right angle to the beam axis, plays a significant role to augment pulse filamentation. Figure 2.5 shows a series of longest possible single-shot void structures micromachined near the rear surface with average pulse energy of 30 µJ. In absence of glass plate after

the objective, the void height is noticeably small (Fig. 2.5a), whereas, void height keeps on increasing significantly as the thickness of glass plate gradually increases. With an increase in glass thickness, stronger focusing lifts up power density in a tinier region and thus gradually increases the height and decreases the width of voids in Fig. 2.5 (b-f). In addition, a narrow ionization column initiated by squeezing a modest amount of laser energy into an extremely small spatial region likely to undergo low MPI losses per unit length compare to a wider ionization column formed in loosely focusing condition.

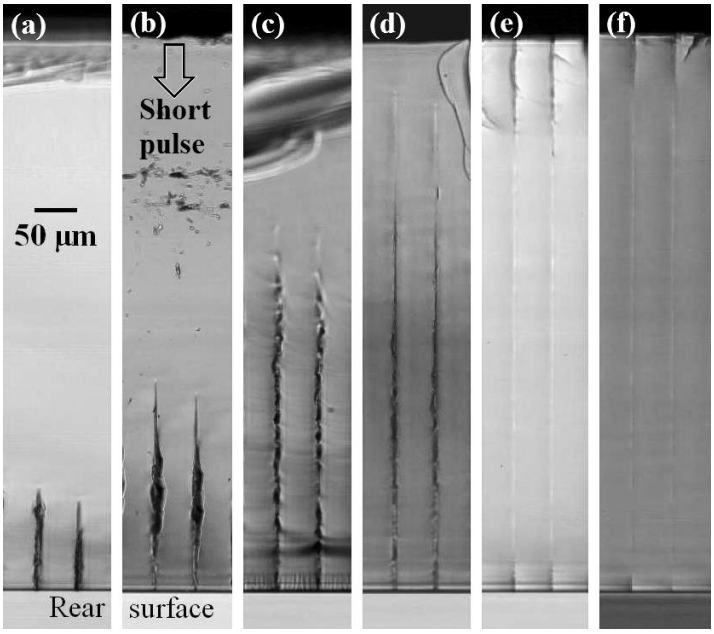

Figure 2.5 Cleaved surfaces of longest possible single shot voids fabricated at rear surfaces when (a) no glass plate, (b) 1 mm glass plate, (c) 2 mm glass plate, (d) 3 mm glass plate, (e) 5 mm glass plate, and (f) 6 mm glass plate are placed after objective lens

The single shot voids in Fig. 2.5 appear as a result of nonlinear-focusing and defocusing induced series of discrete hot plasma spots formed in Corning glass along the propagation axis. Consequently, the most primitive hot spot at focal point manipulates the successive plasma spots. For a tiny focal volume, the resulting small plasmas in

propagation axis are likely to have insignificant extra diffraction. Therefore, repetitive plasma induced uniform de-focusing and nonlinear re-focusing take place in a shorter period all the way to the end of propagation axis for least energy loss. Consequently, the filaments are steadier, narrower, and longer towards the right hand side of Fig. 2.5. In contrast, power density is low in loosely focused volume and the ionization of bulk molecules in a wider plasma column likely to increase MPI induced power loss per unit length. Consequently, filament length decreases while width increases as exemplified in Fig. 2.5(a). Typical trend of filamentation morphology observed in our experiment is shown in Fig. 2.6. The quadratic curves fitted in Fig. 2.6(a) and 2.6(b) show significant dependency of filament length and width on the thickness of soda-lime plate placed after the objective lens. Thus, for a given laser energy, the length and width of pulse filamentation in dielectric medium can be controlled simply by varying the thickness of the soda-lime glass plate.

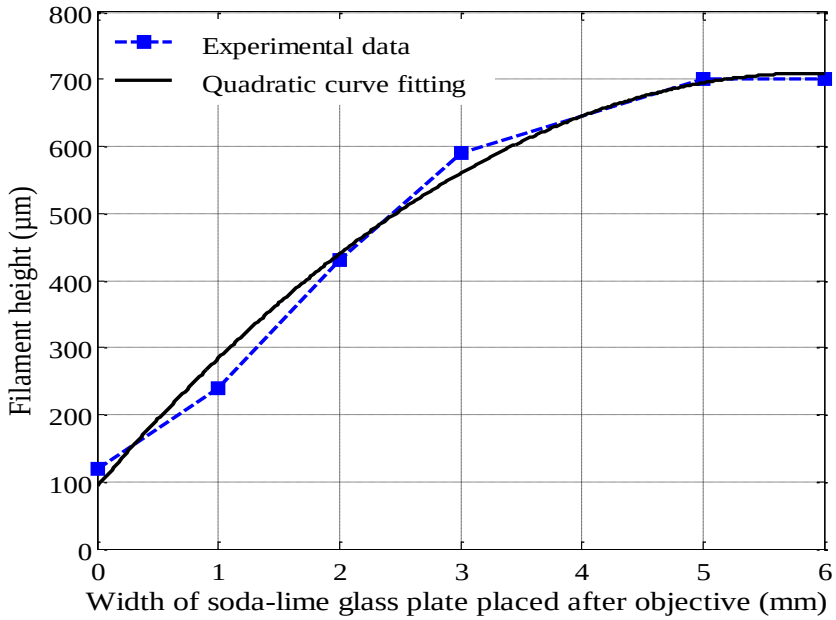

(a)

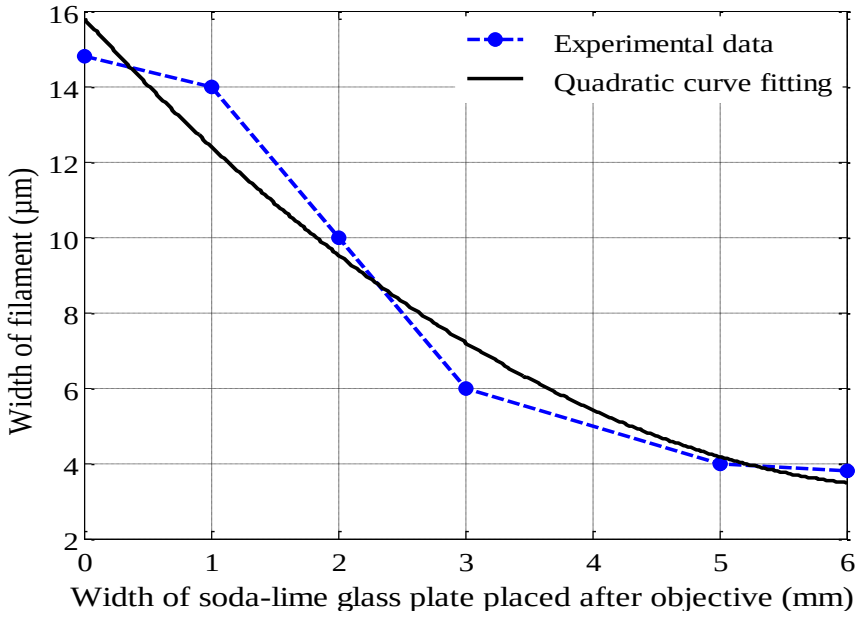

(b)

Figure 2.6 Geometrical characteristics of filament voids written in bulk glass with average pulse energy of 30 μJ measured after objective. The filament height (a) and width (b) are plotted as a function of the thickness of soda-lime glass plate placed next to objective

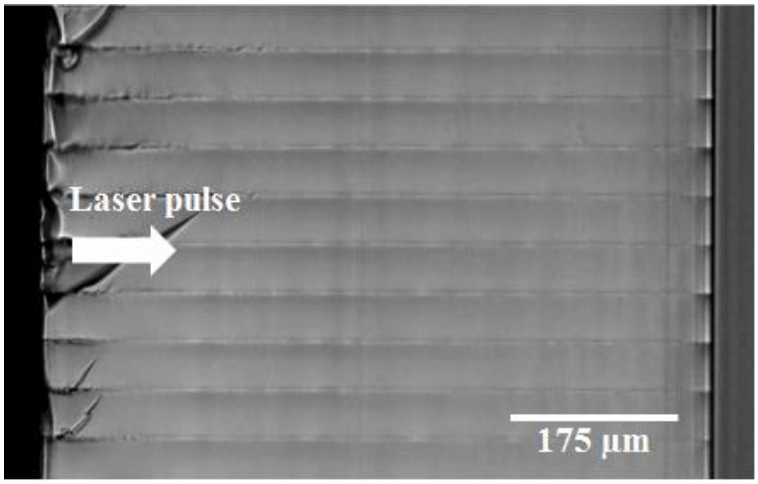

Figure 2.7 Single-shot voids in Corning Eagle^{2000} glass written with pulse energy of 30 μJ when a 6 mm soda-lime glass plate is placed after objective lens

As shown in Fig. 2.7, the single shot narrow waveguides having diameter of 3.8 μm fabricated in our experiments are highly repeatable, which is vital for reliable optical device fabrication. Elevated pulse peak power confined in tiny spot ionizes relatively few dielectric atoms. As a result, the produced plasma spots generated by focusing and subsequent self-defocusing align closely along the propagation axis. So, the single-shot waveguides written in Fig. 2.7 have uniform morphology along its length.

2.4 Conclusion

This work aims to propose an experimental study to demonstrate enhanced and controllable single-shot ultrafast pulse filamentation in Corning Eagle^{2000} glass. When a dense transparent medium (soda-lime glass) is placed after the objective lens, strong focusing elevates power density in a tiny transverse region and likely to reduce ionization induced power loss per unit length as the pulse filament progresses. Filamentary void height increases from 100 μm (in absence of soda-lime glass layer) to 700 μm when a pulsed laser beam is allowed to pass through the soda-lime glass layer of 6 mm before it hits the sample. Single ultrashort pulse induced fabrication of uniform and highly repeatable long waveguides of diameter 3.8 μm is also demonstrated in this study. We believe that, the proposed study has potential applications in fast and reliable fabrication of photonic devices and circuits.

Chapter 3 - Measurement of in-fiber refractive index change induced by ultrafast laser radiation

Accurate, efficient and cost effective measurement of the refractive index profile of an optical fiber is a significant job to design and manufacture in-fiber photonic devices and communication systems [87, 88]. In particular, to design in-fiber gratings, it is required to estimate the refractive index modulation to be inscribed by the fabrication apparatus such as ultraviolet or infrared lasers. Characterization of refractive indices written in standard single mode fiber and micro-fiber by femtosecond laser radiation is presented in this chapter. Bragg grating based Fabry-Perot cavity structure (cavity length, L= 10 mm) and microfiber based Mach-Zehnder are used to measure refractive index change in standard telecommunication fiber and microfiber, respectively. Demonstrated methods provide simple yet very effective on-site measurement of index change in optical fibers.

3.1 Introduction

Inscription of adequate periodic RI in the core of an optical fiber is crucial in fabrication of optical gratings. Hence, the quantification of in-fiber index modulation is essential to design and reliably fabricate grating devices in optical fibers. Several techniques are available to measure refractive index profile (RIP) of optical fibers. One of the popular techniques is the Refracted near-field (RNF) measurements [68, 89, 90]. This method offers RI measurements with high index resolution [68, 91], but RNF technique involves cleaving and subsequent polishing of the cleaved face. In addition, this method cannot map the RIP along fiber axis. The multi-wavelength interferometry (MWI) approach permits direct measurement of RIP of an optical fiber employing Fourier-transform

spectroscopy [69, 92]. A microscopy approach called differential interference contrast (DIC) measures RIP using image contrast from the phase variation in optical fiber [93]. Another method called computerized tomography (CT) that enables three-dimensional measurement of RIP in optical fiber, for instance, at a grating [94]. Most of the reported techniques are either expensive and/or require a complex reconstruction method. Bragg-grating Fabry-Perot interferometers have been reported as effective tools to measure UV radiation induced index change [95] and ultra-fast laser made index variation as a function of exposure time [74] in standard telecommunication fibers.

In this study, we propose the fiber Bragg grating based Fabry-Perot cavity structure (cavity length, L= 10 mm) to characterize femtosecond pulse filamentation induced refractive index change in the core of SMF. To demonstrate the process, higher RI is inscribed in the core length of 100 μm within the cavity of in-fiber Fabry-Perot cavity sensor, and the corresponding spectral shift of the cavity interference fringe is utilized to measure the change in RI of the core. The reason of choosing 100 μm length of fiber is to later simulate long period grating's index modulation using *OptiGrating*. Identical index modulation is then inscribed by femtosecond laser pulse filamentation in pure silica fiber to write LPGs (next chapter). The resulted transmission spectrum of the fabricated LPG is also validated using *OptiGrating* simulation software.

In order to measure femtosecond laser induced index modification in microfiber (core dia: 3.75 μm and cladding dia: 40 μm in this case), the same microfiber is used to construct Mach-Zehnder interferometer. The microfiber is fusion spliced between standard SMFs to form a sandwiched configuration of MZI (Fig. 3.7). The input light is split at first splice point and guided through both core and cladding and finally

recombined at second splice point. Therefore, when RI modification is written in the core of microfiber, the index measurement can be performed from the spectral shift of MZI's transmission valley. Positive and negative index inscription provide red or blue shift, respectively.

3.2 Experimental procedure

Schematic of experimental setup is shown in Fig. 3.1 (a). The femtosecond laser system operating at center wavelength of 800 nm, pulse duration of 120 fs, and repetition rate of 1 kHz, was used to carry out the in-fiber index characterization. A computer controlled half-wave polarizer was used to tune laser output power suitable for writing index modulation. Using an iris diaphragm, the laser beam's diameter was reduced to 1.5 mm (initial diameter: 6 mm). Then the beam was focused by an achromatic objective lens (Numerical aperture: 0.55) into a small focal volume to elevate pulse peak power necessary for writing filamentary voids in fiber core. An electronic shutter was used to selectively turn on/off the laser beam in a scanning trajectory and write index changes at desired location in the fiber core. A computer controlled 4-axis stage was used to align and scan the fiber with laser radiation. With the aid of rotational stage shown in Fig. 3.1(a) fiber is align along the X-axis of the stage with submicron precision. The fiber was coupled with a broad band light source (AFC BBS-1550) and a spectrum analyzer (PHOTONETICS Walics) to monitor and record both the spectral shifts of Fabry-Perot cavity fringe when RI was modified within the cavity structure and MZI when RI was modified in the core of microfiber. An index change over a length of 100 μm within the cavity structure of standard SMF provided a reasonable shift in the fringe pattern. Figure 3.1(b) shows a detail scanning of core length of 100 μm where the fiber was scanned with

a period of 1 µm to achieve the index modification in the core. To measure RI written in microfiber, the microfiber MZI is scanned with the femtosecond laser pulses for a length of 200 µm. The shift in MZI transmission spectrum is then used to calculate the amount of written RI.

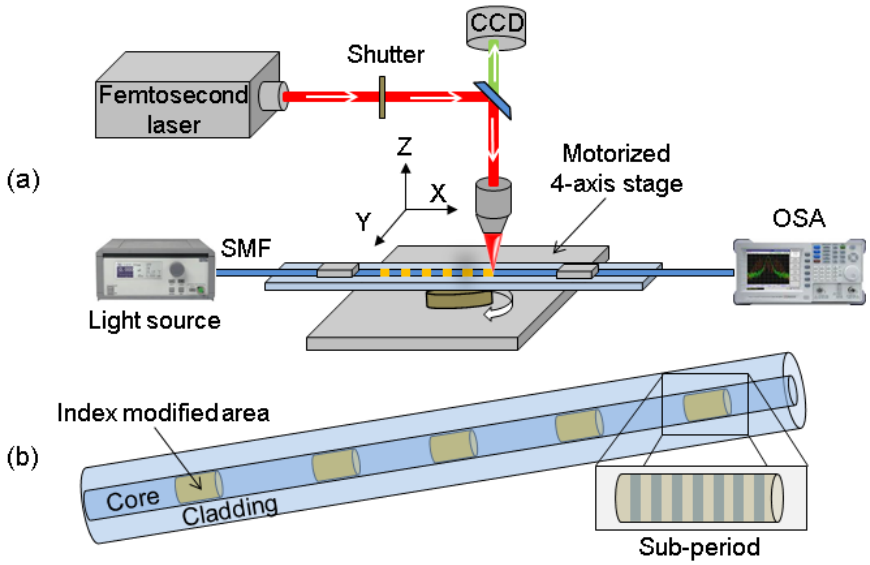

Figure 3.1 Schematic of the experimental setup (a), and the magnified image of refractive index modified region by laser radiation (b)

3.3 In-fiber RI measurement: results and discussion

3.3.1 RI characterization in standard SMF

Femtosecond laser is an effective tool to modify index in transparent dielectric materials. Permanent refractive-index can be efficiently inscribed in glass medium using focused IR-radiation of femtosecond laser pulses [96, 97]. Ultra-short pulses of femtosecond laser exhibit unique filamentation property which has been investigated extensively [76, 80]. Filamentary propagation of femtosecond pulses provides the opportunity to write index change only in the filament region. Tuning laser parameters, it is possible to control the width and length of filament [98], which offers a unique way to spatially control index

modification in the core of fiber. The width and the length of the filamentary voids found in this study were about ~1 µm and 10 µm, respectively. When the pulses are tightly focused in the transparent dielectric, due to pulse filamentation, filamentary void structures of higher index appear at the focal point. This provides an opportunity to spatially control local index modification in the core of an optical fiber. Quantification of in-fiber index modification was achieved in this work using a fiber optic Fabry-Perot cavity sensor.

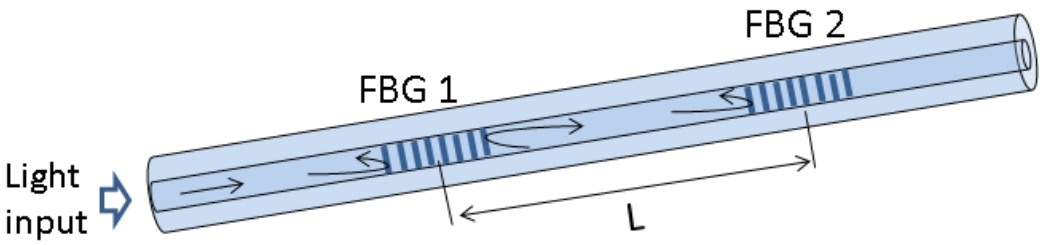

Figure 3.2 Schematic of a Fabry-Perot cavity structure constructed from a pair of fiber Bragg gratings in standard telecommunication fiber

Fringe shift of a grating based in-fiber Fabry-Perot cavity structure was employed to quantify the RI inscribed in the core of a Ge-doped standard SMF. Two identical FBGs with very low spectral noise are required to form in-fiber cavity. Figure 3.2 shows the schematic of a Fabry-Perot cavity structure in an optical fiber. In this study, the cavity structure was constructed by writing twin FBGs 10 mm apart in standard Ge-doped SMF by UV radiation. The FBGs have reflectivity of ~15% and center wavelength of 1541.9 nm with a tolerance of ±0.2 nm. The interference fringe of the Bragg grating cavity is shown in Fig. 3.3. A magnified image of the fringe pattern is shown in Fig. 3.4. In a

Fabry-Perot cavity, resonances occur when the round-trip of the light is a multiple of the wavelength:

$$2nL = m\lambda \tag{3.1}$$

where L is the spacing between the mirrors (gratings), n is the refractive index of the core, λ is the center of the reflection spectrum of the FBGs, and m is an integer. Therefore, a change in the refractive index n, over a distance d (which can be shorter than L), will shift the wavelength of a resonance fringe by:

$$\frac{\delta\lambda}{\lambda} = 2\frac{\delta n}{n}.\frac{d}{L} \tag{3.2}$$

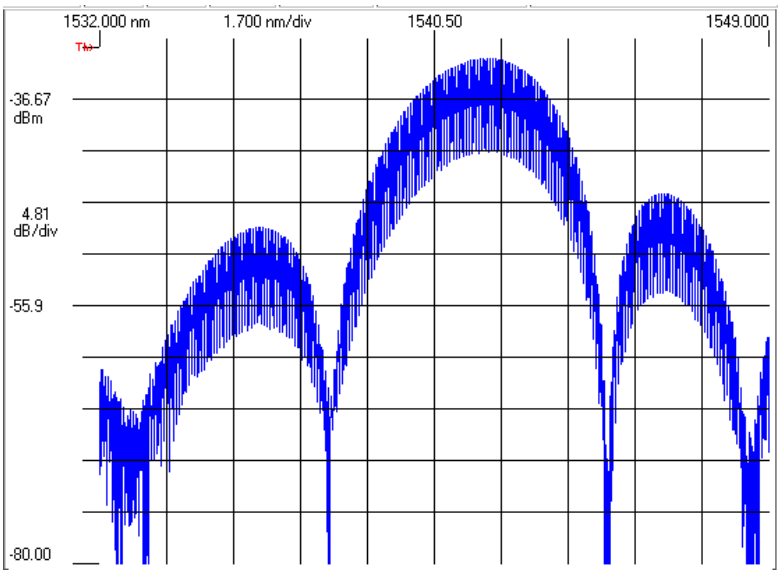

Figure 3.3 Interference fringe pattern of the fiber Bragg grating based Fabry-Perot cavity interferometer in standard telecommunication fiber

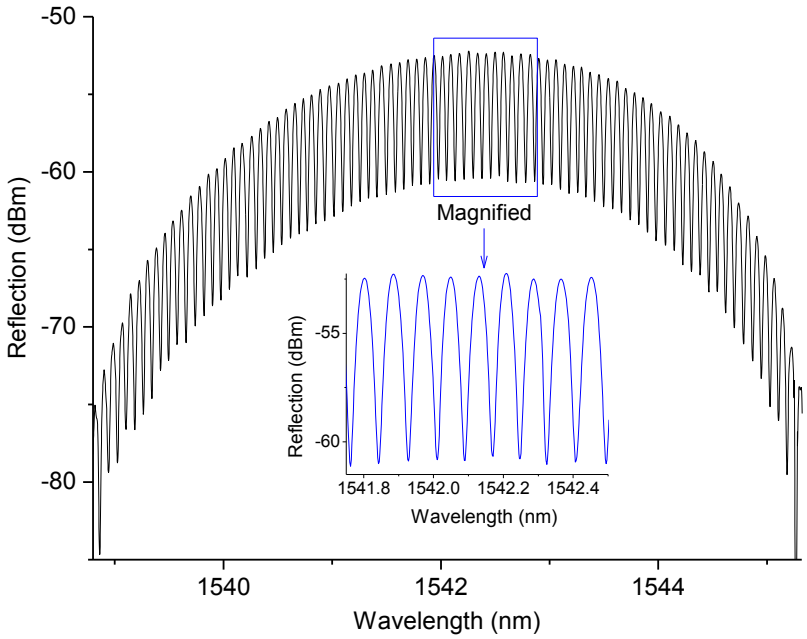

Figure 3.4 Resonance spectrum of the in-fiber Fabry-Perot cavity structure and the inset shows the magnified fringe pattern

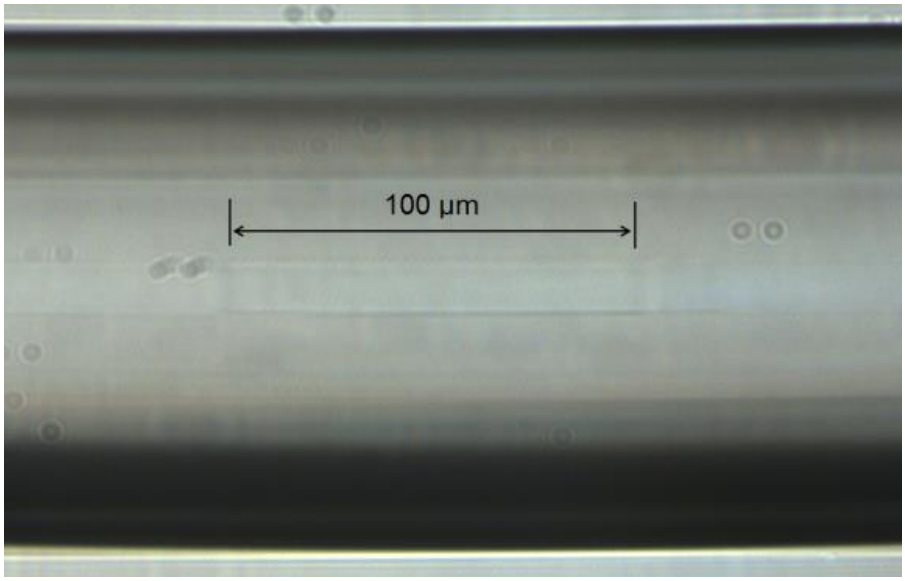

Figure 3.5 Femtosecond laser induced Index modification in the fiber core for a length of 100 micron. The fiber core is scanned transverse to its propagation axis with a period of 1 µm at the speed of 50 µm/ Sec

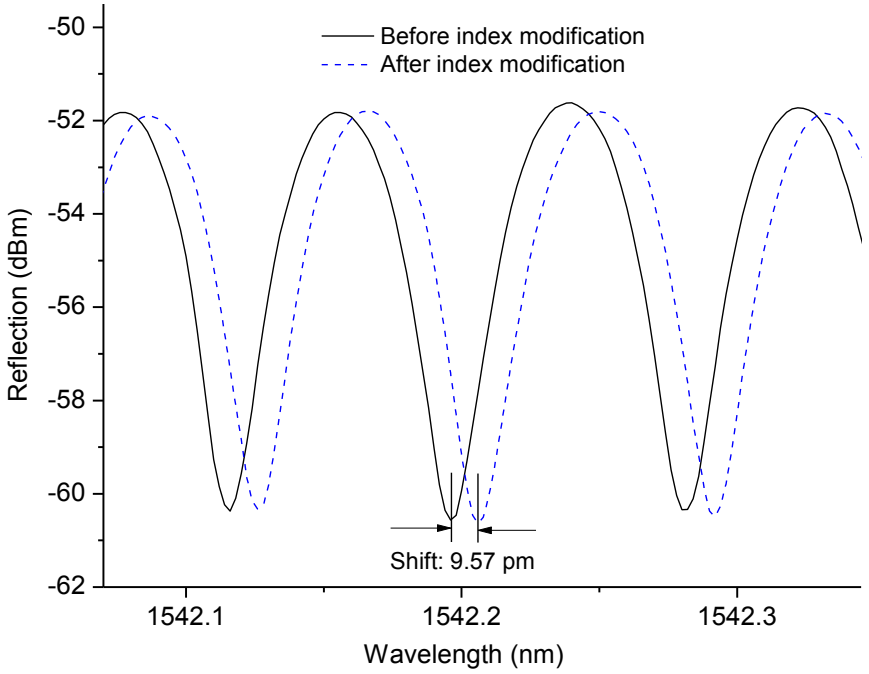

Figure 3.6 The plot showing a fringe shift of 9.57 pm of the cavity spectrum for femtosecond laser induced index change over a length of 100 µm in the core within the cavity structure

Prior to index inscription in the cavity region, the fiber was firmly fixed on the 4-axis stage as shown in Fig. 3.1(a), so that the tension on the fiber remains constant for the duration of entire experiment. At this point, the initial fringe spectrum was recorded. Next, a core length of 100 µm within the cavity was periodically (period: 1 µm) scanned with 1 kHz ultrashort pulses (pulse energy: 0.96 µJ) at the speed of 50 µm/Sec. The femtosecond pulses inscribe an array of closely packed filamentary voids (width: 1 µm) in the core and enhance the local RI. Any change of RI in the cavity region is expected to shift the resonance spectrum according to Equation 3.1. When higher RI was inscribed in the core for a length of 100 µm within the cavity as shown in Fig. 3.5, a spectral shift was observed. At this point, the fringe spectrum was recorded again. As shown in Fig. 3.6, the spectrum before and after index change is plotted to examine the total spectral shift. The

index inscription over the length of 100 μm fiber core provides 9.57 pm spectral shift of the cavity fringe. For λ= 1541.9 nm, δλ= 9.57 pm, n= 1.4470, L= 10 mm, and d= 100 μm, the Equation 3.2 provides an approximate RI change of 4.49×10-4. Identical RI was later (Chapter 4) periodically inscribed in pure silica core fiber to write LPGs.

3.3.2 RI characterization in microfiber SMF

Mach-Zehnder Interferometers have been widely used in different sensing applications [7, 8, 99, 100]. Typically, a MZI has a reference and a sensing arm. A fiber coupler splits an incident light into two arms which are then recombined by a second coupler. The recombined light interferences with each other and produces interference fringe depending on the optical path difference (OPD) between the two arms. For sensing a quantity, the reference arm is kept isolated while the sensing arm is exposed to the measurand. The signal deviation in the sensing arm induced by a measuring quantity changes the OPD of the MZI that can be sensed by examining the variation in the interference pattern. This sensing mechanism offers a unique approach to measure any refractive index change in optical fiber core. More details on MZI sensors will be discussed in chapter 6 and 7.

Figure 3.7 (a) shows the microscope image of the MZI which is constructed by splicing a microfiber between standard single mode fibers. The Fujikura (FSM-40PM) splicer set at arc power of 10 bit, and arc exposure time of 1000 millisecond, was used to splice the microfiber with standard pure silica core SMFs. To measure the RI written by infrared femtosecond laser, 200 μm blocks of higher RI was written in the core one after

another. As the higher index were written in each 200 µm blocks shown in Fig. 3.7 (b), MZI's transmission spectrum followed red shift.

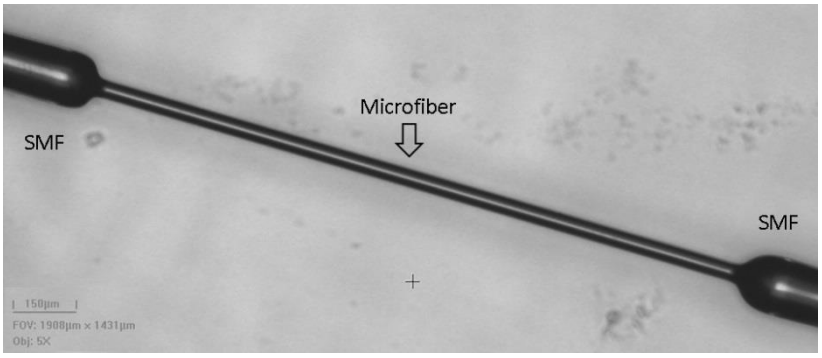

(a) Microscope image of the microfiber MZI

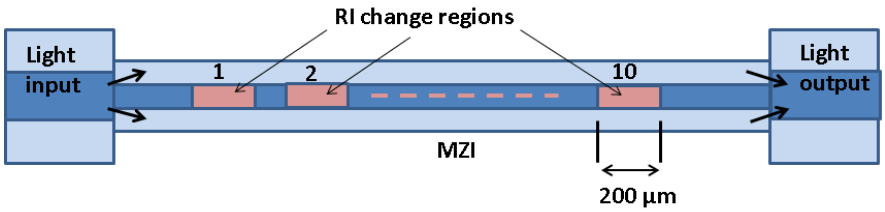

(b) Microfiber MZI schematic

Figure 3.7 (a) Microscope image of microfiber sandwiched between SMFs that form the MZI, and (b) schematic of operating principle of MZI and the blocks index change to be measured by the MZI sensor

The transmission spectral mode spacing was found to be ~35 nm when the MZI has a length of 3.25 mm as shown in Fig. 3.8. In response to the core index change over a length of 200 µm, the MZI showed a constant spectral red shift. This spectral shift can be used to calculate the amount of RI change inscribed by the femtosecond irradiation. As showed in Fig. 3.9, for each bock of laser written refractive index change, the MZI spectrum shift was recorded to be ~0.80 nm. The index change was written over 10 blocks to observe the consistency of MZI's corresponding spectral responses. As shown

in Fig. 3.10 and Fig. 3.11, using *Comsol* simulation, the value of index change required for MZI spectral shift of ~0.80 nm is found to be 0.00038.

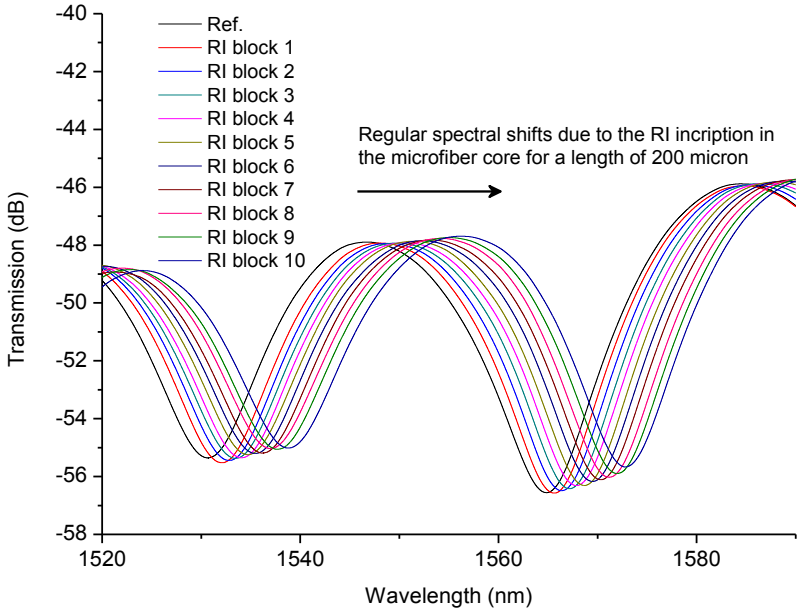

Figure 3.8 Spectral shift of the transmission spectrum of the microfiber MZI due to refractive index change over a length of 200 µm in the core. As the blocks of higher RI change add up, the spectrum experiences a steady red shift

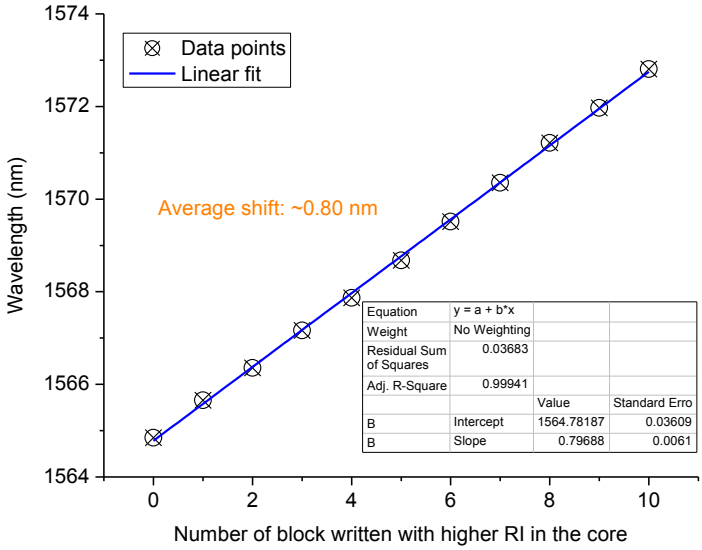

Figure 3.9 For each higher refractive index block in the microfiber core, a consistent ~0.80 nm positive spectral shift was observed as demonstrated by the slope of the characterization plot

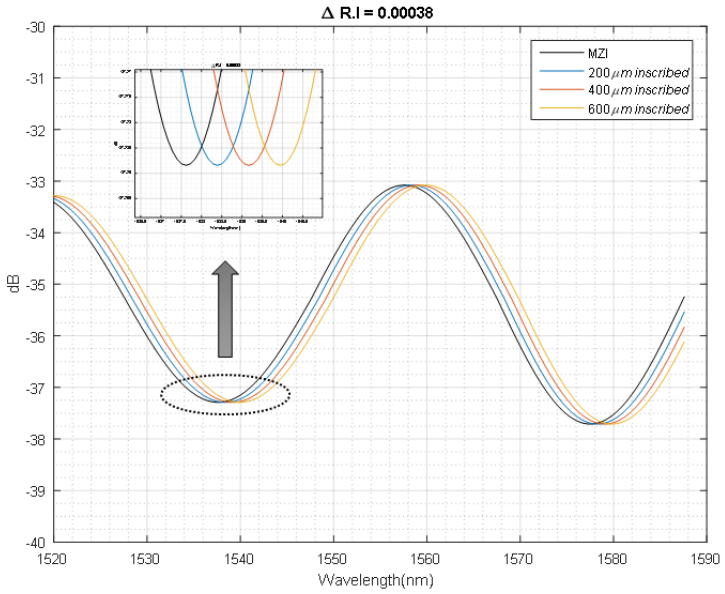

Figure 3.10 Comsol simulations to measure in-fiber refractive index modification using ultrafast laser radiation. A spectral shift of 0.775 nm was observed for RI modification of + 0.00038 over a length of 200 µm in the core

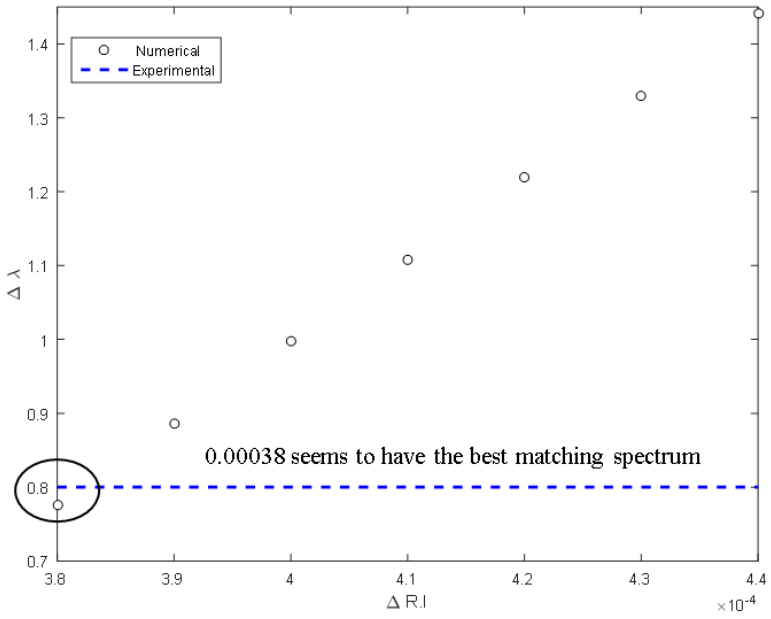

Figure 3.11 Simulation results showing optimization of core RI change required over a length of 200 µm to cause a spectral shift of 0.796 nm

3.3.3 Conclusion

In-fiber Fabry-Perot cavity structure is employed to quantify the amount of RI inscribed in standard SMF by femtosecond pulse filamentation induced voids. For the specified set of laser inscription parameters, the index change of 0.000449 is measured over the core length of 100 μm in the standard SMF using the cavity sensor.

MZI based in-fiber RI measurement technique also provides an in-situ measurement of refractive index change written by the inscription device (such as laser). Since MZI can be constructed in diverse fiber types, this technique offers flexibility to quantify index change in various optical fibers. For the specified set of laser inscription parameters, the index change of 0.00038 is measured over the core length of 200 μm in the microfiber SMF using the microfiber MZI sensor.

Chapter 4 - Ultrashort pulse filamentation based LPG fabrication in Ge-doped and pure silica core fibers

The discovery of fiber optic long period grating (LPG) has noteworthy influence on research and development of fiber sensing technologies. The LPG operates by wavelength dependent coupling of light from core mode into forward propagating cladding mode where it is lost via absorption and scattering. Therefore, these intrinsic devices can manipulate the properties of light propagating within the fiber. External environmental conditions such as ambient refractive index and temperature perturb the light propagation properties within long period gratings. This opens up wide-range studies of LPGs and their applications as sensor devices. This chapter discusses basic properties of long period gratings and application dependent manufacturing challenges and proposes femtosecond laser based fabrication of LPGs as a potential solution to overcome limitations of UV laser based gratings manufacturing.

4.1 LPG refractive index sensing

The condition for phase matching between forward propagating core mode and cladding mode in an LPG is given by [10]:

$$\lambda_{PM} = \left[n_{eff}^{core}(\lambda) - n_{eff}^{cl(m)}(\lambda)\right]\Lambda_L \tag{4.1}$$

where n_{eff}^{core} is the effective index of the core mode, $n_{eff}^{cl(m)}$ is the effective index of the m^{th}- order cladding mode, and Λ_L is the period of the grating. The cladding modes can escape from the fiber into the atmosphere due to absorption and scatterings. For this unique property, LPGs are excellent tools for refractive index sensing.

The coupling mechanism of wavelengths between fundamental core mode and forward propagating cladding modes (known as phase-matching condition), explains the LPG's refractive index sensing principle. According to the Equation 4.1, the coupling resonant wavelength is a function of the effective indices of the guided and cladding modes as well as the grating period. The effective indices are dependent on the indices and radii of core and cladding. The effective indices of the cladding modes are strong functions of the ambient RI (n_3). A change in ambient index modifies the effective index (n_{eff}^{cl}) of the cladding modes, with the higher order modes experiencing greater index variations. The coupling wavelength corresponding to a particular cladding mode is dependent on n_{eff}^{cl}. Hence, a change in ambient index (n_3) will shift the value of λ_{PM}. Let us restrict the RI measurements to a region where the ambient index (n_3) is less than the effective index of cladding mode (n_{eff}^{cl}). For a typical single mode fiber, the fundamental mode is well guided into the fiber core and is not altered by ambient index modulation. In case of a constant strain and temperature, the grating period is expected to remain unchanged. Hence, the shift of resonance cladding mode under the effect of ambient index n_3 ($d\Lambda_L/dn_3 = 0$) is given by [47]:

$$\frac{d\lambda_{PM}}{dn_3} = \frac{d\lambda_{PM}}{dn_{eff}^{cl}} \frac{dn_{eff}^{cl}}{dn_3} \tag{4.2}$$

For the operational band in normal region, an increase in effective index of the cladding mode causes a negative shift of the coupling wavelength($d\lambda/dn_{cl}$) < 0. Hence, a typical RI response of LPG shows a negative spectral shift of transmission dip when it comes in contact with higher ambient RI than air.

4.2 LPG temperature sensing

Temperature characterization is crucial for a LPG based refractive index sensor because any temperature variation in test chamber may alter the RI sensing. The phase matching condition of a long period grating is given in Equation (4.1) as a function of the mode index of core and the cladding. There are two factors that affect the temperature sensitivity of wavelength of attenuation band, $d\,\lambda_{PM}/dT$:

- the change in effective indices due to the temperature dependence of the material refractive index;
- the change in the periodicity of LPG due to thermal expansion of fiber.

The temperature dependency of the long period gratings is given by [101]:

$$\frac{d\lambda_{PM}}{dT} = \frac{d\left(n_{eff}^{core} - n_{eff}^{cl}\right)}{dT} + \left(n_{eff}^{core} - n_{eff}^{cl}\right)\frac{d\Lambda_L}{dT} \tag{4.3}$$

4.3 Fabrication of LPG in Ge-doped fiber

4.3.1 Introduction

The rapid advancement in fiber optic sensing systems has accelerated the quest to develop devices that overcome the existing limitations and offer solution to specific applications. Fiber optic sensors have shown great potential as practical and commercial measurement systems due to their inherent small size and immunity to external interferences [12]. LPGs have grating periods on the order of 100 micrometers, to a millimeter, and they couple light from a guided core mode into forward propagating cladding modes where it is lost due to absorption and scattering. LPGs, first demonstrated by Vengsarkar et al. in 1996 [10], are fast gaining approval as simple yet versatile devices for multitude of sensing applications. In-fiber long period gratings have been

demonstrated as effective and efficient tools for RI sensing [14, 18, 21, 45, 58, 102-107]. Novelty of fiber optic grating sensors depends on their performance characteristics and the transition from laboratory to commercial market depends on their fabrication simplicity. There has been a lot of progress, yet more work needs to be done to promote and develop their use in specific and advanced applications.

Various methods have been developed to fabricate long period gratings, including the use of ultraviolet [28, 30] and CO_2 laser radiation [32] exposure to electric arcs [33], mechanical pressure [34] and period corrugated structure [36]. Currently, the LPG fabrication method with UV radiation in photosensitive optical fiber is the most typical method used in in the grating fabrication. RI modulation can be written in the core of photosensitive optical fiber by the influence of an electric field. It has been demonstrated that germanosilicate glasses when tread with hot hydrogen show increase photosensitivity [38] and this phenomenon was used to write permanent periodic index in germania-silica waveguides [39]. The addition of hydrogen to Ge-doped glass breaks the Si-O-Ge bonds and forms Si-OH bonds and germanium- oxygen deficiency centers. Both of this effect leads to the increase of RI. To load a photosensitive fiber with hydrogen, the fiber is exposed with gaseous hydrogen at high pressure (100- 700 atm) and temperatures ranging from 20 to 100 ^{0}C [64]. After the completion of UV radiation based gratings fabrication in fiber, typically some excess hydrogen remains in the fiber. The post fabrication residual hydrogen enhances local index of refraction, and any further diffusion to retain equilibrium causes grating instability. Therefore, it is necessary to get rid of excess hydrogen from the fiber before using it in a particular application. Annealing the fiber at

high temperature for a short period of time provides better stability for operation at lower temperatures [64].

Because LPGs fabricated by UV radiation requires these extra pre- and post-processing steps, use of UV radiation increases fabrication complexity and heightens manufacturing cost. In contrast, femtosecond laser has brought simplicity and innovation to in fiber grating fabrication. Focused femtosecond laser pulses offer permanent RI increase in various glasses and these short pulses demonstrated a novel techniques to fabricate fiber gratings [41-44, 65, 66, 108, 109]. High pulse intensity is common for a femtosecond laser system due to its short pulse duration, which is four to five orders of magnitude less than that of an Excimer laser [43]. Light intensity is highly localized at the focal point, and hence femtosecond laser can induce period RI modulation in the core of fiber without affecting cladding or polymer coatings. A major advantage of femtosecond laser fabrication is that the fabricated gratings have higher temperature resistance; hence they have a greater aging characteristic [47].

4.3.2 Femtosecond laser system

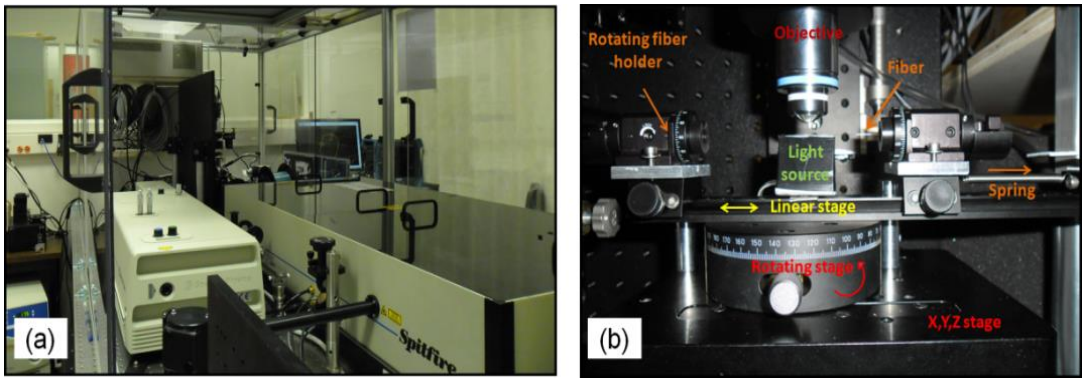

Figure 4.1 The femtosecond laser system (Spectra-Physics, U.S.A) (a) and the computer-controlled 4-axis stage to align fiber along x-axis (b)

The femtosecond laser (Spectra-Physics ultrafast Ti: Sapphire laser) shown in Fig. 4.1, was used to write RI change in the fiber core. The kilohertz ultrafast laser has a pulse width of 120 femtosecond with the center wavelength of 800 nm. A computer controlled 4-axis stage was used to align and scan the fiber with laser radiation.

4.3.3 Experimental setup

The schematic of experimental setup for the fabricating long period gratings is shown in Fig. 4.2. A set of neutral density (ND) filters was used to primarily tune down the pulse energy. After the ND filters, a computer controlled variable attenuator (based on a half wave-plate and polarizer combination) was used to further adjust laser output power to the desired level. A computer controlled electronic shutter was used to selectively turn on/off the laser beam and write index at desired location in the fiber core. An iris diaphragm was used to reduce beam diameter to 1.5 mm. Then the laser beam was guided into a microscope and focused by objective lens (Numerical aperture: o.55) into the core. The features fabricated during focused irradiation of femtosecond pulses were observed through a CCD camera mounted above the dichroic mirror. Fiber jacket was removed and cleaned with acetone before writing LPGs in bare fiber. The optical fiber was fixed on a computer-controlled 4-axis stage that allows aligning it along x-axis with submicron precision. Laser beam focusing was done with an achromatic lens under incident angle of zero degree onto the sample. Line-by-line technique was used to fabricate LPGs. The software, GOL3D was used to generate scanning path of the laser head. The schematic of in-fiber RI inscription for long period gratings fabrication is shown in Fig. 4.3. The period of refractive index modulation in fabricated LPGs is 435 μm. In the index modified area of Fig. 4.3, the RI was written for a length of 100 μm by the laser scanning

(period: 2 μm) at the speed of 50 μm/sec. The fiber was coupled with a broad band light source (AFC BBS-1550) and a spectrum analyzer (PHOTONETICS Walics) to monitor the growth of LPG during fabrication. The high index periods are gradually added one after another until LPG's transmission valley reached at its maximum value. Once an individual LPG's transmission dip reaches its highest and optimum value, any further increase in length of index modulation degrades transmission spectrum.

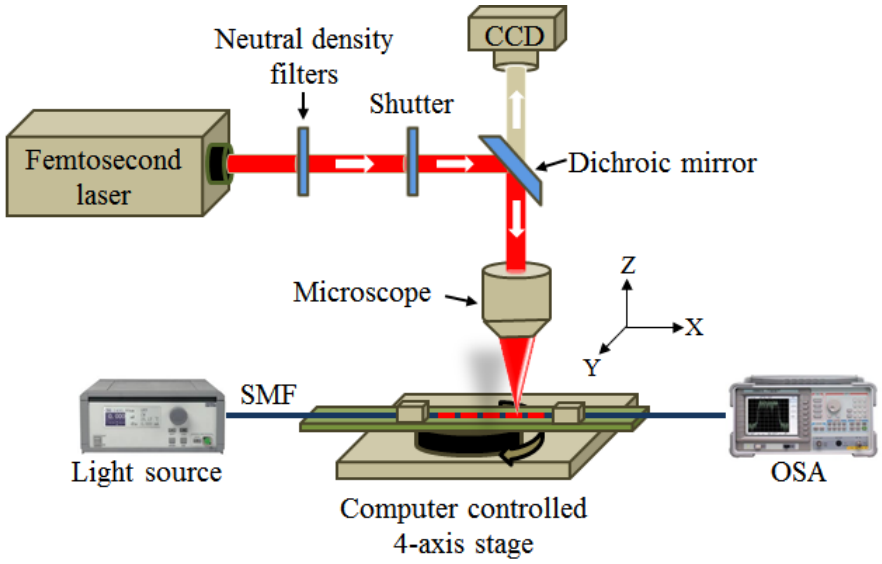

Figure 4.2 Schematic of experimental setup for writing fiber gratings

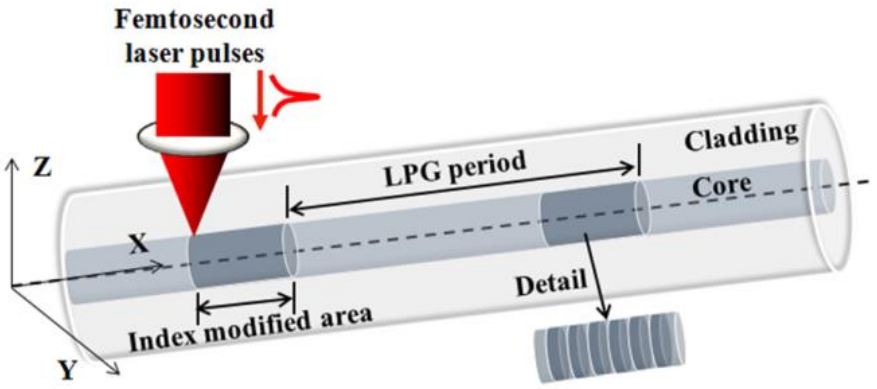

Figure 4.3 Schematic long period in-fiber grating fabrications

4.3.4 Pulse filamentation to write RI

Femtosecond lasers are effective tools to write index in transparent dielectric materials. Permanent refractive-index can be efficiently increased in glass medium using focused irradiation of femtosecond laser pulses [96, 97]. Intense femtosecond pulse when tightly focused reaches high enough intensity to ionize the medium in its path and leave behind a narrow column of plasma. Along the filament axis, alternative Kerr self-focusing and self-defocusing of self-generated plasmas continue to add up regularly spaced plasma spots in a narrow channel until pulse peak power remains higher than critical power for pulse filamentation [80]. In its progression, the pulse losses it's energy due to ionization so that the self-focusing gradually weakens. Eventually the filament terminates because the self-focusing is overcome by diffraction and plasma defocusing. The plasma column quickly solidifies and creates a void of higher refractive index in the transparent medium. Filamentary propagation of femtosecond pulses provides the opportunity to write index only in the filament region. Tuning laser parameters, it is possible to control the width and length of filament, which offers a unique way to better control index modification in the core of fiber.

Pulse self-focusing is a crucial parameter for its filamentation to occur. An ultra-short laser pulse can self-focus in an optical medium due to 3rd order nonlinear process called Kerr effect explained in Chapter 2. In such case, medium shows pulse intensity dependent index of refraction and is given by [76, 110]:

$$n_1 = n_0 + n_2 I(r,t) \tag{4.4}$$

where n_0 is the linear RI, n_2 is the nonlinear RI, and *I(r,t)* is the intensity profile of the ultrafast pulse. When pulse focusing occurs, the photons start to gather towards the center of the pulse and enhance pulse intensity. The intense pulse creates plasma in the central region of the pulse due to multi-photon ionization as shown in Fig. 4.4. Excess electron densities decrease the susceptibility of the medium and reduce the local index of refraction. So, the central part of the pulse tends to de-focus while the peripheral region continues to self-focus. This leads to interesting energy dynamics within the pulse at it propagates [110]. The balance between self-focusing and de-focusing leads to a sustained filamentary propagation of ultrafast pulse. However, pulse losses energy when ionizing the medium. So, the filament terminates as soon as the pulse peak power becomes less than the critical power required for pulse filamentation. Because the ultrashort pulses carry limited energy, the pulse propagation medium almost immediately re-solidifies leading to a change in RI. Consequently, with the proper laser parameters, it is possible to control the local RI in the bulk of glass materials. Inscription of waveguides using filamentary propagation of ultrafast pulse is demonstrated in several studies [111, 112]. That specifies that the RI is highest at the center of the filament and gradually decreases toward the periphery.

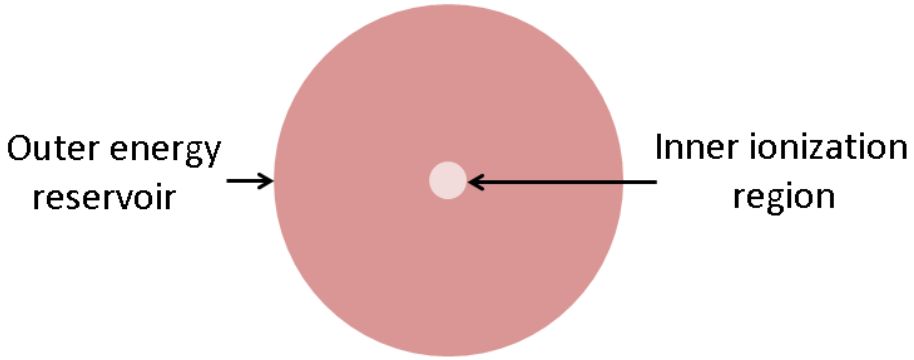

Figure 4. 4 Transverse profile of ionizing region of a filament

Spatial control of RI modification in the core is one of the key requirements to efficiently write fiber gratings. When the pulses are tightly focused in the transparent dielectric, due to pulse filamentation, higher index of filamentary void structures appear in the focal point. This gives an opportunity to spatially control local index modification at focal point. With the elevated pulse intensity confined in a tiny focal volume, we have employed ultra-fast pulse filamentation technique to inscribe submicron void inside the core of single mode fiber. Prior to working with single mode optical fiber, we investigated the index morphology written by femtosecond laser radiation in the bulk of borosilicate glass. Figure 4.5 shows the femtosecond laser induced single-shot voids inscribed in borosilicate glass of thickness 150 µm. Average pulse energy of 10 µJ was used to inscribe the voids. The period of horizontal scan, the amount of index change and their location relative to the core of fiber determine the location peak attenuation band in transmission spectrum.

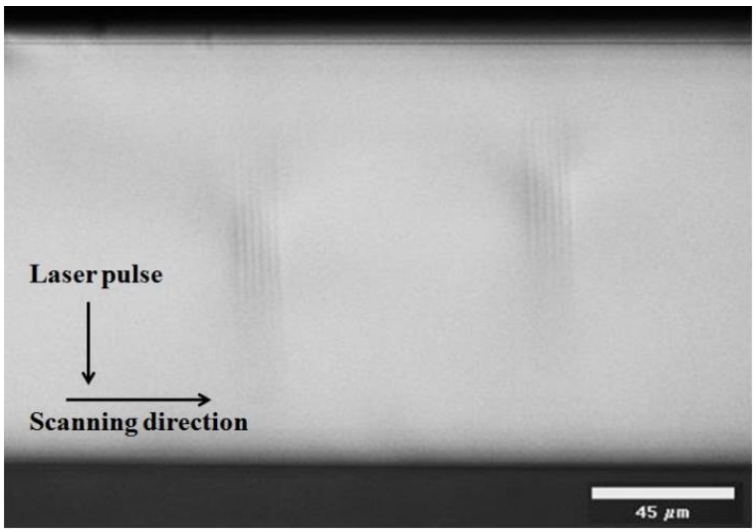

Figure 4.5 Periodic index change written in borosilicate glass (thickness 150 µm) by single-shot femtosecond pulse filamentation with pulse energy of 10 µJ

4.3.5 Fabrication results and discussion

Figure 4.6 shows the growth of LPG's transmission spectrum. Both LPGs were written for a period of 435 µm but the total lengths of index modulation were different. The LPG written in Figure 4.6 (a) was relatively short (total length: 22.62 mm). The transmission spectrum shows an attenuation dip of 20dB at 1552 nm. The first 30 periods of the LPG shown in Figure 4.6 (a) were written with average pulse energy of 24 µJ. Periods from 31 to 52 were written with average pulse energy of 26 µJ. The index modulation was written for a total length of 34.8 mm with average pulse energy of 24 µJ for the LPG shown in Fig 4.6 (b). The transmission spectrum has a smaller attenuation dip (~18 dB) at 1537 nm, but the spectrum valley is narrower than the previous one which is better for sensing applications. The FWHM of the attenuation band is 5 nm and the sharp transmission dip can offer high resolution in RI measurement.

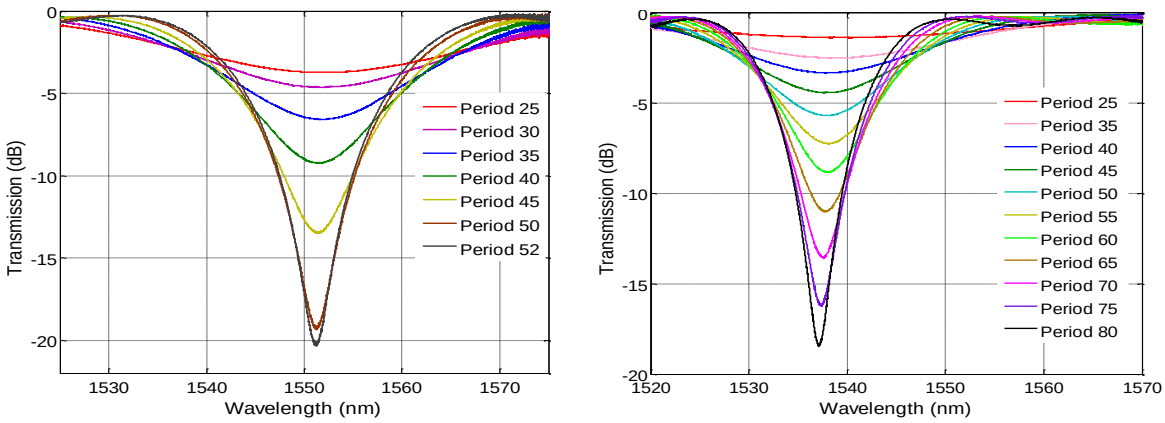

(a) (b)

Figure 4.6 Gradual growth of LPG in Ge-doped fiber for different number of periods. The total length of LPG in (a) and (b) are 22.62 mm and 34.8 mm give the transmission dip at 1552nm and 1537 nm respectively

4.3.6 Refractive index characterization

For the operational band in normal region shown in Fig. 4.7 and Fig. 4.8 (a), an increase in effective index of the cladding mode causes a negative shift of the coupling wavelength ($d\lambda/dn_{cl}$) < 0. For a grating operating at $d\lambda/dn_{cl} = 0$, the transmission valley disappears and the LPG fails to work as a RI sensor near that index value. This property is demonstrated in Fig. 4.8 (b). When the ambient index equals the effective index of cladding mode, the outer cladding interface disappears and the coupling of the guided mode is expected to occur to a continuum of guided modes [47]. Since each cladding mode has a unique effective index, the corresponding resonance bands should disappear at different values of the ambient index. For grating operation in the region where ($d\lambda/dn_{cl}$) > 0, the grating exhibits opposite behavior as shown in Fig. 4.8 (c). An increase in ambient index n_3 near the value of the effective index boosts ($dn_{cl}/dn_3 > 0$) and thus results in shifts in opposite directions.

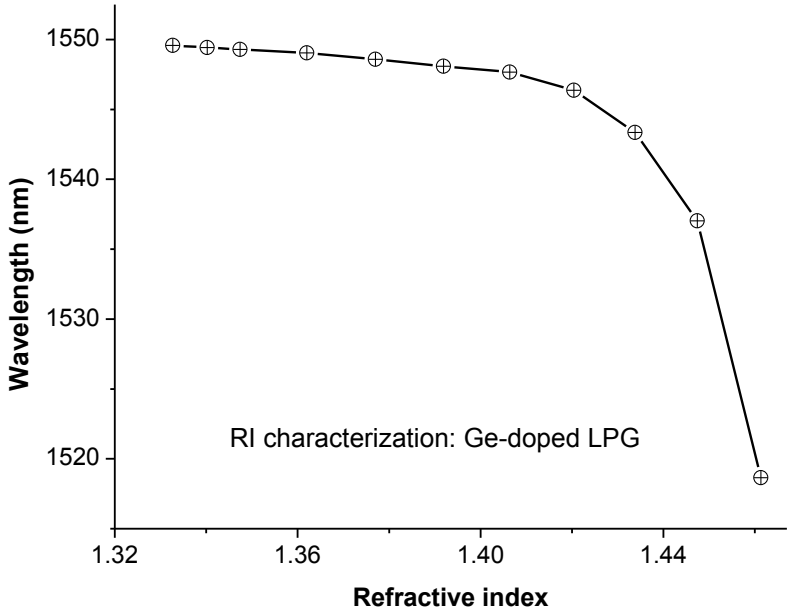

Figure 4.7 Refractive index characterization of LPG fabricated with femtosecond laser radiation

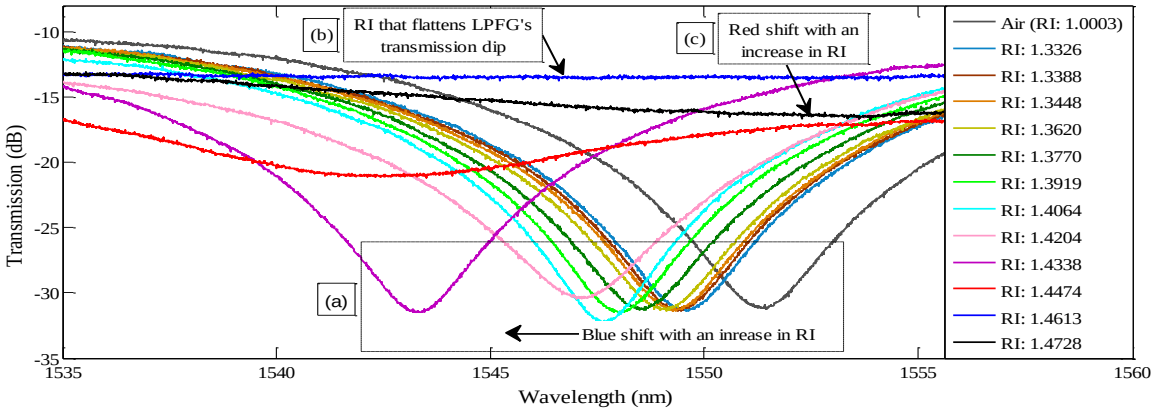

Figure 4.8 Shift of transmission valley and attenuation height when the LPG is exposed to solutions of different RI. Regular blue shift is observed for the attenuation band enclosed in rectangular box (a). The attenuation band is flattened for the ambient RI value of 1.4613 (b). Further increase in ambient RI results in a red shift of the transmission band (c)

4.3.7 Conclusion

Ultrashort pulse filamentation induced writing of refractive index modulation in the core of standard SMF is demonstrated to fabricate LPGs. Reported RI inscription technique shows steady growth of in-fiber long period gratings. The proposed method exhibits negligible insertion loss in LPG fabrication which is a vital to many sensing applications. LPG's sharp transmission valley (FWHM of 5 nm) offers better resolution in RI measurement of a test solution. The position of transmission dip can be tailored relatively easily simply by varying the period.

4.4 Fabrication of LPG in pure silica fiber

4.4.1 Introduction

As mentioned in section 4.3, ultraviolet excimer lasers are mostly used to inscribe LPGs in standard SMFs. In UV laser based techniques, RI modulation is written in the core of a photosensitive optical fiber by UV radiation and photo-mask [10, 67]. The UV laser based gratings fabrication can only be used in photosensitive optical fibers (e.g. Ge-doped core) and this process requires pre and post fabrication steps. To increase photosensitivity of the core, the germanosilicate fibers are treated with hot hydrogen [38] prior to writing periodic index modulation in UV laser based fabrication. Hence, a post fabrication annealing at high temperature for a short period of time is necessary to get rid of excess hydrogen from the fiber and provide better grating stability [64]. In addition, the performance of UV LPGs degrades over time due to hydrogen darkening in harsh environmental conditions, a phenomenon that occurs when hydrogen gas diffuses into the Ge-doped fiber and darkens the core through chemical reaction [113, 114]. Photo insensitive pure silica fibers are considerably more resistant to ionizing radiation environments compared to Ge-doped fibers. Therefore, gratings inscribed in pure silica fibers are good candidates for sensing applications in hazardous environments. Hindle et al. have demonstrated fabrication of LPG in pure silica fiber, however, the reported grating has weak rejection band and wider full width at half maximum (FWHM) [46]. Besides, the weak focusing condition of ultrashort pulses reported in that study may account for higher insertion loss due to material darkening.

In this work, identical index modulation measured in section 3.3.1 is inscribed in pure silica fiber to write LPGs. The resulted transmission spectrum of the fabricated LPG

is also validated by the grating simulation software called *OptiGrating*. The simulation and experimental results of LPG fabrication show that for the same laser inscription parameters, the written index change in pure silica fiber is identical to the RI modification measured in Ge-doped standard SMF using Fabry-Perot cavity. Demonstrated line-by-line gratings fabrication exhibits simple and flexible writing of LPGs in pure silica SMF with an attenuation dip of 22.22 dB in the transmission spectrum. The LPG sensors are also characterized for temperature and refractive index sensing.

4.4.2 Fabrication results and discussion

Prior to LPG fabrication, the '*OptiGrating*' simulation software was used to optimize grating parameters such as period, index modulation, grating length etc. For index change of 0.000449 over core length of 100 µm found in the cavity based characterization (Section 3.3.1) and period of 435 µm, the *OptiGrating* simulation was used to predict LPG's transmission valley in pure silica fiber (more *OptiGrating* LPG simulation can be found in Appendix B). Figure 4.9 shows a comparison between LPG's transmission spectra obtained in simulation and femtosecond laser fabrication. Both the transmission spectra (simulation and fabrication) have a common valley at ~1534.67 nm which was achieved for the period of 435 µm (total number of periods: 62) and the index modulation of 0.000449 found in RI characterization process. The transmission spectrum of fabricated LPG shows an insertion loss of 0.54 dB. The simulation and experimental results show that the femtosecond pulses write index change in Ge-doped standard telecommunication fiber and pure silica fiber to identical magnitude.

In line-by-line inscription, the index modified area was achieved by scanning the fiber transverse to its propagation axis with the speed of 50 µm/ sec and sub-period of 1 µm as shown in Fig. 4.3. The pulse energy of 0.96 µJ was used to write total 62 periods and the gradual buildup of the transmission spectrum was monitored and recorded in-situ in the optical spectrum analyzer. To investigate the growth behavior of LPG's transmission valley, the spectrum was recoded at period number 30, 40, 45, 50, 55, 60, and 62 then plotted as depicted in Fig. 4.9. When the total number of period reached to 62 (grating length: 26.97 mm), the transmission spectrum showed highest dip of - 22.22 dB centered at 1534.674 nm. Any farther increase in grating length causes a reduction of the depth of transmission valley. The FWHM of the attenuation band is 7.5 nm.

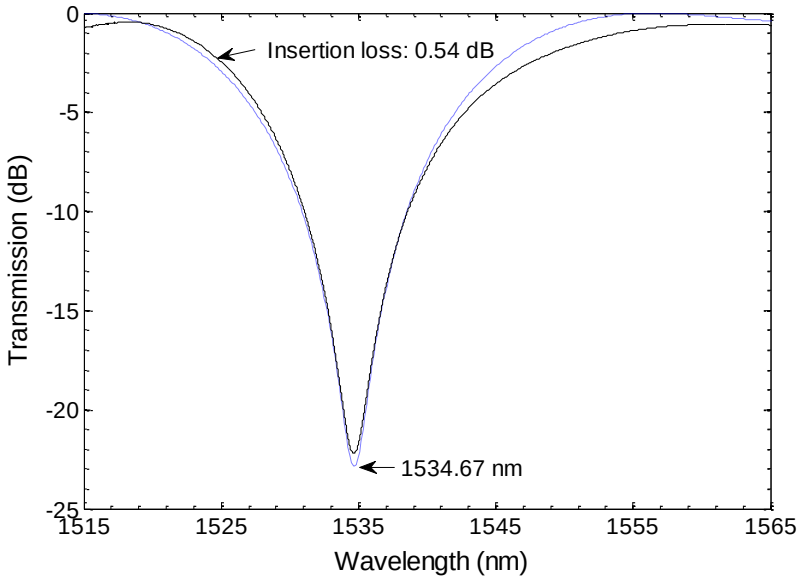

Figure 4.9 Comparison between the transmission spectra of the gratings simulated in OptiGrating software and actually inscribed by femtosecond laser pulse filamentation based index modulation. Both simulation and fabrication spectra of the long period grating are in good agreement. The spectrum of the fabricated grating shows as insertion loss of 0.54 dB which is very low in ultra-short laser inscription

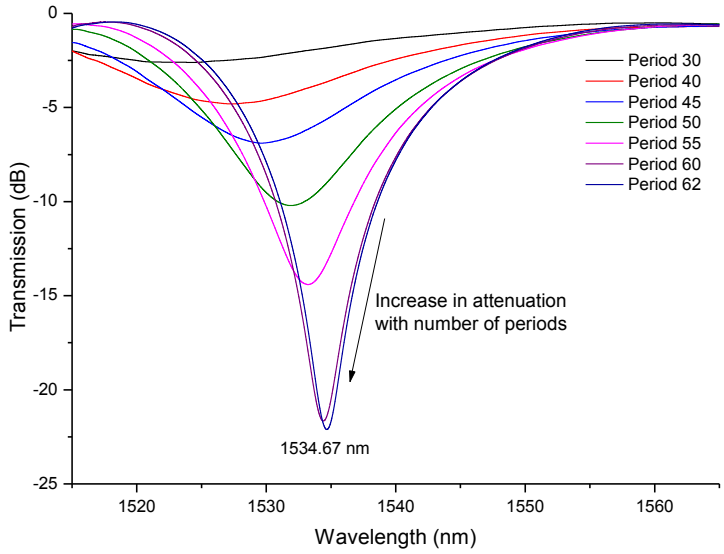

Figure 4.10 Growth of LPG's transmission spectrum during fabrication process. Height of the transmission valley is maximum when the total number of periods reaches to 62

4.4.3 Refractive index characterization

The experimental results show good RI measurement capability of LPG. The experiments were done at room temperature. The grating was immersed in a custom made small container fillable with difference concentration of glycerin solutions. The LPG was firmly supported on two sides of the container by fiber holders to subside any bending or strain induced spectral shift. Then the grating was separately immersed in difference concentration of glycerin solutions of variable RI ranging from 1.3325 to 1.4615. After interrogating the LPG with particular glycerin solution, the container was cleaned carefully to remove the residual solution. The typical refractive index dependence of the loss peak wavelength in transmission spectrum for the LPG written in pure silica core SMF is shown in Fig. 4.11. The spectral shift of the transmission valley increases non-linearly with increasing RI. The overall spectral shift of -13.96 nm was measured for RI range n_3 = 1.3325 to 1.4615. When the ambient RI approaches to 1.4615, the

transmission valley gradually flattens as the coupling from the guided mode to the corresponding cladding mode weakens. As shown in Fig. 4.11, the LPG's index sensitivity is fairly low for ambient index values from 1.33 to 1.39. Sensitivity in that RI window can be considerably increased by reducing cladding diameter in grating region [23] or depositing nanoscale overlays on LPGs that have higher RI compared to the cladding one [115].

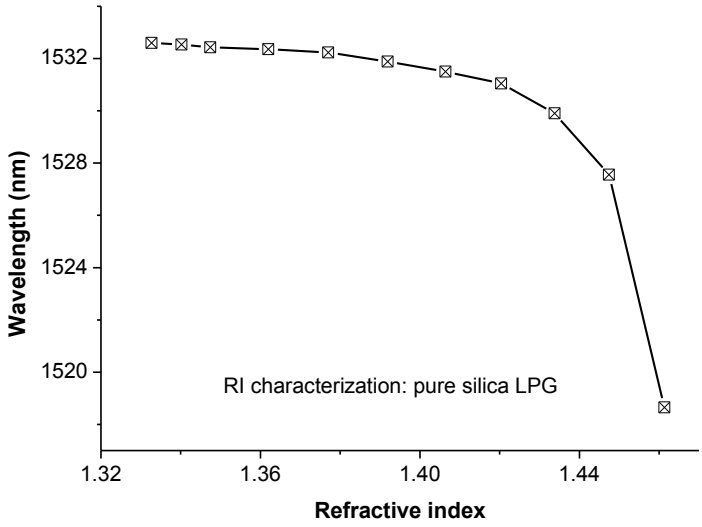

Figure 4.11 Refractive index characterization of the pure silica core in-fiber LPG sensor

Unlike UV laser, ultra-fast laser based grating fabrication offers permanent and stable RI modulation in core of SMF, and does not require any pre or post processing. Compared to UV LPGs, they can stand higher temperature which is often required for many industrial applications. Hydrogen diffusion in photosensitive fiber can darken the fiber core through chemical reaction and can erase the index modulation of the grating in long term sensing applications. In contrast, femtosecond LPGs written in pure silica fibers, are suitable for long term environmental monitoring since they do not experience any significant hydrogen darkening.

4.4.4 Temperature characterization

For temperature characterization, the grating was immersed in a water bath ($n_3 = 1.33$) and the water was progressively heated from 28.50 ^{0}C to 96.80 ^{0}C. The shift in resonance band as a function of temperature is shown in Fig. 4.12, where a positive temperature induced spectral shift was observed. A total spectral shift of ~ 1.98 nm (measured at $n_3 = 1.33$) was observed for the temperature variation of 68.30 ^{0}C. The linear curve fit in Fig. 4.12 shows a temperature sensitivity of ~30 pm/ ^{0}C.

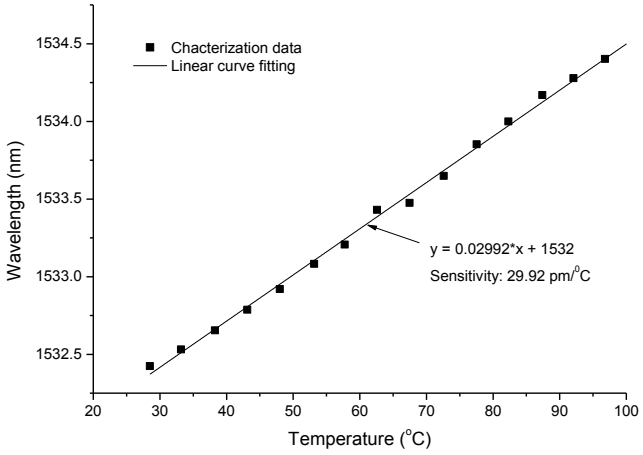

Figure 4.12 Temperature response of the LPG written in pure silica core fiber

4.4.5 Conclusion

Fabrication of LPG is demonstrated with very low insertion loss. The LPGs fabricated in pure silica fiber are potentially promising in contaminated/ down-hole sensing applications because unlike doped fibers, pure silica fiber are immune to ionizing radiation environments. The ultrafast laser written index modulation would likely to withstand higher temperature compare to UV laser written gratings in doped fibers. Therefore, the pure silica fiber LPGs are also expected to cope well in higher temperatures.

Chapter 5 – Fabrication of helical LPGs in pure silica fiber

A comparative study of LPG fabrication in both doped and pure silica fibers using UV excimer laser and infrared femtosecond laser is provided in chapter 4. Until recently, the UV laser based fabrication is commercially viable, even though they have few limitations such as poor ageing characteristics, unreliable in extreme environmental conditions such as high temperature and chemically hazardous atmosphere, excess pre and post fabrication steps that increase production cost, etc. Femtosecond laser based fabrication may bring solution to these problems; however, femtosecond gratings are still not commercially available because of high fabrication cost and/or due to the lack of reliability in manufacturing. This chapter proposes fabrication of helical LPGs using femtosecond laser to improve reliability in long period grating fabrication.

5.1 Introduction

As revealed in chapter 4, besides UV laser inscription, there are several methods available up to date for manufacturing LPGs [29, 32-36, 43, 48, 49, 65-67]. The ultrafast laser inscription is reported to be the most popular and viable technique after UV laser based method. In fact, compare to UV radiation, gratings fabricated by infrared radiation have superior properties such as better ageing characteristics, potentially suitable to operate in higher temperature and chemically hazardous environments that are key requirements for many industrial applications. Direct, rapid, and permanent in-fiber RI writing capabilities of ultrafast pulses also make femtosecond lasers suitable for large

scale grating fabrication. Nevertheless, the femtosecond laser manufacturing has far to go before it becomes a commercial success in gratings manufacturing.

Asymmetric index inscription and Low tolerance on fiber alignment are two common sources of unreliability in direct writing of long period gratings in ultra-short laser manufacturing. In ultrafast direct writing, typically the refractive index is written in the core along the direction orthogonal to the fiber propagation axis. The length of a LPG can be as long as few centimeters. Thus in ultrafast laser fabrication, confinement of index modulation in the core for the entire grating length is unforgiving to fiber misalignment. Therefore, for the same laser inscription parameters, the transmission spectra of two LPGs may differ if the fiber alignment changes. In contrast to conventional gratings, the core index modulation of a helical grating has the helical structure like a screw. Therefore, compared to conventional LPGs, the helical LPGs (HLPG) are expected to be more forgiving of pre-fabrication fiber alignment which is vital for mass production.

Polarization dependent loss (PDL) in optical components can degrade overall system performance in long-haul communication [116]. Wavelength dependent loss and longer grating length (few cm) of long period grating make it vulnerable to PDL. Asymmetric index change in transverse plane is reported to be one the main reason that accounts for PDL in LPGs and grating inscription by multiple exposure or rotating exposure are proposed to overcome it [117, 118]. HLPG was first demonstrated by helical micro-bending induced by winding wire around a two-mode fiber [119]. The period of that grating is hard to control as it is determined by the thickness of the wire. Oh *et al.* reported fabrication of HLPG in single mode fiber by using CO_2 laser [120]. To

be best of our knowledge, fabrication of HLPG is not yet been reported using any ultra-fast laser. In this study, we present pulse filamentation based helical long period grating inscription in pure silica fibers using femtosecond laser radiation. Reliability of gratings fabrication has also been demonstrated in this work.

5.2 Experimental setup

To rotate the fiber at constant speed with minimal rotating run-out, a custom fiber fixture was developed. As shown in Fig. 5.1, the fiber fixture is mainly composed of a tilt & rotation platform (Newport), a miniature optical rail (Newport), two mini rail flat carriers (Newport) and a DC motor. To hold the fiber while in rotation, the fiber was guided though two close fit channels (sitting on rail flat careers) that were machined using femtosecond laser. The channels were created by machining slots (width: 125 um, length: 15 mm, depth: 130um) on a microscope slide and letting a second microscope slide to firmly sit on it when the fiber is rested on the slots. As shown in the figure, between the two rail careers, the fiber jacket was removed. One rail career is fixed on the rail while other can travel back and forth. Therefore, adjusting the position of moveable rail career, an adequate tension is applied on the fiber to keep it straight while allowing it to rotate. The fiber is coupled with a DC motor that runs at 45 RPM for 12 VDC. The measured run-out while the fiber rotates was less than 1 um. The fiber fixture assembly was mounted on a computer controlled 3-axis stage. A computer controlled polarization based attenuator was used to tune down the laser power suitable for grating fabrication. The laser pulses were focused with a microscope lens (Numerical aperture: 0.55) on to the fiber core. To inscribe the LPGs, the rotating fiber was moved at constant speed (10 μm/ s) along its propagation axis, while an electronic shutter was selectively turned on and off

to write higher refractive index at desired location in the core to create grating period. The transmission spectra of the fabricated LPGs were examined using a spectrum analyzer (PHOTONETICS Walics) connected to broad band light source (AFC BBS-1550).

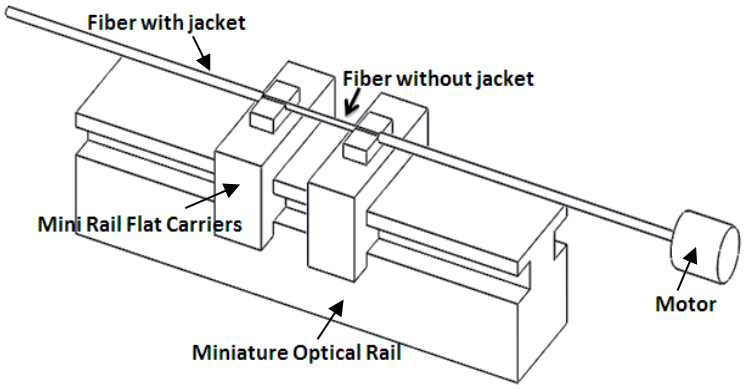

Figure 5.1 Schematic of rotational stage used for ultra-short laser based HLPG fabrication

5.3 Fabrication results

The schematic of in-fiber helical index modification is illustrated in Fig. 5.2. For a given RPM of the fiber, the period of the helix can be selected simply by changing the linear speed of the fiber along its core axis. This allows adjusting the index modification over a distance to achieve a desired index modulation in the core.

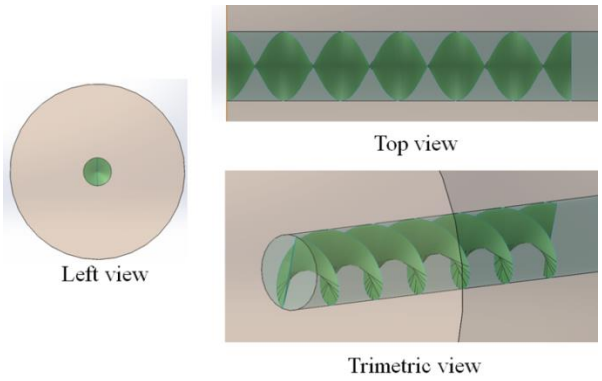

Figure 5.2 Schematic of the helical index change in the core of standard SMF

Figure 5.3 shows details of index modification over a period length of 435 µm. As mentioned in 'experimental setup' section, the electronic beam shutter was open for a length of 100 µm for the whole period of 435 µm to achieve the periodic index. Length of index modified region was varied by allowing the laser to radiate over a projected length of the core. The effect of the length of index modified region on spectral growth of LPG's transmission dip is also examined in this work.

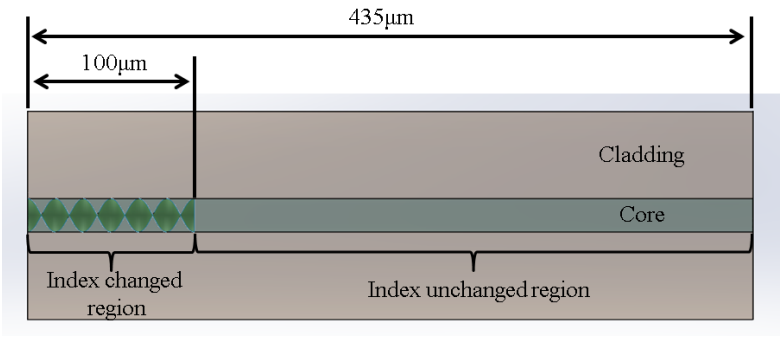

Figure 5.3 Schematic of index modulation proposed in HLPG fabrication

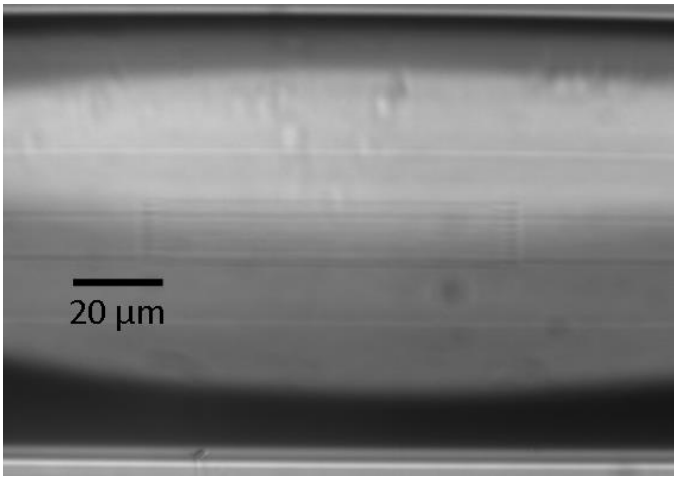

Figure 5.4 Filamentary index alterations over a core length of 100 µm in pure silica core fiber

Femtosecond pulse filamentation induced core index modification over a length of 100 µm is presented in Fig. 5.4. As shown in the figure, voids written by pulse filamentation technique allows even index alteration without significant material

darkening. Index modification without substantial material darkening enables inscription of fiber gratings with minimum insertion loss.

5.3.1 Test of fabrication reliability

Helical index modification turned out to provide greater fabrication reliability of fiber gratings. Figure 5.5 shows the transmission spectra of three different LPGs fabricated with same writing conditions (pulse energy: 25 µJ, beam diameter: 2 mm, and grating period: 450 µm) but different number of periods. In absence of rotational stage, the gratings are usually inscribed by scanning the fiber with laser pulses orthogonal to its propagation axis. It is challenging to confine asymmetric index modification (written in conventional technique) within the fiber core when the fiber is not aligned precisely. The helical index modification seems to improve consistency in writing of index modulation and thus writing of reliable LPGs. A maximum spectral deviation of 0.22 nm is overserved in Fig. 5.5, which may also appear due to the tension manually applied on the fiber prior to grating fabrication. It is worth noting that we aimed to apply a constant pre-fabrication tension on the fiber in this experiment.

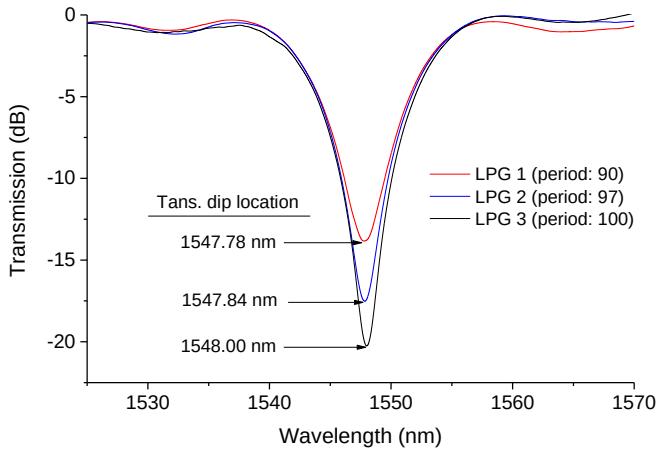

Figure 5.5 Transmission dips of three different LPGs fabricated with same writing parameters (i.e. radiation conditions, periodic length, etc.) for different number of periods. The maximum

fluctuation of spectral locations of transmission dips appears to be 0.22 nm which is overwhelmingly good for ultrafast laser based grating fabrication.

Figure 5.6 shows spectra of four different LPGs fabricated using identical laser writing conditions (pulse energy: 25 µJ, beam diameter: 2 mm, period: 450 µm, number of period: 100). A maximum spectral deviation of 3.78 nm was observed between the transmission dips of the LPGs which is fairly satisfactory in LPG fabrication. It is worth to mention here that the spectral fluctuation may appear due to the manual strain applied on the fiber before laser index inscription.

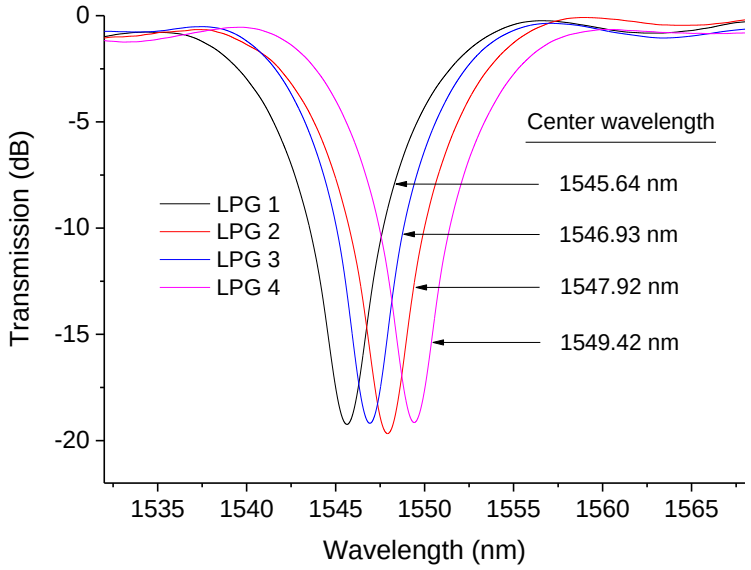

Figure 5.6 The fluctuation 3.78 nm among the center wavelengths for 4 consecutive LPGs fabricated with rotational inscription method. The authors believe the wavelength deviation results from variable tension applied prior to fabrication

5.3.2 Effect of index change length on spectral dip

Effect of index modification length (within the period) on LPG's spectral location and attenuation loss is investigated in this section. Figure 5.7 shows how the transmission spectra of three different LPGs evolve when length of index modified region was chosen

to be 50 µm, 100 µm, and 200 µm. As shown in the figure bellow, it requires fewer numbers of periods to reach a specific attenuation loss in LPG's transmission spectrum when the length of index modified region increases. Also it is apparent that the transmission dip experiences a red shift when length of index modified region increases.

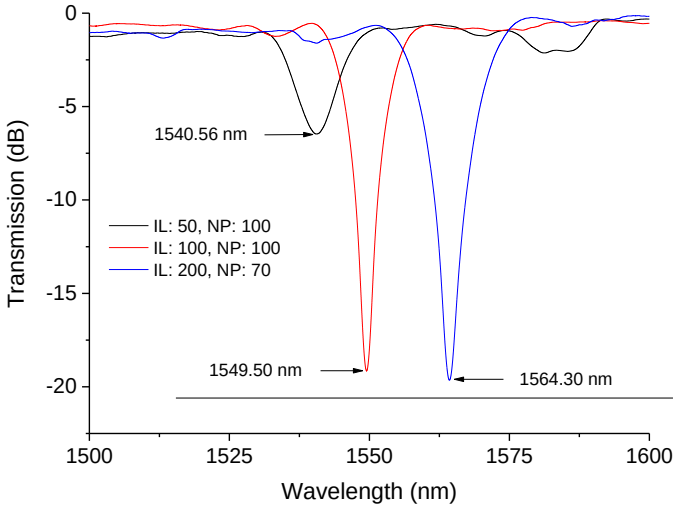

Figure 5.7 The effects of RI change length (in a period) on spectral location of attenuation loss. For the fixed period of 450 µm, longer index change length (IL) provides more attenuation loss for less number of periods (NP)

5.4 RI and temperature characterization

The refractive index dependence of the loss peak wavelength in transmission spectrum for the HLPG written in pure silica core single mode fiber is shown in Fig. 5.8. The fiber optic sensor was first firmly fixed horizontally on an aluminum fixture to subside any effect of strain on the grating. All the measurements were taken at room temperature. To measure the shift of transmission spectrum with refractive indices, the LPG was immersed in different concentration of glycerin solutions ranging from 0% to 80%. As

the ambient refractive index increases, the HLPG shows blue spectral shift which is typical for long period gratings.

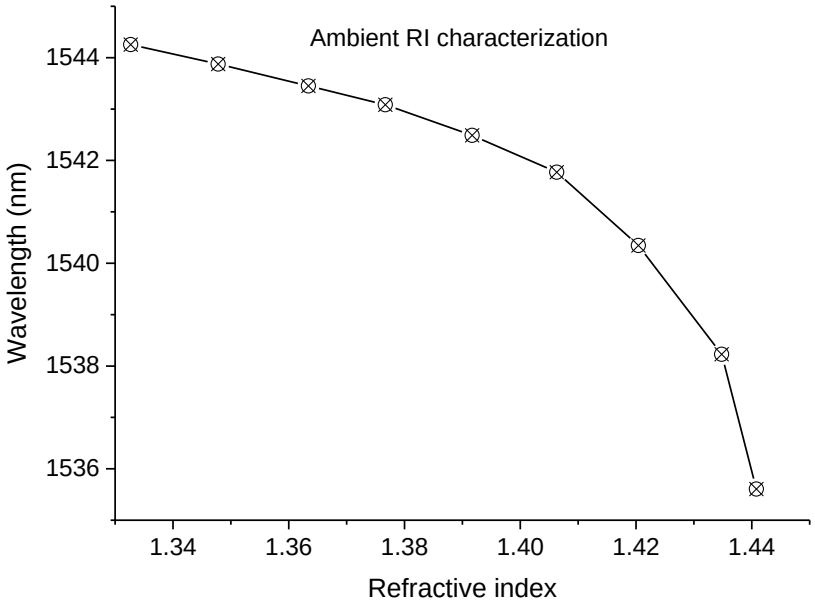

Figure 5.8 Ambient refractive index characterization of HLPG using different concentration of glycerin solutions

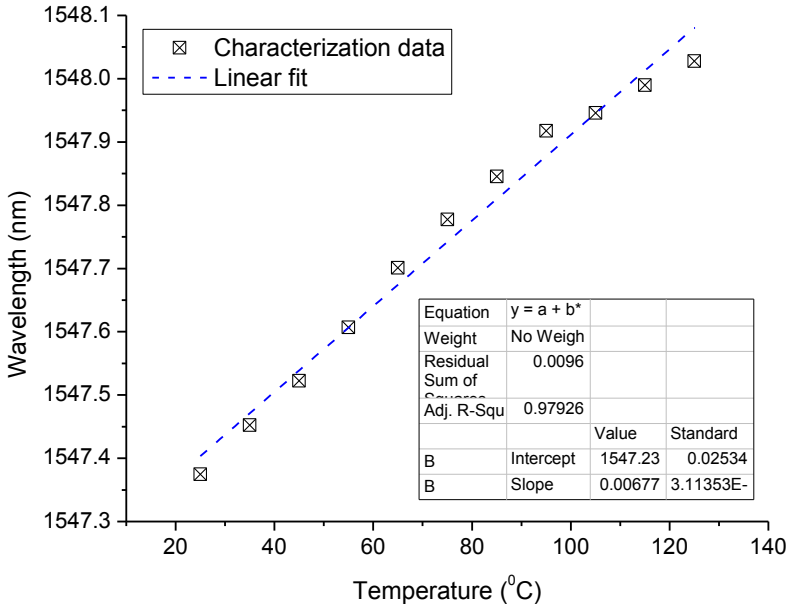

Figure 5.9 Temperature calibration of HLPG for temperature range between 25 ^{0}C to 125 ^{0}C. The HLPG shows a temperature sensitivity of ~6.8 pm/ ^{0}C

Fig. 5.9 shows the temperature characteristic behavior of the in-fiber HLPG sensor. Linear temperature dependency of the HLPG's attenuation valley is observed for difference temperature range. For the temperature range: 25 to 125 ^{0}C, the sensor shows a sensitivity of 6.8 pm/ ^{0}C.

5.5 Conclusion

As demonstrated in this chapter, employing in-fiber rotational index modification technique, long period gratings can be fabricated using ultra-short pulses more reliably and effectively. In contrast to conventional transverse scanning technique, LPGs inscribed in the helical index modification reduce polarization dependent loss when used in optical communications. The ambient refractive and temperature response of the HLPG seems to follow typical behaviour of long period gratings.

Chapter 6 – Fiber optic Mach-Zehnder interferometers for improved refractive index sensing

The interference of light in optical fibers has been used in precision measurement systems and sensors. Optical fibers can be configured to allow splitting and recombination of light, and to control their optical paths. Creating optical path difference between two modes in an optical fiber that eventually undergo recombination, it is possible to construct sensor devices in optical fibers that are extremely compact and economic. The fiber optic Mach-Zehnder interferometers (MZI) are simple yet effective tools for measurement of ambient refractive index. MZIs are very simple to fabricate compare to fiber grating but in general they show high sensitivity to ambient refractive index changes. This chapter demonstrates microfiber and tapered photonic crystal fiber based MZI sensors for ambient refractive index measurement.

6.1 Introduction

The distinctive properties such as miniature, light weight, immunity to electromagnetic wave, and ability for high resolution detection of fiber optic interferometric sensors have made them superior candidates over conventional sensors for environmental monitoring applications. In-fiber Mach-Zehnder interferometers, in particular, offer high sensitivity not only to temperature, strain and pressure, but also to ambient refractive index changes. A typical MZI has a reference and a sensing arm. A fiber coupler is used to split the incident light into two arms which are then recombined by a second coupler. The two lights recombine at the second coupler and produces interference fringe depending on the

optical path difference (OPD) between the two arms. For MZI based ambient RI sensing, the reference arm is kept isolated while the sensing arm is exposed to solutions of variable RI. The signal deviation in the sensing arm induced by ambient RI changes the OPD of the MZI that can be sensed by examining the variation in the interference pattern.

The long period gratings are the widely used RI sensors where the shift in transmission spectrum generated by intermodal coupling between forward-propagating core modes and cladding modes is used for sensing applications [23, 45, 65, 121]. To further enhance RI sensitivity, MZI has been constructed using a pair of LPGs [59]. However, the LPGs are often expensive and working only in a limited band(s) of wavelengths due to phase matching phenomenon of fiber gratings [122]. In addition, both LPGs in two arms are required to be identical for maximum performance. Considerable research work has been conducted to achieve alternative MZI configurations including core mismatch, use of multimode fiber segments or small core SMF in standard SMF, air-hole collapsing of PCF and fiber tapering [8]. Sensors based on PCL are attracting considerable attention because photonic crystal fibers show unique optical properties due to their periodic microstructure along fiber length [123]. The modal and light guidance properties of PCFs are appealing for ambient refractive index sensing. Fiber optic MZI sensors in diverse structural configurations have been used in many sensing applications. MZI sensors in SMF-PCF-SMF configuration have been demonstrated for RI sensor [61, 124, 125]. Li et al. have proposed MZI sensor with tapered PCF for high RI sensing, however, the sensor has a length of 2.4 cm [126]. In many applications, sensor with smaller dimension and localized sensing are required. To keep the sensor length considerably small, acid etching of the PCF also has been reported [61, 127]. Chemical

etching using hydrofluoric acid is probably not the best method for many laboratory setups. So, alternative approaches are required to achieve miniature MZI that has considerable sensitivity for ambient RI sensing.

In this work, we propose microfiber based MZI interferometer, which shows good surrounding RI sensitivity. The sensor is built by splicing a stub of small diameter SMF (core diameter: 3.75 μm, cladding diameter: 40 μm) between two standard single mode fibers. Small fiber diameter allows the cladding modes to extend much closer to the surrounding solution; hence, the sensor shows high sensitivity to any change of RI in the surrounding environment. We also present a simpler and cost effective method for the construction of a taper PCF based in-fiber core-cladding inter-modal interferometer that shows high ambient RI sensitivity. The sensor is built by splicing a stub of PCF between two standard single mode fibers. The PCF is then tapered using a custom made tapering machine. The core mode is confined in the core while the propagation characteristic of the cladding modes depends on the RI difference at cladding-ambient interface. Smaller diameter of the PCF allows the cladding modes to extend much closer to the ambient solution; hence, the sensor shows high sensitivity to any change of RI in the ambient environment.

6.2 Microfiber Mach-Zehnder interferometer

6.2.1 Device fabrication

Figure 6.1 shows the schematic of the sensor configuration and the fusion splicing of standard SMF with reduced diameter SMF. As pointed out in Fig. 6.1 (a), the incident light when interacts with the first interface (SMF and small diameter SMF), it spreads into both core and cladding of small diameter SMF and then recombine at the second

interface (small diameter SMF and SMF). The core mode is confined in the core while the propagation characteristic of the cladding modes depends on the RI difference at cladding-surrounding interface. Figure 6.1 (b) shows the splicing of standard SMF with microfiber. The Fujikura (FSM 40PM) fusion splicer was used to splice standard SMF to microfiber with an arc power of 10 bit exposed for 1000 millisecond.

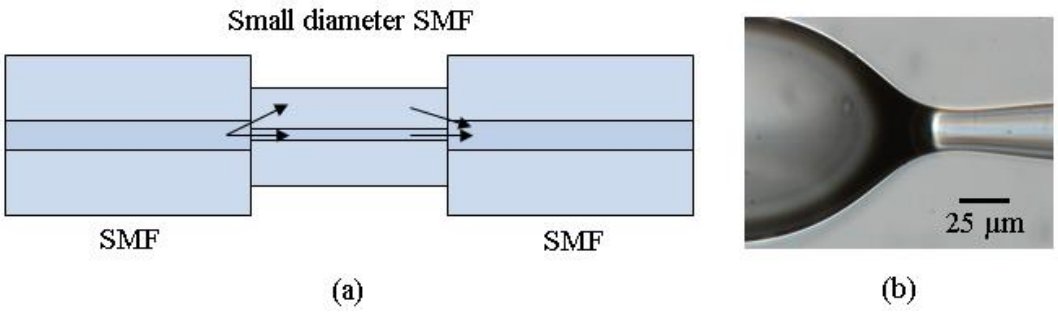

Figure 6.1 Schematic of the proposed fiber optic MZI interferometer (a), and the microscope image showing fusion splicing of a regular SMF with a reduced diameter SMF (b)

6.2.2 Output spectral response

The spectral response of the interferometry sensor was recorded using an ASE broadband light source and an optical spectrum analyzer (Photonetics 3650 HR 15). Figure 6.2 shows the transmission spectrum over 200 nm spectral window, the transmission dips appear at periodic spectral locations. The total length of the MZI was 5.25 mm. Modal spacing of the MZI's transmission spectrum varies with device length. The fringe spacing as a function of the length of the microfiber single mode fiber is also given in Fig. 6.3. Mode spacing exponentially decreases as the length of small diameter SMF gradually increases. FWHM of the individual dip of microfiber MZI goes down as the sensor length gradually increases.

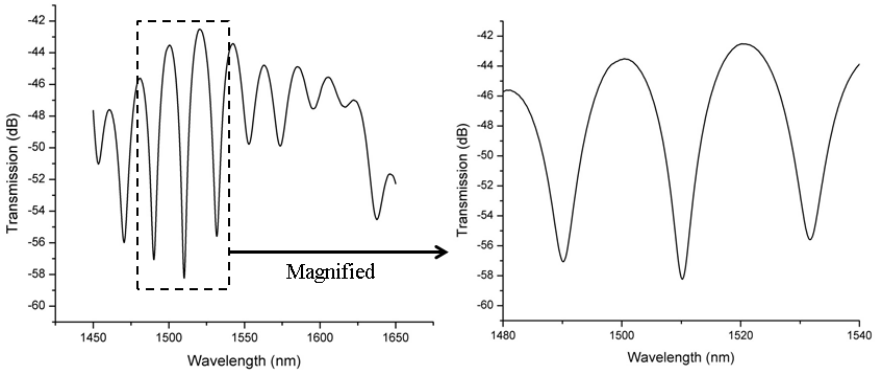

Figure 6.2 Transmission spectrum of the in-fiber MZI interferometer sensor (left), and the magnified image showing three major transmission valley (right)

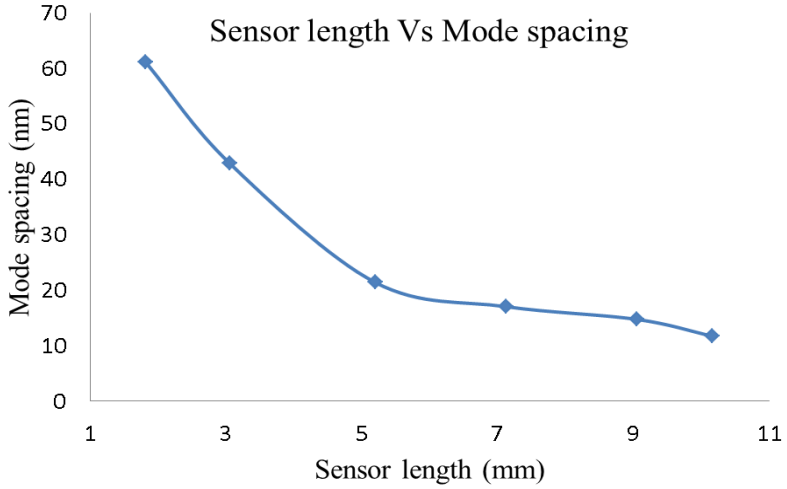

Figure 6.3 Small diameter fiber length dependent modal separation of the output spectrum of the MZI sensor

6.2.3 Sensing results and discussion

The shift of interference fringe as a function of the ambient refractive index change was observed for device length of 6 mm. The sensor was characterized with difference concentration of glycerin solutions at room temperature. To achieve characterization data, the device was immersed in different glycerin solutions of gradually varying

concentration. After each test, the sensor was thoroughly cleaned before immersing it in subsequent higher concentration glycerin solution. Figure 6.4 shows the wavelength shifts due to the change of surrounding refractive index between the values of 1.3327 to 1.4408. As the surrounding RI increases, the dip wavelength of the transmission wave experiences a blue-shift. The sensor demonstrates average sensitivity of -38.91 nm/RIU for ambient refractive index value between 1.3327 ~ 1.4063 and -98.85 nm/RIU for refractive index value between 1.4133 ~ 1.4408.

To examine the temperature sensitivity, the MZI sensor was immersed in a temperature controlled water bath. The sensor was tested by increasing temperature of the water bath between 25^0C to 95^0C with a step of 10^0C. Prior to taking wavelength shift readings, a waiting time of 10 min was allocated for the system to stabilize at set temperature. The temperature response is shown in Fig. 6.5. The temperature sensitivity of the MZI sensor is 51.65 pm/^{0}C.

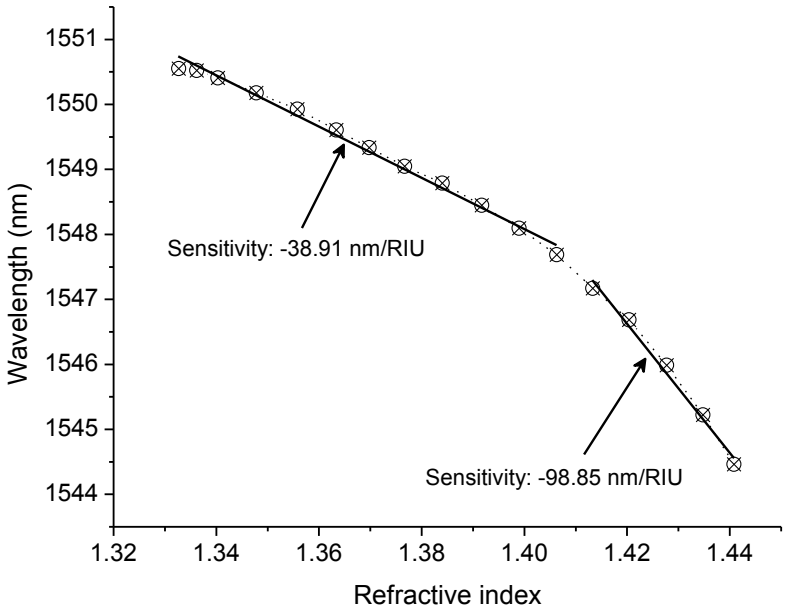

Figure 6.4 Refractive index characterization of microfiber MZI sensor

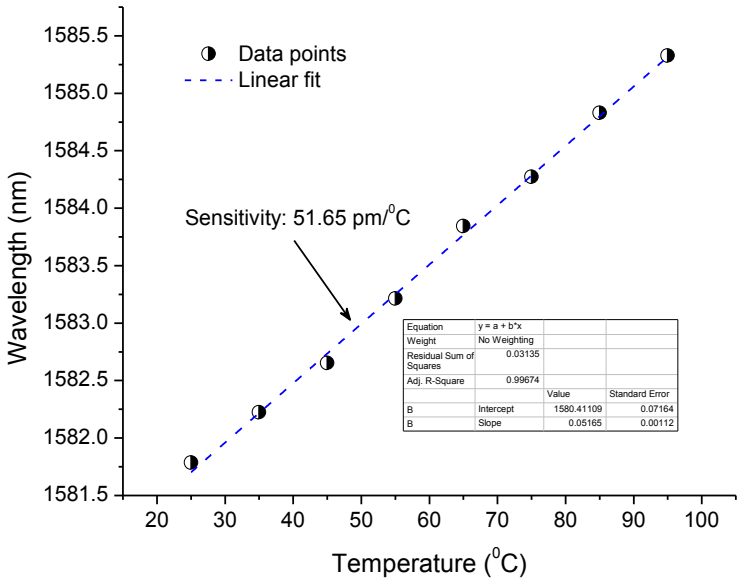

Figure 6.5 Temperature characterization of microfiber MZI sensor

6.2.4 Conclusion

We have fabricated and tested a simple and cost effective fiber optic MZI based RI sensor by fusion splicing a small diameter SMF between standard SMFs. Refractive index sensitivity of the sensor is -38.91 nm/RIU and -98.85 nm/RIU for ambient refractive index value between 1.3327 ~ 1.4063 and 1.4133 ~ 1.4408, respectively. The microfiber MZI shows higher ambient RI sensitivity than commercially available LPGS. The temperature sensitivity of the sensor is 51.65 pm/^{0}C for operating temperature range of 25^{0}C to 95^{0}C.

6.3 Tapered photonic crystal fiber Mach-Zehnder interferometer

6.3.1 Device schematic

Figure 6.6 illustrates the two step process of the sensor fabrication. As shown in Fig. 6.6 (a), the basic MZI interferometer is constructed by splicing a small stub of PCF between standard SMFs. In the second step, the PCF is tapered while the SMFs on both sides remain unchanged. During splicing, a small segment of PCF collapse that diffracts the fundamental core mode. As pointed out in Fig. 6.6 (b), the incident light when interacts with the first interface (SMF and PCF), it spreads into both core and cladding of PCF and then recombine at the second interface (PCF and SMF).

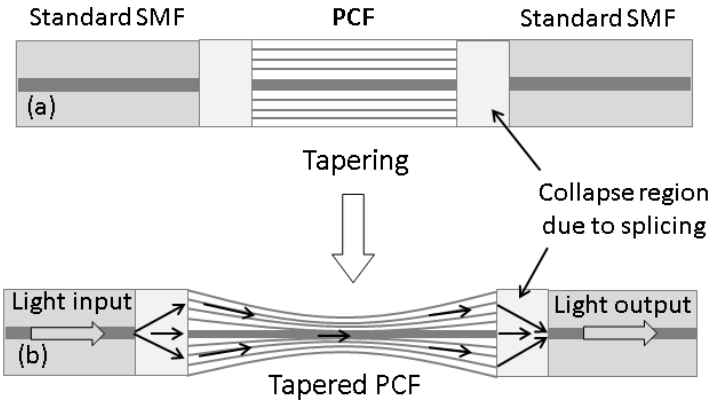

Figure 6.6 Schematic of the PCF interferometer (a), and tapering of the PCF to enhance ambient refractive index sensitivity (b)

6.3.2 Sensor fabrication and spectral response

A small piece of single mode PCF is spliced between a lead-in and a lead-out SMF-28 fiber. Both the standard SMF and PCF are stripped off from polymer coating before fusion splicing. In such case, the surrounding air acts as a low index cladding and confines the higher order modes within the PCF. The Fujikura (FSM 40PM) fusion splicer was used to splice standard SMF to PCF with an arc power of 10 bit exposed for

1500 millisecond. Fig. 6.7 (a) shows the splicing of SMF with PCF where a small segment of the PCF collapses due to the applied arc heat. At the first splicing, the input light splits into core and cladding modes while the modes recombine at the second splicing to construct the MZI structure. The PCF is tapered down to ~ 60 µm using a custom made equipment to enhance RI sensitivity.

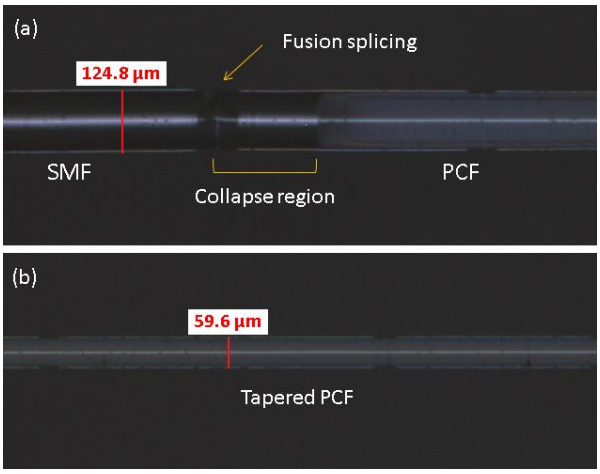

Figure 6.7 Fusion splicing of PCF with standard SMF (a) where the hollow structures of the PCF collapse that splits the incoming light from the SMF. The PCF is then tapered down to ~ 60 µm (b)

The holey structure of the PCF has much lower softening point than that of SMFs, and thus at each splicing point the air holes of the PCF entirely collapse over a short length. In a typical splicing machine, the intensity and arc exposure duration of the fusion process can be tuned. This allows controlling the collapse length in the PCF at the splicing point. As shown in Fig. 6.7 (b) the collapse length in our experiment was found to be 156 µm for arc power of 10 bit and exposure time of 1500 ms. Let's consider the evolution of propagating beam shown in Fig. 6.6 (b) as it travels from the lead-in SMF, through the PCF and finally to the lead-out SMF. When the fundamental SMF mode reaches the collapsed region of PCF it starts to diffract, and thus the mode broadens. For

a beam centered at wavelength λ, the initial spot size w_0 (at the first SMF-PCF interface) broadens to a new size of w when it propagates a length l_1 of the collapse region and is given by [61]:

$$w = w_0 \sqrt{1 + \left(\frac{\lambda l_1}{\pi n_f w_0^2}\right)^2} \tag{6.1}$$

where, n_f is the refractive index of the collapse region of PCF. When the center wavelength λ = 1.577 μm, collapse length of PCF l_1 = 156 μm, index of collapse region n_f = 1.444 and initial spot size w_0 = 5 μm, the new spot size at the end of collapse region of PCF will be w = ~12 μm. Therefore, at the end of collapse region, the PCF will be excited with a Gaussian beam of diameter 2w = 24 μm which is much larger than its core size. The combine effect of mode field mismatch and the modal characteristics of the PCF [128] excite certain core and cladding modes in the PCF that have difference propagation constants [129]. Both modes propagate along the PCF and enter the second collapse region of the PCF. The collapse region causes further diffraction and finally the core and cladding modes recombine due to the filtering of the subsequent SMF. The core and cladding mode interfere and provide transmission spectrum given by [130]:

$$I = I_{co} + I_{cl} + 2\sqrt{I_{co} I_{cl}} \cos(\delta + \varphi_0) \tag{6.2}$$

$$\delta = (2\pi/\lambda) \int_L^{(n_{cl} - n_{co})} dz \tag{6.3}$$

where I is the intensity of the interference signal, I_{co} and I_{cl} are the intensities of the core and cladding modes, δ is the phase difference of the two modes, n_{co} and n_{cl} are the effective indices of the core and cladding modes. L and λ are the length of the PCF and wavelength, respectively. Typically the MZI sensors are very sensitive to fiber bending, so the sensor was firmly fixed on a fiber holder. Then the fiber was coupled with a broad

band light source (AFC BBS-1550), and a spectrum analyzer (PHOTONETICS Walics) to analyze the optical characteristics of the tapered PCF MZI. Figure 6.8 shows the transmission spectra that have a single notch for the given spectral window (1550~1600 nm) with an attenuation dip centered at ~1577 nm. The waist diameter of the PCF was ~60 μm. The intensity of the cladding mode decreases with decrease in waist diameter because the transition region of the taper PCF is nonadiabatic [126].

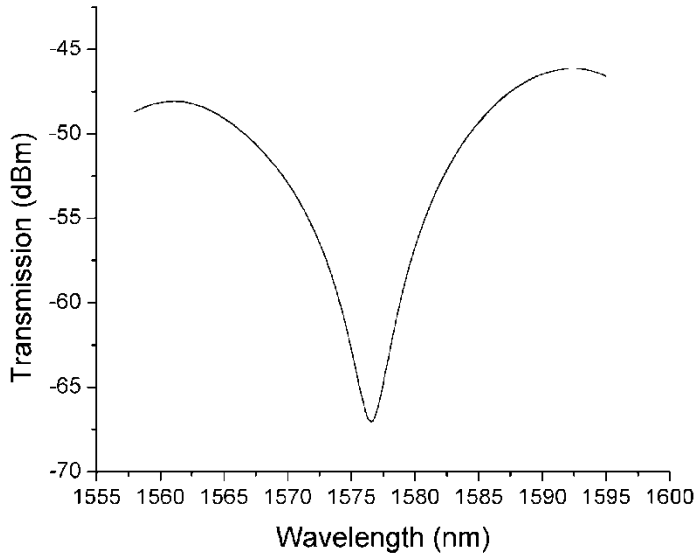

Figure 6.8 Transmission spectrum of the in-fiber MZI in SMF-Tapered PCF-SMF configuration. The length of the sensor is ~6 mm

6.3.3 Refractive index sensing

The sensor was characterized with difference concentration of glycerin solutions at room temperature. To achieve characterization data, the device was immersed in glycerin solution whose concentration was gradually increased. After each test, the sensor was thoroughly cleaned before immersing it in subsequent higher concentration glycerin solution. Figure 6.9 shows the wavelength shifts due to the change of surrounding

refractive index between the values of 1.3327 to 1.4063. As the surrounding RI increases, the dip wavelength of the transmission wave experiences a red-shift.

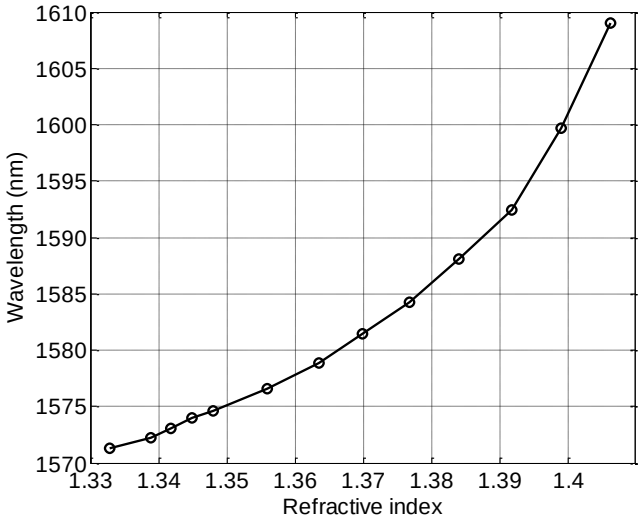

Figure 6.9 The overall refractive index sensitivity plot of the in-fiber MZI interferometer in SMF-taper PCF-SMF configuration

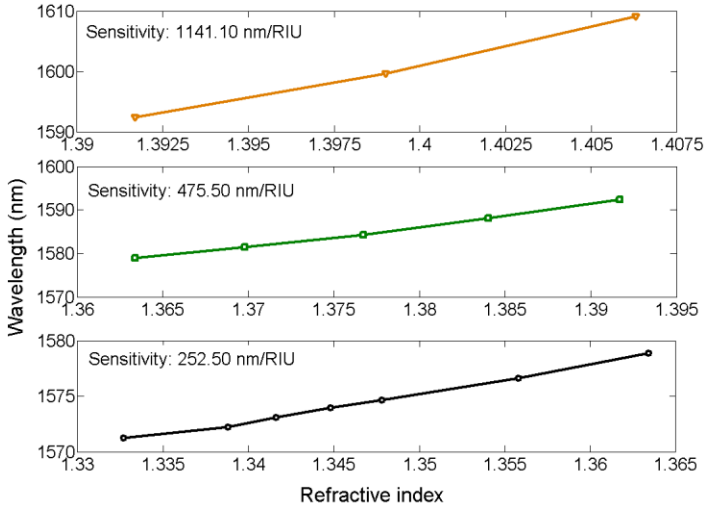

Figure 6.10 Elaborated refractive index sensitivity analysis of the MZI sensor for different index ranges of the solutions. The interferometer shows highest sensitivity of 1141 nm/RIU for RI range of 1.39 17 to 1.4063

The performance of the taper PCF MZI is evaluated by its sensitivity which is defined as the amount of resonance wavelength shift divided by the change in refractive index of the solution that causes the spectral shift. To analyze RI sensitivity, the entire plot of Fig. 6.9 is divided into subplots for the solution index range of 1.332 to 1.363, 1.364 to 1.392 and 1.393 to 1.406 as shown in Fig. 6.10. The sensor shows RI sensitivity of 252.50 nm/RIU for RI range of 1.332 to 1.363, 475.50 nm/RIU for RI range of 1.364 to 1.392 and 1141.10 nm/RIU for RI range of 1.393 to 1.406, respectively.

6.3.4 Conclusion

We propose highly sensitive miniature RI sensor based on tapered PCF MZI. The MZI is constructed by fusion splicing a PCF between two standard single mode fibers. When the PCF is tapered down to ~ 60 μm, a maximum RI sensitivity of ~ 1141 nm/RIU can be achieved. Small fiber diameter of the PCF allows the cladding modes to extend much closer to the surrounding solution; hence, the sensor shows high sensitivity to any change of RI in the surrounding environment. Similar PCF MZI sensor shows temperature sensitivity of ~8 pm/ ^{0}C [126], which is negligible compare to its RI sensitivity. Low temperature sensitivity makes it an effective RI sensor. The sensor shows RI sensitivity of 252.50 nm/RIU for RI range of 1.332 to 1.363, 475.50 nm/RIU for RI range of 1.364 to 1.392, and 1141.10 nm/RIU for RI range of 1.393 to 1.406.

Chapter 7- Microfiber FBG and MZI for temperature and refractive index sensing

Various unique properties of microfibers including their extended evanescent fields, compactness, flexibility, and configurability offer new opportunities and solutions to various telecommunication and sensing applications [131, 132]. This chapter reports the direct ultrafast laser inscription of miniature FBG in microfiber and the integration of FBG and MZI in microfiber for applications in ambient temperature and refractive index measurements. Enhancing temperature sensitivity of microfiber FBG and simultaneous measurement of refractive index and temperature are also proposed in this chapter.

7.1 Fabrication of FBG in microfiber

7.1.1 Introduction

Fiber Bragg grating (FBG) is a band stop filter that works on the principle of Bragg reflection phenomenon. The property to reflect particular wavelengths of light while transmit all others is achieved by forming a periodic index modulation in the core of an optical fiber [133]. An extensive amount of research has been conducted on FBG devices to uncover their applications in telecommunication and sensing [134-136]. In particular, FBG sensors have been demonstrated as effective and reliable tools for individual or simultaneous measurement of temperature and strain [137-140]. Grating embedded in standard single mode fibers (core diameter: 8μm, cladding diameter: 125 μm) sensors have shown great promise in diverse sensing platform because of their accurate measurement, real time response, and capabilities of multi-parameter measurements. However, recently there has been a lot of research focus on microfibers [131, 141],

because the photonics devices fabricated in microfibers have many unique and interesting properties. The flexibility and configurability of microfibers are expected to provide easy manipulation of the microfiber based devices such as FBGs and in-fiber interferometers.

Currently, there are two major technologies available for fabrication of FBGs in single mode fiber: ultraviolet (UV) laser radiation with phase mask method [2, 9] and ultrafast laser radiation method [142, 143]. Fabrication of FBG in microfiber using UV laser and phase mask has been demonstrated for diverse sensing applications [144]. The inscription of fiber grating by UV laser radiation method requires pre and post fabrication steps. To enhance photosensitivity of the core, the fibers are first treated with hot hydrogen [38] before writing periodic index modulation. To get rid of excess hydrogen from the fiber and provide better grating stability, a post fabrication annealing at high temperature for a short period of time is required [64]. Besides, sensing performance of UV FBGs may degrade over time due to hydrogen darkening in harsh environmental condition, a phenomenon that occurs when hydrogen gas diffuses into the photosensitive fiber and darkens the core or even erases the index modulation [113, 114]. In general, the phase mask techniques are expensive and they require different phase masks of variable period to achieve flexibility in Bragg resonance Bragg wavelengths. In contrast, femtosecond laser based fabrication offers arbitrary resonance wavelength of FBGs simply by varying scanning speed in point-by-point method and scanning period in line-by-line method. Fabrication of FBG in microfiber using phase mask and femtosecond laser for refractive index sensing has been demonstrated in a recent research work [3]. The reported study illustrates FBG fabrication in SMFs of diameter between 2-10 μm and their resonance spectrum shows higher order modes suitable for refractive index sensing.

Higher background noise in the spectrum and weaker Bragg resonance reflection are most likely be an outcome of excess/ inefficient energy deposition by ultrafast laser pulses.

This work proposes writing of FBGs in microfiber (core diameter: 3.75 μm, cladding diameter: 40 μm) by femtosecond laser based point-by-point direct inscription method. Ultrashort pulse filamentation technique is employed to better control deposition of femtosecond pulse energy and achieve clean index modulation in the core of microfiber. The experimental results show strong Bragg reflection even for a grating length as small as 1 mm. To write a 1 mm long grating in the proposed method takes less than 2 second. The fabricated FBGs are also characterized for temperature and strain sensing to evaluate their sensing performance.

7.1.2 System specification and setup

A femtosecond laser was used to write pulse filamentation induced RI change in the fiber core. The kilohertz ultrafast laser has a pulse width of 120 femtosecond with the center wavelength of 800 nm. A motorized attenuator was used to tune laser output power suitable for FBG fabrication. The laser beam was selectively turned on/off by an electronic shutter to control power delivery in the experiment. An iris diaphragm was used to reduce beam diameter to 1.75 mm. Then the laser beam was guided into a microscope and tightly focused by objective lens (Numerical aperture: o.75) into the fiber core. Focusing was done with an achromatic lens under incident angle of zero degree onto the sample. The fiber jacket was removed and cleaned before writing gratings in bare fiber. The optical fibers were mounted on a computer controlled 4-axis stage to periodically write index inside the core. Fiber alignment was done using the rotary stage

and live image feedback from the CCD camera attached to the system. The fiber was coupled with a broad band light source (AFC BBS-1550), a spectrum analyzer (PHOTONETICS Walics), and a circulator to monitor the growth of Bragg resonance reflection spectrum during fabrication. As shown in Fig. 7.1, the index modulation in the fiber was created by point-by-point inscription method. The scanning speed was chosen for the kilohertz pulse laser so that the filamentary voids partially overlap to create the desired index modulation in the core of the microfiber.

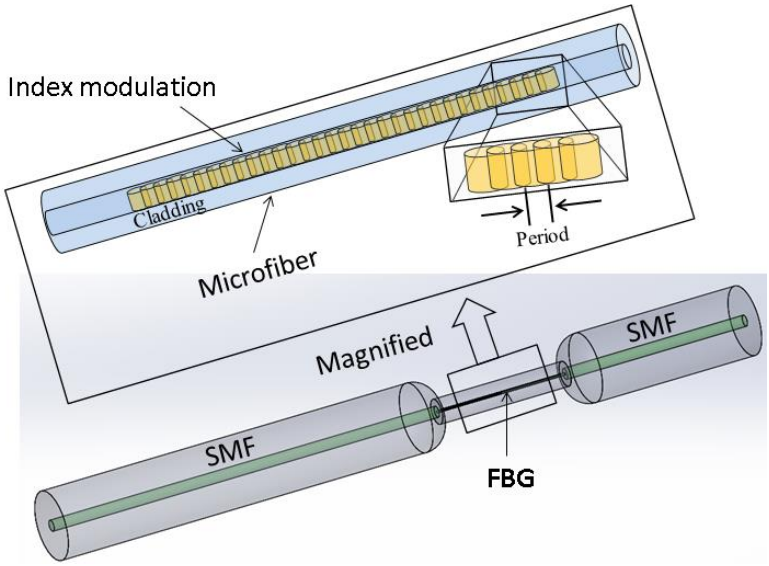

Figure 7.1 Schematic of the index modulation written in the core of microfiber by femtosecond pulse filamentation induced periodic void structures

7.1.3 Grating fabrication

As shown in Fig. 7.2, the microfiber (core diameter: 3.75 μm, cladding diameter: 40 μm) was spliced between two standard SMFs prior to grating fabrication. Splicing with SMF facilitates fixturing of the microfiber prior to FBG fabrication, and temperature and strain characterization of the grating sensor. A Fujikura (FSM-40PM) splicer set at arc power

of 10 bit, and arc exposure time of 1000 millisecond, was used to splice the microfiber with standard pure silica core SMFs.

Figure 7.2 Splicing of the microfiber between two standard SMFs prior to grating fabrication in order for improve handling of the fiber during modulated index inscription

Typical periods of FBGs written in SMF that have resonance spectrum about 1550 nm are usually around 500- 550 nm. In addition, due to the miniature core size of the microfiber (3.75 µm), it is necessary to write spatially confined periodic index modulation in the fiber core. Femtosecond pulse filamentation was employed to write submicron periodic voids in the core. . Ultra-short pulse filamentation is basically a serious of hot plasma spots appear along its propagation axis produced due to focusing and defocusing of pulse until the peak power remains higher than the critical power necessary for filamentation [76]. An objective lens with high numerical aperture of 0.75 was used to strongly focus the ultrafast pulses into a very small focal volume and elevate pulse peak power. Elevated pulse intensity confined in a tiny spot forms a filamentation induced void at focal point in transparent medium. When the microfiber was axially scanned with the kilohertz pulse train at the speed of 534 nm/ sec, the filamentary voids

were overlapped as shown in Fig. 7.1 to create an index modulation period of 534 nm. As shown in Fig. 7.3, when 1 mm length of the fiber core was scanned with the focused femtosecond pulses (pulse energy: 42.5 μJ) with the period of 534 nm, it inscribed a FBG in the microfiber that has a resonance Bragg reflection spectrum centered at 1550.22 nm.

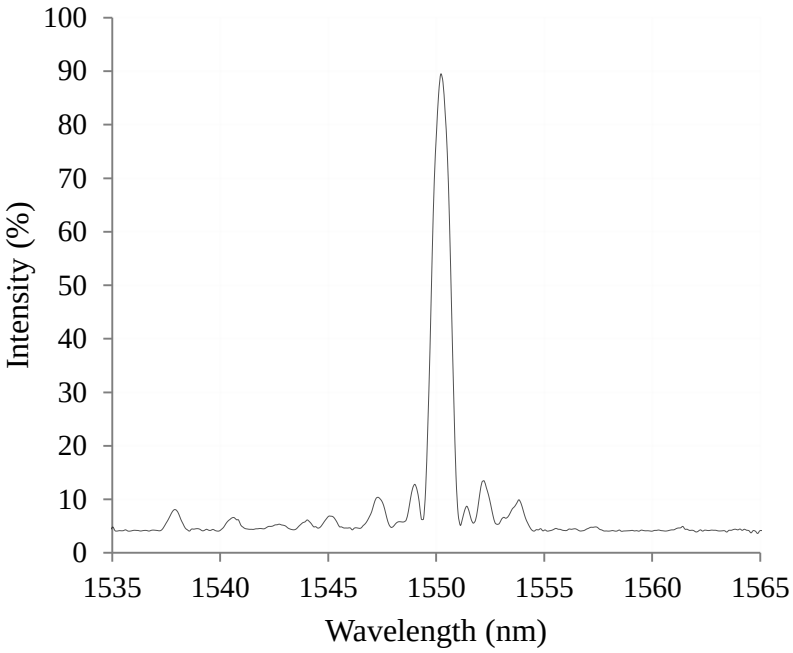

Figure 7.3 The Bragg resonance reflection spectrum centered at 1550.22 nm for the grating written in microfiber with a period of 534 nm

7.1.4 Sensing temperature and strain using FBG

Fiber Bragg gratings are suitable sensing elements to directly measure temperature and strain. The resonance condition of the Bragg wavelength is given by [145]:

$$\lambda_B = 2n\Lambda \tag{7.1}$$

where, n is the effective index of the core and Λ is the Bragg grating period. For a given FBG, a change in its refractive index profile and grating pitch shifts the Bragg resonance wavelength according to Equation 7.1. These changes generally appear under the influence of strain and temperature. When a strain is applied on the fiber, the Bragg

wavelength shifts due to the elongation of the FBG and changes in its refractive index through photo-elasticity effect [16]. Similarly, a change in ambient temperature alters the Bragg wavelength due to thermal expansion of fiber material that changes both grating period and index modulation. A temperature and/or strain induced Bragg wavelength shift *($\Delta\lambda_B$)* caused by applied three dimensional strains (ε_x , ε_y , and ε_z) is given by [146]:

$$\frac{\Delta\lambda_B}{\lambda_B} = \varepsilon_z - \frac{n_0^2}{2}\left[\varepsilon_z p_{12} + \frac{1}{2}\left(p_{11} + p_{12}\right)\left(\varepsilon_x + \varepsilon_y\right)\right] \tag{7.2}$$

where p_{11} and p_{12} are dimensionless photo-elastic constants and have the values of 0.113 and 0.252 respectively. The x-y-z is a right handed Cartesian coordinate systems with z-axis pointing along the fiber axis.

7.1.5 Temperature response of microfiber FBG

The FBG based temperature sensors have great potential and are promising alternatives to classical temperature measurement techniques. Temperature sensing using microfiber FBG with no further modification is demonstrated in this study. The Bragg wavelength of the FBG sensor experiences linear red shift with ambient temperature. Figure 7.4 depicts the experimental setup used to measure temperature induced red shift in the resonance wavelength of the FBG sensor. The broadband light was launched into the port 1 of the circulator and the reflection spectrum from port 2 is recorded using the optical spectrum analyzer (OSA) connected at port 3. The water temperature of the water bath was gradually increased from 22.5 ^{0}C to 95 ^{0}C with a step of 2.5 ^{0}C. The temperature dependent change of the Bragg resonance wavelength as a function of increasing temperature is shown in Fig. 7.5. A temperature change of 72.5 ^{0}C caused the Bragg wavelength to red shift 0.72 nm. The data points measured at each temperature interval of

2.5 ^{0}C are fitted with a liner line to measure the sensitivity of the device. The temperature sensitivity of the unmodified FBG sensor written in microfiber was measured to be 0.01 nm/ ^{0}C.

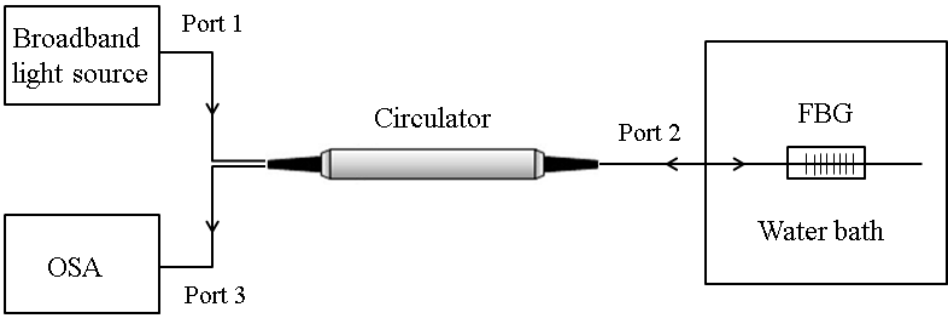

Figure 7.4 Schematic diagram of the temperature measurement system. The experiment was conducted in constant ambient refractive index and atmospheric pressure

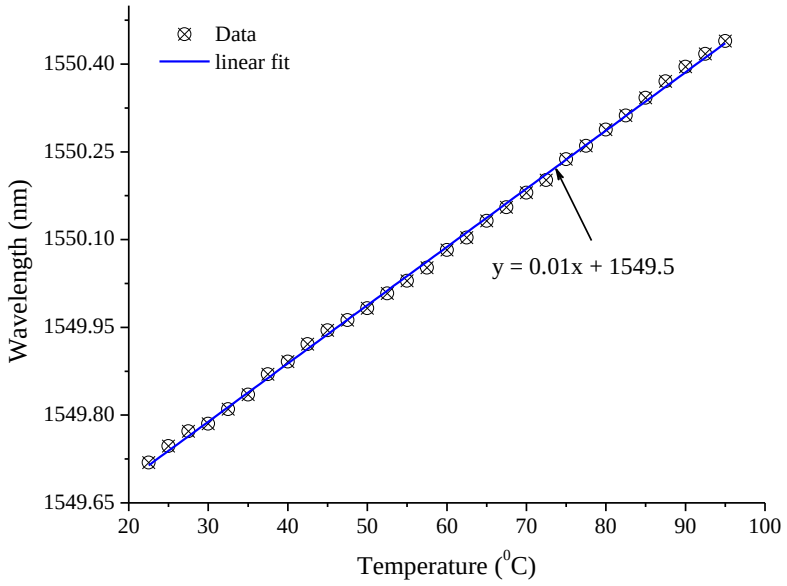

Figure 7.5 Temperature calibration of the FBG written in microfiber. The temperature dependent spectral red shift of the sensor is measured to be 0.01 nm/ ^{0}C

7.1.6 Strain response of microfiber FBG

Typically, standard FBGs show linear axial strain sensitivity. The schematic of applying axial strain on the microfiber FBG sensor is shown in Fig. 7.6. Acquisition and recording of characterization data was done using the similar setup shown in Fig. 7.4, except the FBG in port 2 was subjected to axial strain as depicted in Fig. 7.6. The microfiber length of 1.5 mm spliced between two regular SMF accommodates the Bragg grating. One end of microfiber (spliced to the standard SMF) is secured on the stationary fixture while the other end is fixed on the micrometer driven linear stage as shown in Fig. 7.6. The axial strain was applied on the grating using the micrometer attached to the right hand side fixture. The amount of strain applied on the FBG is easily calculated using its original length (1.5 mm) of the microfiber and increased length calculated from the micrometer reading. When a uniform axial strain is applied on the FBG, the Bragg resonance wavelength red shifts proportionally. The strain characterization plot shown in Fig. 7.7 exhibits linear dependency to the applied strain. The microfiber FBG strain sensor has a sensitivity of ~ 1 pm/micro-strain.

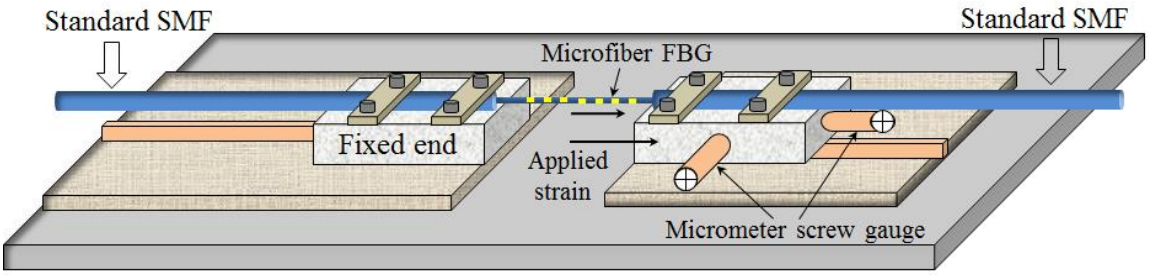

Figure 7.6 Experimental setup schematic for applying axial strain on the microfiber FBG. The experiment was conducted in constant ambient refractive index, room temperature, and atmospheric pressure

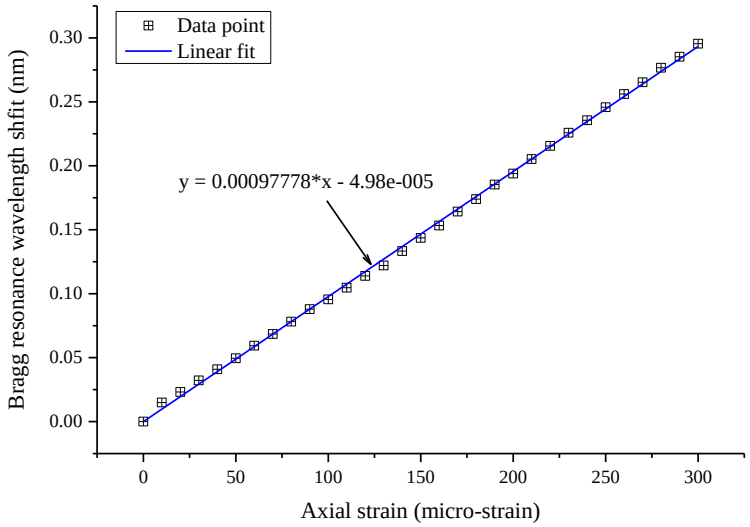

Figure 7.7 Characterization of the microfiber FBG for strain measurement. The slope of the solid regression line shows the strain sensitivity of ~1 pm/micro-strain

7.1.7 Conclusion

This study demonstrates direct fabrication of fiber Bragg gratings in microfiber (core diameter: 3.75 μm, cladding diameter: 40 μm) by ultra-fast laser radiation. Femtosecond pulse filamentation is employed in point-by-point inscription of refractive index modulation in microfiber to write FBG. For the scanning speed of 534 nm/ sec, the kilohertz femtosecond pulse stain creates partially overlapping void structures with the period of 534 nm. The in-fiber index modulation of period 534 nm produces the Bragg resonance spectrum centered at 1550.22 nm. A variation in resonance reflection spectrum can easily be obtained simply by changing the scanning speed of the translation stage. The temperature and strain sensitivity of the microfiber FBG are 10 pm/ ^{0}C and 1 pm/micro-strain, respectively.

7.2 Microfiber FBG based enhanced temperature sensor

7.2.1 Introduction

Fiber Bragg grating based devices has been widely studied for optically sensing diverse physical parameters such as temperature, strain, refractive index, and pressure [9, 20, 138, 139, 147]. FBGs inscribed in standard single mode fiber (SMF) have great potential in diverse temperature sensing applications and these fiber optic sensors are functional over a wide range of temperature [148]. However, the small thermo-optic coefficient and thermal expansion coefficient (TEC) of silica based optical fibers limit the temperature sensitivity of FBGs to about ~10 pm/ ^{0}C [149, 150] for a Bragg wavelength of 1550 nm. Temperature sensitivity goes down for shorter wavelengths because it is proportional to Bragg wavelength. Limited resolution of a sensor may affect accurate temperature measurement or require a costly detecting device.

Extensive studies have been carried out to enhance FBG's temperature sensitivity. Specialty optical fibers doped with heavy metal such as PbO-GeO_2 have higher TECs and hence the FBGs inscribed in such fibers show greater temperature sensitivity without any further modification [151]. However, limited TECs of the reported fibers only able to improve temperature sensitivity few times compared to FBGs written in regular SMFs. Different packaging techniques have been proposed to modify FBG sensors in order to enhance their temperature sensitivity. Higher temperature sensitivity has been demonstrated by coating the FBG written in standard SMF with metals and metal compounds of high thermal expansion coefficients [152-155]. Feasibility of using of polymer coating to enhance temperature sensitivity of fiber grating device has also been shown promising because applying a polymer cladding layer around the fiber can be done

simply by a general coating process [156-158]. Coating or molding of the fiber with materials of higher TECs has been shown very promising to significantly enhance sensitivity of fiber Bragg grating temperature sensors. The temperature monitoring systems where the sensor undergoes lots of heating and cooling cycles, the adhesive strength between the coating material and the fiber may degrade due to the large disparity in thermal expansion coefficients between them. If the coating material fails to apply consistent thermal strain on the fiber, the sensor can no longer operate reliably.

Recently, there has been a considerable research focus on microfibers and the gratings written in reduced diameter fibers have inherent properties to enable high resolution measurements. Use of UV laser and phase mask has been reported as the most common method to inscribe in photosensitive microfibers [159, 160]. However, the gratings inscribed by UV laser are not always suitable for temperature sensing particularly in chemically harsh environments because of hydrogen darkening effects [113, 114]. Stable index modulation of FBGs written in microfibers by infrared radiation and phase mask [3, 161] has better stability and thus suitable for temperature monitoring. However, the use of phase mask in the reported studies increases fabrication complexity and cost. Direct writing of FBGs in microfiber using infrared radiation has not yet been reported, to the best of our knowledge.

In this work, femtosecond pulse filamentation based direct inscription of FBG in microfiber spliced between standard SMFs and subsequent molding with materials of higher TECs are proposed to demonstrate enhanced temperature sensitivity. The structural configuration of the sensor shown in Fig. 7.8 (b) provides strong grip when molded with materials of high thermal expansion coefficients. No adhesion is required,

thus the sensor is expected to be suitable for long term applications. The sandwich microfiber FBG when molded with Sn-Ag-Cu alloy shows temperature sensitivity of 31.32 pm/ ^{0}C. Acetal molding further improves temperature sensitivity to ~ 202.33 pm/ ^{0}C for temperature range of 22.5 ^{0}C to 60 ^{0}C and ~ 479.48 pm/ ^{0}C for temperature range of 60 ^{0}C to 95 ^{0}C. The authors believe, the bare microfiber FBG sandwiched between SMFs proposed in this work can be coated or molded with suitable materials to achieve desired sensitivity with operational reliability.

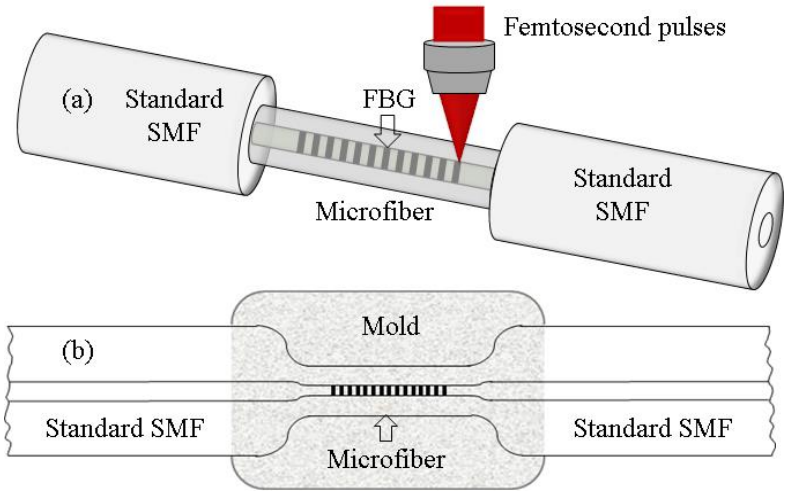

Figure 7.8 The schematic of a microfiber spliced between standard SMFs and point-by-point inscription of FBG in microfiber by femtosecond laser radiation (a), and molding of the microfiber grating with a material of higher thermal expansion coefficient (b)

7.2.2 Experimental procedure

The experimental schematic is depicted in Fig. 7.8. A small stub of microfiber (core diameter: 3.75 μm, cladding diameter: 40 μm) was first fusion spliced between two standard single mode fibers as shown in Fig. 7.8(a). The Fujikura (FSM 40PM) fusion splicer was used to splice standard SMF to microfiber with the arc power of 5 bit exposed for 1000 millisecond. Detail fabrication FBG fabrication in microfiber is provided in

section 7.1.3. To achieve a Bragg resonance spectrum at around 1550 nm, an index modulation period of 500 nm to 550 nm is required. Tight spatial control of core index modulation is crucial to write such grating in microfiber (core diameter is 3.75 μm in this study). In infrared laser inscription method, even though the use phase mask facilities the writing of desired periodic index, it increases manufacturing cost. With an aim to better control spatial index modulation in direct writing, primary focus of this work was given to write submicron single-shot periodic index change. Femtosecond pulse filamentation was employed to write submicron periodic voids in the core. When the microfiber was axially scanned with the kilohertz pulse train at the speed of 534 nm/ sec, the filamentary voids were overlapped to create an index modulation period of 534 nm. As shown in Fig. 7.3, when 1 mm length of the fiber core was scanned with pulse energy of 425 μJ and the period of 534 nm, the resonance Bragg reflection appeared at 1550.22 nm. As shown in Fig. 7.8 (b), the microfiber FBGs were then molded with acetal and Sn-Ag-Cu alloy that have much higher coefficients of thermal expansion. The molded microfiber FBGs were placed in a temperature controlled oven and their responses were recorded for both climb in temperature and fall in temperature. The oven temperature was measured using a thermocouple located close to the molded FBG.

7.2.3 Enhancement of temperature sensitivity

The reflection wavelength of a fiber Bragg grating relies on its periodic index modulation and is influenced by a change in ambient conditions (temperature, strain, refractive index, etc.). The center wavelength of a fiber Bragg grating shifts as a function of the ambient temperature. Such temperature dependency of a FBG results from change in fiber refractive index and thermal strain of the fiber. The effects of temperature induced

change in core effective index and fiber strain on Bragg wavelength shift can be given by differentiating Eq. (7.1):

$$\Delta\lambda_B = 2\Delta n\Lambda + 2n\varepsilon_z\Lambda \tag{7.3}$$

where n is the initial refractive index of the core, Δn is the change in refractive index, Λ is the grating period, and $\varepsilon_z$is the axial strain of the fiber. For a change in temperature ΔT, the change in refractive index of the core is given by [162]:

$$\begin{aligned}\Delta n &= \left(\frac{\partial n}{\partial T}\right)_\rho \Delta T + \left(\frac{\partial n}{n}\right)_T n \\ &= \left(\frac{\partial n}{\partial T}\right)_\rho \Delta T - \frac{n^3}{2}[(P_{11} + P_{12})\varepsilon_r + (P_{12}\varepsilon_z)]\end{aligned} \tag{7.4}$$

where $P_{11}$and $P_{12}$are Pockels coefficients of the fiber core, and ε_z is the radial strain in the fiber. When a bare FBG is subjected to variable temperatures, the Bragg wavelength shift in Eq. (7.3) happens mainly due to temperature dependent index change Δn because the thermally induced strain ε_z is relatively very small. The value of Δn in this case can be calculated by solving the equation that relates stress and strain in the fiber [155]. The thermal response of the fiber material can be enhanced by molding or coating the fiber grating. FBG undergoes greater thermal strain when it is molded or coated with materials that have higher thermal expansion coefficients. Hence, it provides an effective means to enhance FBG's temperature sensitivity.

Figure 7.9 shows the proposed structural configuration of the sensor and two exemplary temperature sensitivity enhancement schemes that involve burying the sensor in materials of higher expansion coefficients. The sensor can be customized for desired sensitivity and operating temperature range by choosing the suitable molding material.

Using point-by-point inscription method, a millimeter long FBG was first inscribed in the 1.5 mm long microfiber spliced between standard SMFs. After the FBG inscription, 150 μm length of standard SMF was cut at the far end of the microfiber by femtosecond laser micromachining as shown in Fig. 7.9 (a). The edge of the laser cut has a small angle to minimize any reflection from fiber edge and air interface. The FBG was then molded with Sn-Ag-Cu alloy and acetal (polyoxymethylene) as demonstrated in Fig. 7.9 (b) and (c), respectively to demonstrate improved temperature sensitivity. The step structure shown in Fig. 7.9 (a) provides good grip if the sensor is buried in foreign materials and requires no adhesion. In addition, the microfibers are likely to show less resistance to external strain variation compared to standard SMFs. Thus the molded microfiber FBG sandwiched between standard SMFs, when subject to the axial strain ε_z in Eq. (7.3) is expected to easily follow the thermal response of the molding material.

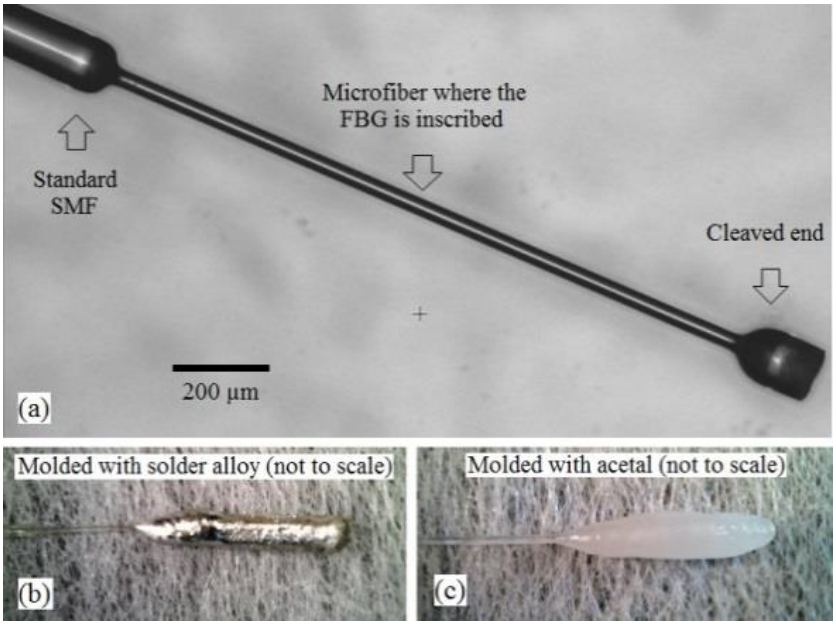

Figure 7.9 Sandwiched microfiber between standard SMFs where the FBG is inscribed (a). Photographs of the FBG sensors molded with Sn-Ag-Cu alloy (b) and acetal (c)

In this study, Sn-Ag-Cu alloy and acetal were used as molding materials. The alloy has a thermal expansion coefficient of 24×10^-6/ ^{0}C while the acetal shows thermal expansion coefficients of 122×10^-6/ ^{0}C for temperature range 0 ^{0}C to 60 ^{0}C and 137×10^ -6/ ^{0}C for temperature range of 60 ^{0}C to 105 ^{0}C. Those coefficients are much larger than that of silica which has a thermal expansion coefficient of 0.55×10^-6/ ^{0}C.

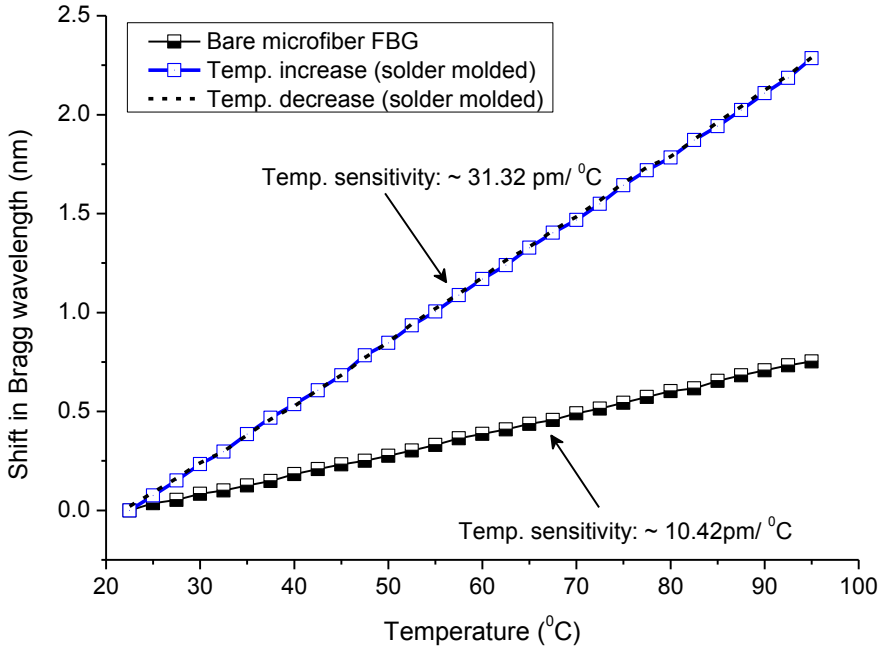

Figure 7.10 Bragg wavelength shift with temperature for bare and Sn-Ag-Cu alloy molded microfiber FBG

To calibrate the sensor, the measurement of the temperature dependent Bragg wavelength shift was conducted using the SmartScan interrogator with wavelength stability of <5 pm and a temperature-controlled oven with the temperature accuracy of 0.1 ^{0}C. Ambient FBG temperature was measured using a thermocouple placed closed to it. The oven temperature was gradually changed from 22.5 ^{0}C to 95 ^{0}C with a step interval of 2.5 ^{0}C. Figure 7.10 shows the temperature response of bare microfiber FBG and when it was molded with alloy. The experimental data of increasing and decreasing

temperature for the Sn-Ag-Cu alloy molded microfiber FBG are shown in solid line with unfilled rectangular marker and dotted line, respectively. Alloy molded microfiber FBG shows a temperature sensitivity of 31.32 nm/ ^{0}C. Figure 7.11 shows the Bragg wavelength shift against temperature variation for bare and acetal molded microfiber FBG's. The bare microfiber has an ambient temperature sensitivity of 10.42 pm/ ^{0}C. With acetal molding the temperature sensitivity improves to 202.33 pm/ ^{0}C for temperature range of 22.5 ^{0}C to 60 ^{0}C and 479.48 pm/ ^{0}C for temperature range of 60 ^{0}C to 95 ^{0}C. The high thermal expansion coefficient of acetal and corresponding elongation of the microfiber FBG in response to applied temperature accounts for the sensitivity enhancement.

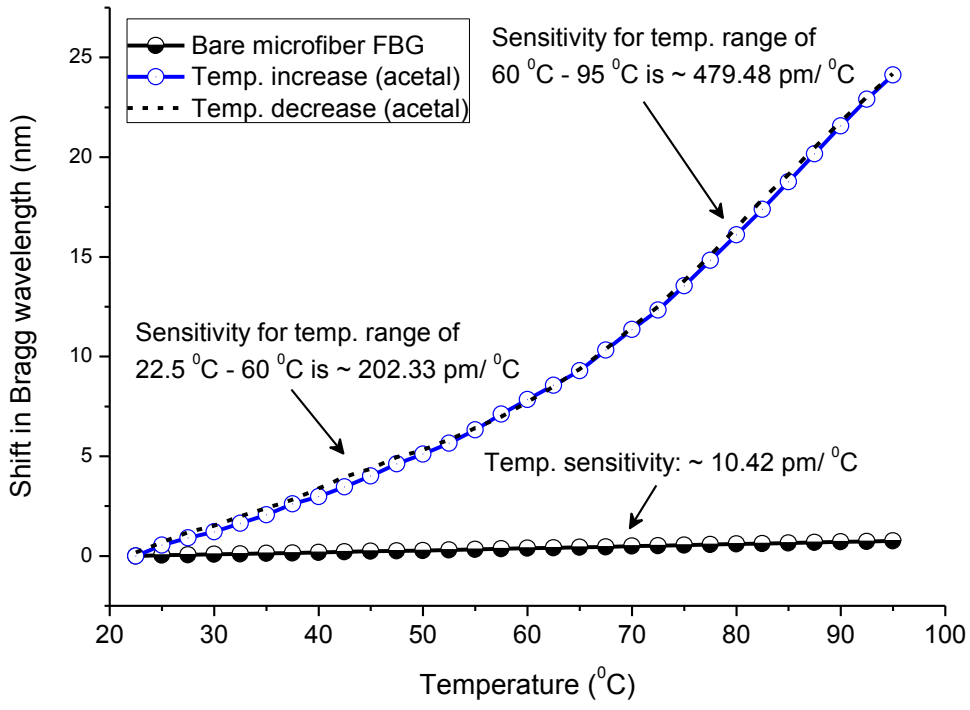

Figure 7.11 Bragg wavelength shift with temperature for bare FBG and acetal molded microfiber FBG. Molding seems to enhance the temperature sensitivity almost 50 times for temperature range of 60 ^{0}C to 95 ^{0}C

7.2.4 Conclusion

Fabrication of FBG in a microfiber spliced between standard SMFs and molding with materials of larger thermal expansion coefficients is presented in this study to demonstrate improved temperature sensitivity. Sandwiched structure of the bare fiber sensor offers inherent and reliable grip when molded with materials. The characterization plots shows that in response to ambient temperature variation, the microfiber FBG easily follows the axial strain applied by the molding materials. Sn-Ag-Cu alloy molding of the microfiber FBG shows temperature sensitivity of 31.32 pm/ ^{0}C. Acetal molding further improves temperature sensitivity to 202.33 pm/ ^{0}C for temperature range of 22.5 ^{0}C to 60 ^{0}C and 479.48 pm/ ^{0}C for temperature range of 60 ^{0}C to 95 ^{0}C. Obviously, with suitable molding material, the sensitivity of temperature measurement can be even further enhanced and tailored for operating temperature range.

7.3 Integrated Microfiber FBG and MZI for multi-parameter sensing

7.3.1 Introduction

Measurement of ambient temperature and refractive index (RI) is crucial to many in-situ environmental monitoring applications. Temperature cross-sensitivity in fiber-optic sensors may lead to incorrect quantification of ambient RI. It is therefore essential to measure both temperature and RI simultaneously and unambiguously. Novel fiber optic measurement systems have been constantly offered to achieve application specific quantification of these parameters. Interferometric fiber optic sensors have been widely studied due their excellent RI sensitivity and moderate temperature sensitivity [12, 163]. Diverse Mach-Zehnder interferometers (MZI) are constructed using structures such as core offset [164, 165], tapered fiber [166], multimode microfiber [167] for simultaneous quantification of temperature and RI. Various configurations of MZI combined with fiber Bragg grating (FBG) have also been explored to measure ambient refractive index (RI) and temperature simultaneously, including peanut-shape and core-offset structure [168], and only core-offset MZI [169]. Formation of MZI has also been illustrated using a pair of long period gratings [58], and splicing a piece of photonic crystal fiber between single mode fibers [170]. However, extended sensor length reported in some works may provide inaccurate sensing location and is undesirable in simultaneous measurement of parameters.

Miniaturization of optical sensors is highly desirable in temperature and RI sensing. A compact femtosecond laser micromachined cavity in single mode fiber is proposed to form a MZI for sensing ambient RI [171]. A miniature MZI embedded in fiber Bragg grating is also reported for simultaneous RI and temperature measurement [172].

Although the sensor demonstrates high sensitivity, the fragile structure and fabrication complexity make it incomputable for many applications. Besides the narrow in-fiber cavity makes it difficult to remove solution residue and reuse without hassle. In general, the key sensing characteristics such as moderate RI and temperature sensitivity, compactness and robustness are hard to achieve simultaneously.

In this study, we present a novel in-fiber sensor that incorporates a 1 mm long FBG in a 4 mm long MZI structure for sensing both RI and temperature. The MZI is constructed by simply fusion splicing a single mode microfiber (core: 3.75 µm, cladding: 40 µm) between standard SMFs. The FBG is inscribed in microfiber by point-by-point inscription of index modulation by femtosecond laser radiation. Because of inherent good RI sensitivity of MZI [171, 173] and insensitivity of FBG to ambient RI change, while both are moderately sensitive to temperature, a simultaneous and unambiguous RI and temperature measurement can be achieved. The embedded FBG is also used to demonstrate temperature compensated RI measurement using MZI.

7.3.2 Experimental

The schematic and of fabrication of the integrated MZI and FBG sensor is shown in Fig. 7.12. The MZI sensor was fabricated by splicing a stub of small diameter SMF (core diameter: 3.75 µm, cladding diameter: 40 µm) between two standard single mode fibers. The Fujikura (FSM 40PM) fusion splicer was used to splice standard SMF to microfiber with an arc power of 5 bit exposed for 1000 millisecond. Afterward, a FBG is inscribed in the microfiber employing a kilohertz femtosecond laser pulse radiation. The femtosecond laser system operating at center wavelength of 800 nm, pulse duration of 120 fs, and repetition rate of 1 kHz, was used to carry out the FPG fabrication

experiment. Using an iris diaphragm, the laser beam's diameter was reduced to 1.5 mm (initial diameter: 6 mm). Then the beam was focused by an achromatic objective lens (Numerical aperture: 0.75) into a small focal volume to elevate pulse peak power necessary for writing filamentary voids in fiber core. The fiber was coupled with a broad band light source (AFC BBS-1550), and a spectrum analyzer (PHOTONETICS Walics) to monitor and record the in-situ growth of transmission valley of FPGs during fabrication. The 1 mm FBG was fabricated by scanning the fiber with the 1 kHz pulse train (pulse energy: 42.5 μJ) along its propagation axis with a speed of 0.534 mm/sec to achieve the index modulation period 534 nm necessary to form its rejection band at 1550.28 nm. Both the transmission spectrum before and after the inscription of FBG in microfiber MZI is shown in Fig. 7.13. The overall spectral shift appears due to the core index modification which is explained in Chapter 3

.

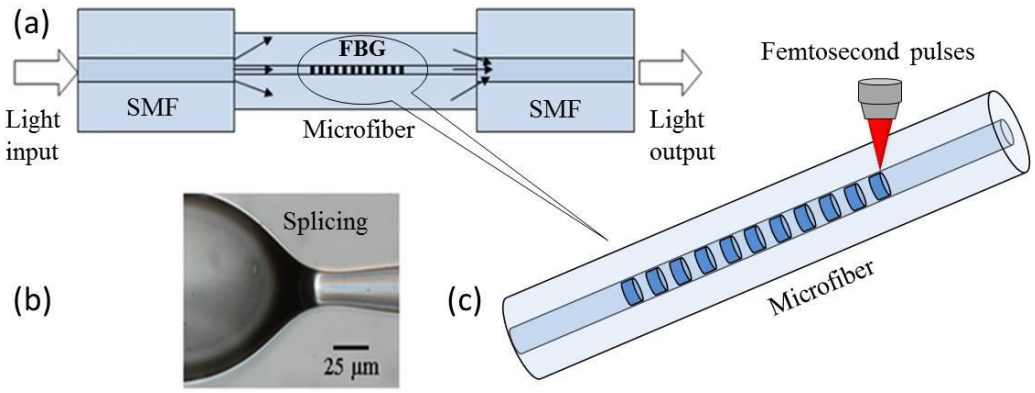

Figure 7.12 Schematic of integrated MZI and FBG sensor (a), splicing of standard SMF to microfiber (b), and schematic of point-by-point fabrication of FBG in microfiber spliced between SMFs (c)

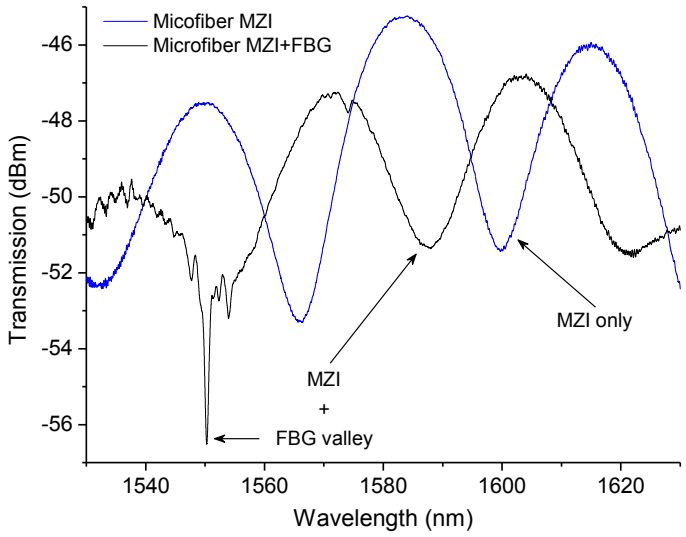

Figure 7.13 Combined FBG and MZI transmission spectrum

7.3.3 Ambient RI and temperature sensing

In ambient refractive index (RI) measurement, temperature cross-sensitivity plays a significant role because the RI of most solutions is a function of temperature. Therefore, it is crucial to measure both RI and temperature of a system to get rid of the temperature effect on RI measurement. This work proposes a compact optical fiber sensor integrating a fiber Bragg grating (FBG) in Mach-Zehnder interferometer (MZI) for RI and temperature measurement with improved sensing resolution.

As illustrated in Fig. 7.12 (a), the incident light when interacts the first interface (SMF and small diameter SMF), it spreads into both core and cladding of small diameter SMF and then recombine at the second interface (small diameter SMF and SMF). Therefore, the core and the cladding of the microfiber act as the two arms of a typical MZI. The core mode is confined in the core while the propagation characteristic of the cladding modes depends on the RI difference at cladding-surrounding interface. Small fiber diameter allows the cladding modes to extend much closer to the surrounding

solution; hence, the MZI sensor shows high sensitivity to any change of RI in the surrounding environment. In contrast, the FBG couples light from forward propagating core mode to the backward propagating core mode in the microfiber. Therefore, the rejection band in FBG's transmission spectrum is also confined in the core. The core mode cannot reach out to the cladding and ambient interface and that explains FBG's very low sensitivity to index change in the vicinity of fiber cladding.

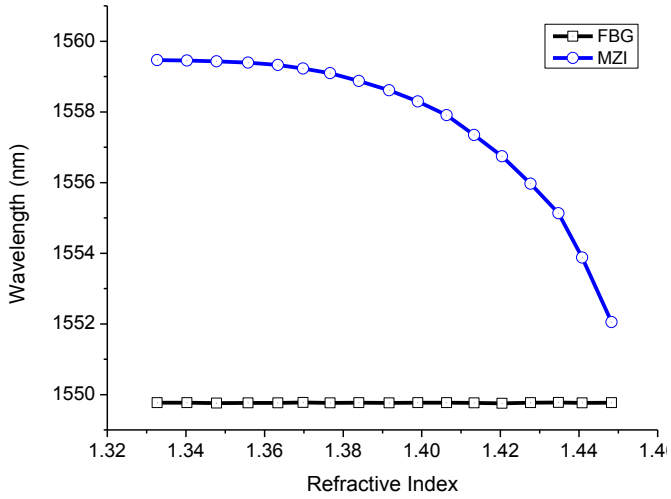

Figure 7.14 Characterization of the sensors to ambient refractive index change. The MZI shows significant RI sensitivity while the FBG is insensitive to ambient RI change

The shift of interference pattern as a function of the surrounding refractive index change was monitored for RI characterization of the 4 mm long MZI. The sensor was characterized with difference concentration of glycerin solutions at room temperature of 22^0C. To achieve characterization data, the device was immersed different glycerin solutions of RI ranging from 1.332 to 1.448. After each test, the sensor was thoroughly cleaned before immersing it in subsequent higher concentration glycerin solution. Figure 7.14 shows the wavelength shifts due to the change of surrounding refractive index. As the surrounding RI increases, the dip wavelength of the transmission wave experiences a blue-shift. FBG's resonance transmission spectrum shows insignificant index sensitivity

as shown by the flat line in Fig. 7.14. The ambient RI sensitivity of the MZI and FBG is summarized in Table 7.1.

Sensor	RI (1.332-1.1.384)	RI (1.384- 1.420)	RI (1.420-1.448)
FBG sensitivity (nm/RIU)	~ 0	~ 0	~ 0
MZI sensitivity (nm/RIU)	-10.65	-58.13	-166.30

Table 7.1 Ambient RI sensitivity of MZI and FBG sensors

The temperature response was examined by placing the sensor in an oven with temperature control range of 30 ^{0}C -95 ^{0}C. The spectral responses with temperature for both FBG and MZI are illustrated in Fig. 7.15 and 7.16, respectively. The MZI shows clearly dominant temperature sensitivity compared to that of FBG. A linear fitting to the measured data gives the temperature sensitivities ($d\lambda / dT$) of 11.80 pm/^{0}C and 51.10 pm/^{0}C, for FBG and MZI, respectively. Therefore, the experimental results show that the MZI is 4.33 times more sensitive than FBG for temperature measurement.

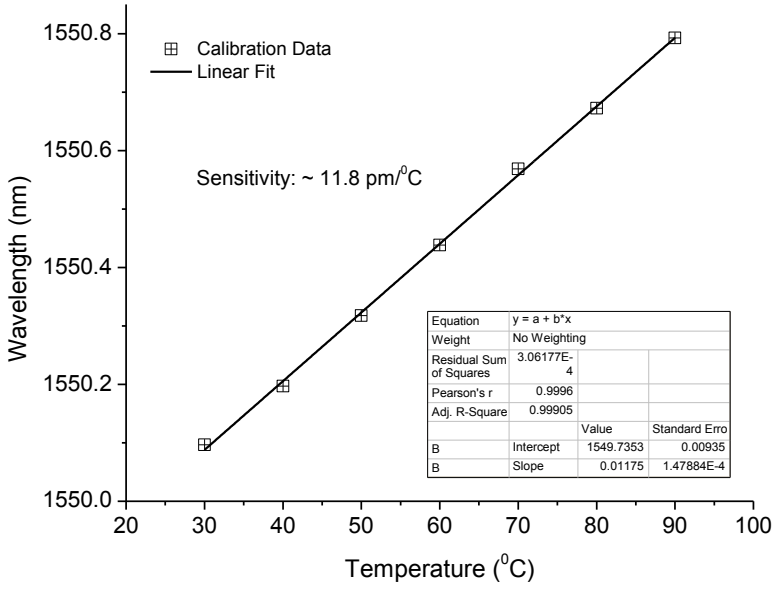

Figure 7.15 Temperature calibration of fiber Bragg grating written in microfiber

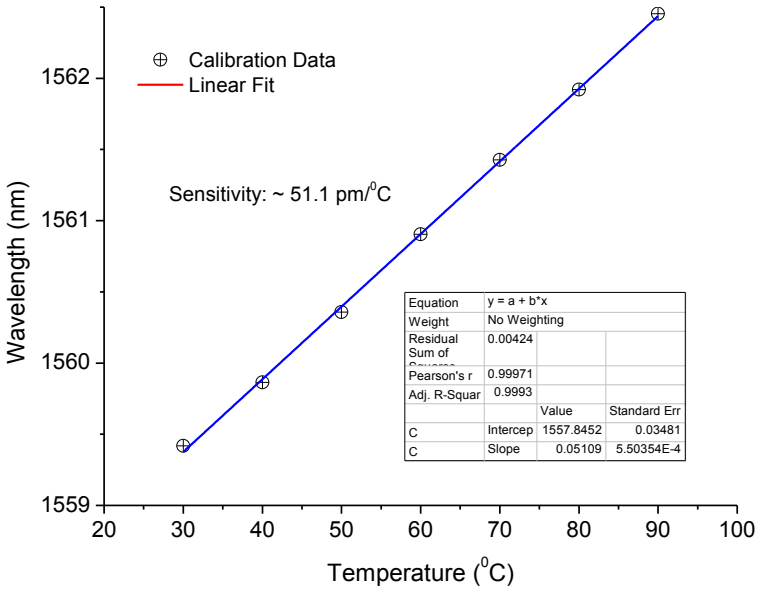

Figure 7.16 Temperature calibration of microfiber MZI

7.3.4 Simultaneous measurement of RI and temperature

Based on sensing characteristics of the MZI and FBG sensors demonstrated in section 7.3.3 above, the RI and temperature can be measured simultaneously using the following matrix equation [173]:

$$\begin{bmatrix} \Delta T \\ \Delta n \end{bmatrix} = \frac{1}{k_{FBGT} \times k_{MZIn} - k_{FBGn} \times k_{MZIT}} \begin{bmatrix} k_{MZIn} & k_{FBGn} \\ k_{MZIT} & k_{FBGT} \end{bmatrix} \times \begin{bmatrix} \Delta\lambda_{FBG} \\ \Delta\lambda_{MZI} \end{bmatrix} \quad (7.5)$$

where, ΔT is the variation of ambient temperature, Δn is the variation of ambient RI, $\Delta\lambda_{FBG}$ and $\Delta\lambda_{MZI}$ are the wavelength change corresponding to the FBG and microfiber MZI, respectively. k_{MZIn} and k_{MZIT} are the index and temperature coefficients of the microfiber MZI sensor, respectively, while k_{FBGn} and k_{FBGT} are the index and temperature coefficients of the microfiber FBG, respectively. Now let's consider the $k_{MZIn} = -58.13$ and $k_{FBGn} = 0$ (RI range: 1.384 - 1.420) from the table 7.1. From Fig. 7.15 and 7.16, we see that $k_{MZIT}$and k_{FBGT} are 0.0511 and 0.0118 respectively. Therefore, the Eq. (7.5) can be rewritten as bellow:

$$\begin{bmatrix}\Delta T\\ \Delta n\end{bmatrix} = -\frac{1}{0.68}\begin{bmatrix}-58.13 & 0\\ 0.0511 & 0.0118\end{bmatrix}\begin{bmatrix}\Delta\lambda_{FBG}\\ \Delta\lambda_{MZI}\end{bmatrix} \quad (7.6)$$

If the resonance wavelength shift of the FBG and the MZI are known, then the temperature and RI coefficients can easily be calculated using Eq. (7.6).

7.3.5 Temperature compensated RI sensing

For temperature compensated refractive index measurement using point sensors, it is vital to achieve both temperature and ambient RI information at a particular point of interest. Often an FBG connected parallel or series is used to quantity the temperature. It raises operation cost, and increases system complexity. In addition, due to the lack of close proximity, it may require the temperature of the whole chamber to stabilize before obtaining temperature reading. The miniature FBG embedded in microfiber MZI appears to minimize the issues explained above. Temperature compensation using embedded microfiber Bragg grating is exemplified in Fig. 7.17.

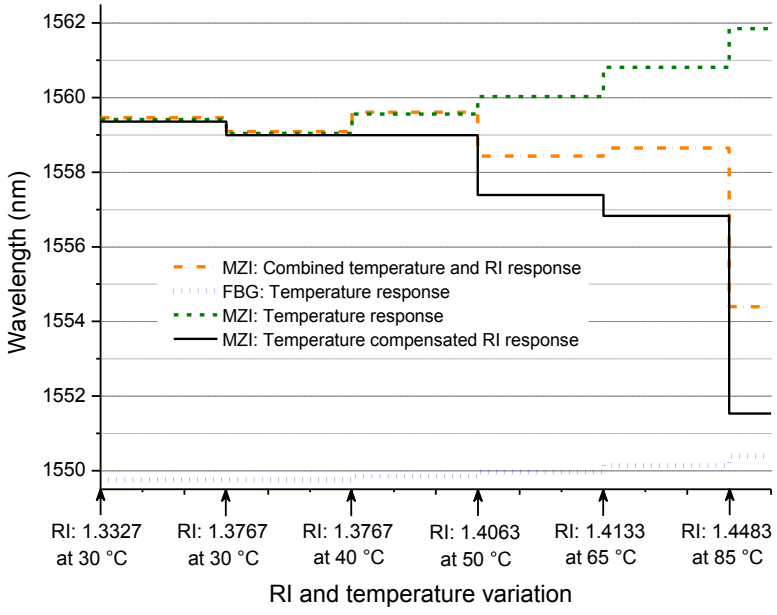

Figure 7.17 Exemplification of temperature compensation using an embedded miniature FBG for ambient RI measurement of microfiber MZI interferometer

Temperature compensation job in the Fig. 7.17 was done following the simple steps provided bellow:

1. Check the FBG response. No shift in FBG spectrum dip indicates constant temperature and no need for compensation. Read the temperature change from FBG if there is any, and go to step 2.
2. Temperature sensitivity of MZI is 4.33 times higher than that of FBG. So, if there is any shift in FBG spectrum in step 1, the MZI's temperature reading can be achieved easily taking FBG as the reference.
3. As shown in characterization plots, the MZI spectral dip displays blue and red shift with increase in ambient RI and temperature, respectively; while the FBG dip shows red shift with increase in temperature and no shift for RI change. Therefore, the following two step observation can be made to isolate temperature effect in MZI based RI measurement:
    a. If both the direction and amount of spectral shift in MZI and FBG are equal to the proportion of their sensitivity, it can be stated that the ambient RI was constant.
    b. If MZI's spectral shift does not correspond to the spectral response of FBG, then the individual spectral shift for both MZI and FBG has to be calculated. Using the following equation the MZI index response (temperature compensated) can be calculated:

       MZI (RI response) = MZI (Total response) – MZI (Temperature response)

7.3.6 Conclusion

A novel optical fiber sensor based on FBG implanted in a MZI of SMF-microfiber-SMF configuration has been proposed for ambient RI and temperature measurement. The MZI is constructed by fusion splicing a 4 mm long microfiber between SMFs. FBG is then fabricated in microfiber by the femtosecond pulse radiation in point-by-point inscription technique. The integrated miniature sensor is demonstrated as a suitable device for both simultaneous RI and temperature measurement, and temperature compensated RI measurement applications.

Chapter 8 - Overall summary and future work

8.1 Overall summary

Development of fiber optic sensors (long period gratings in Ge-doped and pure silica fiber, fiber Bragg gratings in microfiber, and Mach-Zehnder interferometers using microfiber and taper photonic crystal fibers) for ambient refractive index and temperature measurement is presented in this dissertation.

Since the inscription of in-fiber periodic index modulation is the fundamental step to fabricate fiber gratings, the primary focus of this work is given to write positive refractive index in the bulk of transparent dielectric medium. Filamentary propagation of ultra-short pulses in transparent dielectric medium is used inscribe filament voids in corning glass plate. Focusing conditions of femtosecond pulses in glass is investigated in this work to control the morphology of the bulk voids. Quantification of in-fiber refractive index change written by an inscription device is necessary to design a fiber grating sensor. Therefore, two simple and economic yet effective methods are reported in this dissertation to directly measure positive refractive index changed inscribed by femtosecond laser pulses. Both the methods can be configured in various fiber types for refractive index measurement in a particular optical fiber. Then, femtosecond pulse filamentation induced fabrication of long period grating in Ge-doped and pure silica core fiber using asymmetric index inscription. However, asymmetric RI inscription in core is sensitive to fiber misalignment and shows PDL in light propagation. To minimize PDL and enhance reliability in grating fabrication, helical index modulation is introduced. The experimental results of helical long period gratings fabrication show greater consistency

in grating inscription. Writing of fiber Bragg grating in microfiber is demonstrated for enhanced temperature sensing. Finally, sandwiched structure of microfiber MZI and FBG is presented for multi-parameters sensing.

8.2 Future work

Fiber gratings to dominate the existing sensing technologies, the fabrication process needs to be both reliable and cost effective. Even if helical index modification brings reliability in grating fabrication, a single long period grating inscription may take up to 30 minutes. To reduce grating inscription time, the rotary stage needs to be operating at higher RPM without significant vibration and run out. The reported laser system operates at 1 kHz pulse repetition rate which may limit the seed up of grating fabrication using rotary stage. Therefore, it would be worth investigating the use of an ultrafast laser operating at higher pulse repetition rate. Also, a detail study is planned to compare fabrication flexibility and performance characteristics for LPGs fabricated by both asymmetric and helical index modulation.

In order to speed up fabrication as well as enhance ambient refractive index sensitivity of the long period gratings, we aim to inscribe higher index modulation with shorter period and subsequently taper the fiber by applying heat and elongation to match the grating period and reduce cladding diameter. This process is also expected to offer annealing of the fiber that is necessary to minimize micro-crack introduced (if any) in index writing phase.

To confine and strengthen cladding mode field at cladding/air interface, coating the fiber cladding with higher refractive index materials has been demonstrated in numerous research works. Coating the long period grating with higher index materials greatly

enhances the ambient index sensitivity over a specific RI window. However, overlay bonding strength to the fiber and the aging characteristics of the coating materials are not well understood for long term applications. Moreover, to overcome the possibility of any chemical reaction happening between the coating materials and the solution to be measure is a challenge. Therefore, we propose to write a thin layer of higher index at cladding/air interface with laser radiation that would work as a coating overlay.

The detail study on aging characteristics and endurance in chemically hazardous environment of the long period gratings fabricated in pure silica fiber are yet to be achieved. Therefore, future works also include the study of ultrafast laser written grating's survival in high temperature (~ 1000 ^{0}C) and their performance in high pressure and hydrogen rich environment in comparison with gratings inscribed by ultra-violate radiation.

Finally, as discussed in this dissertation, the feasibility and reliability of grating fabrication depends on inscription of adequate RI in the fiber core. Ultrafast laser has the capabilities to inscribe grating based sensors in immerging new fiber types. Since, the fabrication reliability depends on both efficient delivery of ultrafast energy into the bulk glass and alignment of optical fiber, further study in this area would have a great impact on manufacturing of fiber optic sensors.

Bibliography

[1] V. Bhatia, K. A. Murphy, M. J. de Vries, M. B. Sen, and T. D'Alberto, "A comparative evaluation of the types and applications of various sensors," *Photonics Design and Applications Handbook,* 1995.

[2] K. O. Hill and G. Meltz, "Fiber Bragg grating technology fundamentals and overview," *Journal of Lightwave Technology,* vol. 15, pp. 1263-1276, Aug 1997.

[3] X. Fang, C. R. Liao, and D. N. Wang, "Femtosecond laser fabricated fiber Bragg grating in microfiber for refractive index sensing," *Optics Letters,* vol. 35, pp. 1007-1009, Apr 1 2010.

[4] S. W. James and R. P. Tatam, "Optical fibre long-period grating sensors: Characteristics and application," *Measurement Science & Technology,* vol. 14, pp. R49-R61, May 2003.

[5] R. P. Espindola, R. S. Windeler, A. A. Abramov, B. J. Eggleton, T. A. Strasser, and D. J. DiGiovanni, "External refractive index insensitive air-clad long period fibre grating," *Electronics Letters,* vol. 35, pp. 327-328, Feb 18 1999.

[6] V. Bhatia and A. M. Vengsarkar, "Optical fiber long-period grating sensors," *Optics Letters,* vol. 21, pp. 692-694, May 1 1996.

[7] Z. B. Tian, S. S. H. Yam, and H. P. Loock, "Single-mode fiber refractive index sensor based on core-offset attenuators," *Ieee Photonics Technology Letters,* vol. 20, pp. 1387-1389, Jul-Aug 2008.

[8] B. H. Lee, Y. H. Kim, K. S. Park, J. B. Eom, M. J. Kim, B. S. Rho, *et al.*, "Interferometric Fiber Optic Sensors," *Sensors,* vol. 12, pp. 2467-2486, Mar 2012.

[9] K. O. Hill, Y. Fujii, D. C. Johnson, and B. S. Kawasaki, "Photosensitivity in optical fiber waveguides: Application to reflection filter fabrication," *Applied Physics Letters,* vol. 32, pp. 647-649, 1978.

[10] A. M. Vengsarkar, P. J. Lemaire, J. B. Judkins, V. Bhatia, T. Erdogan, and J. E. Sipe, "Long-period fiber gratings as band-rejection filters," *Journal of Lightwave Technology,* vol. 14, pp. 58-65, Jan 1996.

[11] B. H. Lee, J. B. Eom, K. S. Park, S. J. Park, and M. J. Ju, "Specialty Fiber Coupler: Fabrications and Applications," *Journal of the Optical Society of Korea,* vol. 14, pp. 326-332, Dec 2010.

[12] D. J. C. B., *Optical Fiber Sensors: Principles and Componenets*. Boston: Artech House, 1988.

[13] H. J. Patrick, G. M. Williams, A. D. Kersey, J. R. Pedrazzani, and A. M. Vengsarkar, "Hybrid fiber Bragg grating/long period fiber grating sensor for strain/temperature discrimination," *Ieee Photonics Technology Letters,* vol. 8, pp. 1223-1225, Sep 1996.

[14] H. J. Kim, O. J. Kown, S. B. Lee, and Y. G. Han, "Measurement of temperature and refractive index based on surface long-period gratings deposited onto a D-shaped photonic crystal fiber," *Applied Physics B-Lasers and Optics,* vol. 102, pp. 81-85, Jan 2011.

[15] I. W. Jung, B. Park, J. Provine, R. T. Howe, and O. Solgaard, "Highly Sensitive Monolithic Silicon Photonic Crystal Fiber Tip Sensor for Simultaneous

Measurement of Refractive Index and Temperature," *Journal of Lightwave Technology*, vol. 29, pp. 1367-1374, May 1 2011.

[16] D. L. Aybatov, R. R. Kiyamova, O. G. Morozov, and E. V. Suhorukova, "Distributed temperature fiber Bragg grating sensor," 2008, pp. 73740B-73740B-7.

[17] L. Jiang, J. Yang, S. Wang, B. Li, and M. Wang, "Fiber Mach-Zehnder interferometer based on microcavities for high-temperature sensing with high sensitivity," *Optics Letters*, vol. 36, pp. 3753-3755, Oct 1 2011.

[18] J. P. Yang, L. Jiang, S. M. Wang, Q. H. Chen, B. Y. Li, and H. Xiao, "Highly Sensitive Refractive Index Optical Fiber Sensors Fabricated by a Femtosecond Laser," *Ieee Photonics Journal*, vol. 3, pp. 1189-1197, Dec 2011.

[19] S. M. Tripathi, E. Marin, A. Kumar, and J. P. Meunier, "Refractive index sensing characteristics of dual resonance long period gratings in bare and metal-coated D-shaped fibers," *Applied Optics*, vol. 48, pp. G53-G58, Nov 1 2009.

[20] W. Liang, Y. Y. Huang, Y. Xu, R. K. Lee, and A. Yariv, "Highly sensitive fiber Bragg grating refractive index sensors," *Applied Physics Letters*, vol. 86, Apr 11 2005.

[21] I. Del Villar, I. R. Matias, and F. J. Arregui, "Enhancement of sensitivity in long-period fiber gratings with deposition of low-refractive-index materials," *Optics Letters*, vol. 30, pp. 2363-2365, Sep 15 2005.

[22] E. Davies, R. Viitala, M. Salomaki, S. Areva, L. Zhang, and I. Bennion, "Sol-gel derived coating applied to long-period gratings for enhanced refractive index sensing properties," *Journal of Optics a-Pure and Applied Optics*, vol. 11, Jan 2009.

[23] K. S. Chiang, Y. Q. Liu, M. N. Ng, and X. Y. Dong, "Analysis of etched long-period fibre grating and its response to external refractive index," *Electronics Letters*, vol. 36, pp. 966-967, May 25 2000.

[24] N. Chen, B. F. Yun, Y. P. Wang, and Y. P. Cui, "Theoretical and experimental study on etched fiber Bragg grating cladding mode resonances for ambient refractive index sensing," *Journal of the Optical Society of America B-Optical Physics*, vol. 24, pp. 439-445, Mar 2007.

[25] G. Meltz, W. W. Morey, and W. H. Glenn, "Formation of Bragg Gratings in Optical Fibers by a Transverse Holographic Method," *Optics Letters*, vol. 14, pp. 823-825, Aug 1 1989.

[26] K. O. Hill, B. Malo, F. Bilodeau, D. C. Johnson, and J. Albert, "Bragg Gratings Fabricated in Monomode Photosensitive Optical Fiber by Uv Exposure through a Phase Mask," *Applied Physics Letters*, vol. 62, pp. 1035-1037, Mar 8 1993.

[27] D. Z. Anderson, V. Mizrahi, T. Erdogan, and A. E. White, "Production of in-Fiber Gratings Using a Diffractive Optical-Element," *Electronics Letters*, vol. 29, pp. 566-568, Mar 18 1993.

[28] H. J. Patrick, C. G. Askins, R. W. McElhanon, and E. J. Friebele, "Amplitude mask patterned on an excimer laser mirror for high intensity writing of long period fibre gratings," *Electronics Letters*, vol. 33, pp. 1167-1168, Jun 19 1997.

[29] B. J. O'Regan and D. N. Nikogosyan, "Femtosecond UV long-period fibre grating fabrication with amplitude mask technique," *Optics Communications*, vol. 284, pp. 5650-5654, Dec 1 2011.

[30] A. I. Kalachev, V. Pureur, and D. N. Nikogosyan, "Investigation of long-period fiber gratings induced by high-intensity femtosecond UV laser pulses," *Optics Communications,* vol. 246, pp. 107-115, Feb 1 2005.

[31] Y. J. Rao, Y. P. Wang, Z. L. Ran, and T. Zhu, "Novel fiber-optic sensors based on long-period fiber gratings written by high-frequency CO2 laser pulses," *Journal of Lightwave Technology,* vol. 21, pp. 1320-1327, May 2003.

[32] D. D. Davis, T. K. Gaylord, E. N. Glytsis, S. G. Kosinski, S. C. Mettler, and A. M. Vengsarkar, "Long-period fibre grating fabrication with focused CO2 laser pulses," *Electronics Letters,* vol. 34, pp. 302-303, Feb 5 1998.

[33] I. K. Hwang, S. H. Yun, and B. Y. Kim, "Long-period fiber gratings based on periodic microbends," *Optics Letters,* vol. 24, pp. 1263-1265, Sep 15 1999.

[34] S. Savin, M. J. F. Digonnet, G. S. Kino, and H. J. Shaw, "Tunable mechanically induced long-period fiber gratings," *Optics Letters,* vol. 25, pp. 710-712, May 15 2000.

[35] Y. Wang, D. N. Wang, M. W. Yang, and C. R. Liao, "Asymmetric microhole-structured long-period fiber gratings," *Sensors and Actuators B-Chemical,* vol. 160, pp. 822-825, Dec 15 2011.

[36] C. Y. Lin, G. W. Chern, and L. A. Wang, "Periodical corrugated structure for forming sampled fiber Bragg grating and long-period fiber grating with tunable coupling strength," *Journal of Lightwave Technology,* vol. 19, pp. 1212-1220, Aug 2001.

[37] B. E. A. S. M. C. Teich, *Fundamendals of Photonics*. New York: John Wiley, 1991.

[38] A. Tomita and P. J. Lemaire. (1985, Hydrogen-induced loss increases in germanium-doped single-mode optical fibres: long-term predictions. *Electronics Letters 21(2),* 71-72.

[39] G. D. Maxwell, R. Kashyap, B. J. Ainslie, D. L. Williams, and J. R. Armitage. (1992, UV written 1.5 μm reflection filters in single mode planar silica guides. *Electronics Letters 28(22),* 2106-2107.

[40] P. J. Lemaire, R. M. Atkins, V. Mizrahi, and W. A. Reed, "High pressure H₂ loading as a technique for achieving ultrahigh UV photosensitivity and thermal sensitivity in GeO₂ doped optical fibres," *Electronics Letters,* vol. 29, pp. 1191-1193, 1993.

[41] A. Martinez, M. Dubov, I. Khrushchev, and I. Bennion, "Direct writing of fibre Bragg gratings by femtosecond laser," *Electronics Letters,* vol. 40, pp. 1170-1172, Sep 16 2004.

[42] Y. Kondo, K. Nouchi, T. Mitsuyu, M. Watanabe, P. G. Kazansky, and K. Hirao, "Fabrication of long-period fiber gratings by focused irradiation of infrared femtosecond laser pulses," *Optics Letters,* vol. 24, pp. 646-648, May 15 1999.

[43] P. G. Kryukov, Y. V. Larionov, A. A. Rybaltovskii, K. A. Zagorul'ko, A. Dragomir, D. N. Nikogosyan, *et al.,* "Long-period fibre grating fabrication with femtosecond pulse radiation at different wavelengths," *Microelectronic Engineering,* vol. 69, pp. 248-255, 9// 2003.

[44] A. Martinez, I. Y. Khrushchev, and I. Bennion, "Direct inscription of Bragg gratings in coated fibers by an infrared femtosecond laser," *Optics Letters,* vol. 31, pp. 1603-1605, Jun 1 2006.

[45] E. Davies, K. Kalli, C. Koutsides, and L. Zhang, "Highly refractive index sensitive femtosecond laser inscribed long period gratings," *21st International Conference on Optical Fiber Sensors,* vol. 7753, 2011.

[46] F. Hindle, E. Fertein, C. Przygodzki, F. Durr, L. Paccou, R. Bocquet, *et al.*, "Inscription of long-period gratings in pure silica and germano-silicate fiber cores by femtosecond laser irradiation," *Ieee Photonics Technology Letters,* vol. 16, pp. 1861-1863, Aug 2004.

[47] V. Bhatia, "Properties and sensing applications of long-period gratings," PhD, Virginia Polytechnic Institute and State University 1996.

[48] S. J. Liu, L. Jin, W. Jin, D. N. Wang, C. R. Liao, and Y. Wang, "Structural long period gratings made by drilling micro-holes in photonic crystal fibers with a femtosecond infrared laser," *Optics Express,* vol. 18, pp. 5496-5503, Mar 15 2010.

[49] S. J. Liu, L. Jin, W. Jin, Y. P. Wang, and D. N. Wang, "Fabrication of Long-Period Gratings by Femtosecond Laser-Induced Filling of Air-Holes in Photonic Crystal Fibers," *Ieee Photonics Technology Letters,* vol. 22, pp. 1635-1637, Nov 15 2010.

[50] W. H. Tsai and C. J. Lin, "A novel structure for the intrinsic Fabry-Perot fiber-optic temperature sensor," *Journal of Lightwave Technology,* vol. 19, pp. 682-686, May 2001.

[51] Y. J. Rao, "Recent progress in fiber-optic extrinsic Fabry-Perot interferometric sensors," *Optical Fiber Technology,* vol. 12, pp. 227-237, Jul 2006.

[52] S. H. Kim, J. J. Lee, D. C. Lee, and I. B. Kwon, "A study on the development of transmission-type extrinsic Fabry-Perot interferometric optical fiber sensor," *Journal of Lightwave Technology,* vol. 17, pp. 1869-1874, Oct 1999.

[53] Y. J. Rao, M. Deng, D. W. Duan, X. C. Yang, T. Zhu, and G. H. Cheng, "Micro Fabry-Perot interferometers in silica fibers machined by femtosecond laser," *Optics Express,* vol. 15, pp. 14123-14128, Oct 17 2007.

[54] Z. L. Ran, Y. J. Rao, J. Zhang, Z. W. Liu, and B. Xu, "A Miniature Fiber-Optic Refractive-Index Sensor Based on Laser-Machined FabryPerot Interferometer Tip," *Journal of Lightwave Technology,* vol. 27, pp. 5426-5429, Dec 1 2009.

[55] X. K. Wan and H. F. Taylor, "Intrinsic fiber Fabry-Perot temperature sensor with fiber Bragg grating mirrors," *Optics Letters,* vol. 27, pp. 1388-1390, Aug 15 2002.

[56] Y. Zhang, X. P. Chen, Y. X. Wang, K. L. Cooper, and A. B. Wang, "Microgap multicavity Fabry-Perot biosensor," *Journal of Lightwave Technology,* vol. 25, pp. 1797-1804, Jul 2007.

[57] P. Morris, A. Hurrell, A. Shaw, E. Zhang, and P. Beard, "A Fabry-Perot fiber-optic ultrasonic hydrophone for the simultaneous measurement of temperature and acoustic pressure," *Journal of the Acoustical Society of America,* vol. 125, pp. 3611-3622, Jun 2009.

[58] Y. J. Kim, U. C. Paek, and B. H. Lee, "Measurement of refractive-index variation with temperature by use of long-period fiber gratings," *Optics Letters,* vol. 27, pp. 1297-1299, Aug 1 2002.

[59] T. Allsop, R. Reeves, D. J. Webb, I. Bennion, and R. Neal, "A high sensitivity refractometer based upon a long period grating Mach-Zehnder interferometer," *Review of Scientific Instruments,* vol. 73, pp. 1702-1705, Apr 2002.

[60] Y. Zhao, X.-g. Li, and L. Cai, "Mach–Zehnder interferometer formed by a large core-offset splicing fiber for temperature and displacement measurement," *Optics Communications,* vol. 356, pp. 54-58, 12/1/ 2015.
[61] G. A. Cardenas-Sevilla, V. Finazzi, J. Villatoro, and V. Pruneri, "Photonic crystal fiber sensor array based on modes overlapping," *Optics Express,* vol. 19, pp. 7596-7602, Apr 11 2011.
[62] F. F. Pang, H. H. Liu, H. R. Guo, Y. Q. Liu, X. L. Zeng, N. Chen, *et al.*, "In-Fiber Mach-Zehnder Interferometer Based on Double Cladding Fibers for Refractive Index Sensor," *Ieee Sensors Journal,* vol. 11, pp. 2395-2400, Oct 2011.
[63] O. Frazao, S. F. O. Silva, J. Viegas, J. M. Baptista, J. L. Santos, J. Kobelke, *et al.*, "All Fiber Mach-Zehnder Interferometer Based on Suspended Twin-Core Fiber," *Ieee Photonics Technology Letters,* vol. 22, pp. 1300-1302, Sep 1 2010.
[64] P. J. Lemaire, R. M. Atkins, V. Mizrahi, and W. A. Reed, "High-Pressure H-2 Loading as a Technique for Achieving Ultrahigh Uv Photosensitivity and Thermal Sensitivity in Geo2 Doped Optical Fibers," *Electronics Letters,* vol. 29, pp. 1191-1193, Jun 24 1993.
[65] B. Y. Li, L. Jiang, S. M. Wang, H. L. Tsai, and H. Xiao, "Femtosecond laser fabrication of long period fiber gratings and applications in refractive index sensing," *Optics and Laser Technology,* vol. 43, pp. 1420-1423, Nov 2011.
[66] N. Zhang, J. J. Yang, M. W. Wang, and X. N. Zhu, "Fabrication of long-period fibre grainges using 800 nm femtosecond laser pulses," *Chinese Physics Letters,* vol. 23, pp. 3281-3284, Dec 2006.
[67] K. P. Chen, P. R. Herman, J. Zhang, and R. Tam, "Fabrication of strong long-period gratings in hydrogen-free fibers with 157-nm F-2-laser radiation," *Optics Letters,* vol. 26, pp. 771-773, Jun 1 2001.
[68] P. Oberson, B. Gisin, B. Huttner, and N. Gisin, "Refracted near-field measurements of refractive index and geometry of silica-on-silicon integrated optical waveguides," *Applied Optics,* vol. 37, pp. 7268-7272, Nov 1 1998.
[69] A. D. Yablon, "Multi-Wavelength Optical Fiber Refractive Index Profiling by Spatially Resolved Fourier Transform Spectroscopy," *Journal of Lightwave Technology,* vol. 28, pp. 360-364, Feb 15 2010.
[70] J. W. Chan, T. Huser, S. Risbud, and D. M. Krol, "Structural changes in fused silica after exposure to focused femtosecond laser pulses," *Optics Letters,* vol. 26, pp. 1726-1728, 2001/11/01 2001.
[71] E. N. Glezer, M. Milosavljevic, L. Huang, R. J. Finlay, T. H. Her, J. P. Callan, *et al.*, "Three-dimensional optical storage inside transparent materials," *Optics Letters,* vol. 21, pp. 2023-2025, Dec 15 1996.
[72] E. N. Glezer and E. Mazur, "Ultrafast-laser driven micro-explosions in transparent materials," *Applied Physics Letters,* vol. 71, pp. 882-884, Aug 18 1997.
[73] D. Homoelle, S. Wielandy, A. L. Gaeta, N. F. Borrelli, and C. Smith, "Infrared photosensitivity in silica glasses exposed to femtosecond laser pulses," *Optics Letters,* vol. 24, pp. 1311-1313, 1999/09/15 1999.
[74] E. Fertein, C. Przygodzki, H. Delbarre, A. Hidayat, M. Douay, and P. Niay, "Refractive-index changes of standard telecommunication fiber through exposure

to femtosecond laser pulses at 810 cm," *Applied Optics,* vol. 40, pp. 3506-3508, Jul 20 2001.

[75] F. Ahmed, M. S. Lee, H. Sekita, T. Sumiyoshi, and M. Kamata, "Display glass cutting by femtosecond laser induced single shot periodic void array," *Applied Physics a-Materials Science & Processing,* vol. 93, pp. 189-192, Oct 2008.

[76] S. L. Chin, F. Theberge, and W. Liu, "Filamentation nonlinear optics," *Applied Physics B-Lasers and Optics,* vol. 86, pp. 477-483, Feb 2007.

[77] Z. Wu, H. Jiang, Q. Sun, H. Yang, and Q. Gong, "Filamentation and temporal reshaping of a femtosecond pulse in fused silica," *Physical Review A,* vol. 68, p. 063820, 12/23/ 2003.

[78] A. Braun, G. Korn, X. Liu, D. Du, J. Squier, and G. Mourou, "Self-channeling of high-peak-power femtosecond laser pulses in air," *Optics Letters,* vol. 20, pp. 73-75, 1995/01/01 1995.

[79] Z. Wu, H. Jiang, L. Luo, H. Guo, H. Yang, and Q. Gong, "Multiple foci and a long filament observed with focused femtosecond pulse propagation in fused silica," *Optics Letters,* vol. 27, pp. 448-450, 2002/03/15 2002.

[80] S. L. Chin, S. A. Hosseini, W. Liu, Q. Luo, F. Théberge, N. Aközbek, *et al.*, "The propagation of powerful femtosecond laser pulses in opticalmedia: physics, applications, and new challenges," *Canadian Journal of Physics,* vol. 83, pp. 863-905, 2005/09/01 2005.

[81] A. Couairon, "Filamentation length of powerful laser pulses," *Applied Physics B,* vol. 76, pp. 789-792, 2003/07/01 2003.

[82] S. Tzortzakis, L. Sudrie, M. Franco, B. Prade, A. Mysyrowicz, A. Couairon, *et al.*, "Self-Guided Propagation of Ultrashort IR Laser Pulses in Fused Silica," *Physical Review Letters,* vol. 87, p. 213902, 11/02/ 2001.

[83] A. Marcinkevičius, V. Mizeikis, S. Juodkazis, S. Matsuo, and H. Misawa, "Effect of refractive index-mismatch on laser microfabrication in silica glass," *Applied Physics A,* vol. 76, pp. 257-260, 2003.

[84] S. L. Chin, "The physics and the challenge of the propagation of powerful femtosecond laser pulses in optical media," *Physics in Canada,* vol. 60, pp. 273-281, 2004.

[85] J. H. Marburger, " Self-focusing: Theory," *Prog. Quant. Electron,* vol. 4, pp. 35-110, 1975.

[86] Q. Wu, G. D. Feke, R. D. Grober, and L. P. Ghislain, "Realization of numerical aperture 2.0 using a gallium phosphide solid immersion lens," *Applied Physics Letters,* vol. 75, pp. 4064-4066, 1999.

[87] H. El-Ghandoor, E. Abd El-Ghafar, and R. Hassan, "Refractive index profiling of a GRIN optical fiber using a modulated speckled sheet of light," *Optics and Laser Technology,* vol. 31, pp. 481-488, Oct 1999.

[88] J. C. Palais, *Fiber optic communications system*. New Jersey: Prentice-Hall, Englewood Cliffs, 1998.

[89] N. Gisin, R. Passy, and B. Perny, "Optical fiber characterization by simultaneous measurement of the transmitted and refracted near field," *Lightwave Technology, Journal of,* vol. 11, pp. 1875-1883, 1993.

[90] R. Conde, C. depeursinge, B. Gisin, N. Gisin, and B. Groebli, "Refractive index profile and geometry measurements in multicore fibres," *Pure and Applied*

Optics: Journal of the European Optical Society Part A, vol. 5, pp. 269-274, // 1996.

[91] K. W. Raine, J. G. N. Baines, and D. E. Putland, "Refractive-Index Profiling - State of the Art," *Journal of Lightwave Technology,* vol. 7, pp. 1162-1169, Aug 1989.

[92] N. Barakat, "Interferometric Studies on Fibers .1. Theory of Interferometric Determination of Indices of Fibers," *Textile Research Journal,* vol. 41, pp. 167-&, 1971.

[93] Z. Y. Liu, X. M. Dong, Q. H. Chen, C. Y. Yin, Y. X. Xu, and Y. J. Zheng, "Nondestructive measurement of an optical fiber refractive-index profile by a transmitted-light differential interference contact microscope," *Applied Optics,* vol. 43, pp. 1485-1492, Mar 1 2004.

[94] B. L. Bachim and T. K. Gaylord, "Microinterferometric optical phase tomography for measuring small, asymmetric refractive-index differences in the profiles of optical fibers and fiber devices," *Applied Optics,* vol. 44, pp. 316-327, Jan 20 2005.

[95] D. Johlen, H. Renner, A. Ewald, and E. Brinkmeyer, "Fiber Bragg grating Fabry-Perot interferometer for a precise measurement of the UV-induced index change," *24th European Conference on Optical Communication, Vol 1-3,* pp. 393-394, 1998.

[96] K. M. Davis, K. Miura, N. Sugimoto, and K. Hirao, "Writing waveguides in glass with a femtosecond laser," *Opt Lett,* vol. 21, pp. 1729-31, Nov 1 1996.

[97] K. Miura, J. R. Qiu, H. Inouye, T. Mitsuyu, and K. Hirao, "Photowritten optical waveguides in various glasses with ultrashort pulse laser," *Applied Physics Letters,* vol. 71, pp. 3329-3331, Dec 8 1997.

[98] F. Ahmed, M. S. Ahsan, M. S. Lee, and M. B. G. Jun, "Near-field modification of femtosecond laser beam to enhance single-shot pulse filamentation in glass medium," *Applied Physics a-Materials Science & Processing,* vol. 114, pp. 1161-1165, Mar 2014.

[99] M. Wang, J. Cheng, X. Yu, J. X. Dai, G. L. Zhang, and M. H. Yang, "Optical Fiber Hydrogen Sensor based on Micro Interferometer," *22nd International Conference on Optical Fiber Sensors, Pts 1-3,* vol. 8421, 2012.

[100] L. Xu, W. N. Han, P. Wang, and S. M. Wang, "Hybrid Mach-Zehnder interferometric sensor based on two core-offset attenuators and an abrupt taper in single-mode fiber," *Chinese Optics Letters,* vol. 12, Jul 10 2014.

[101] V. Bhatia, "Applications of long-period gratings to single and multi-parameter sensing," *Optics Express,* vol. 4, pp. 457-466, May 24 1999.

[102] Z. T. Gu and Y. P. Xu, "Design optimization of a long-period fiber grating with sol-gel coating for a gas sensor," *Measurement Science & Technology,* vol. 18, pp. 3530-3536, Nov 2007.

[103] L. W. Wang, Y. Liu, M. Zhang, D. S. Tu, X. H. Mao, and Y. B. Liao, "A relative humidity sensor using a hydrogel-coated long period grating," *Measurement Science & Technology,* vol. 18, pp. 3131-3134, Oct 2007.

[104] P. Pilla, V. Malachovska, A. Borriello, A. Buosciolo, M. Giordano, L. Ambrosio, *et al.,* "Transition mode long period grating biosensor with functional multilayer coatings," *Optics Express,* vol. 19, pp. 512-526, Jan 17 2011.

[105] Y. Liu, L. W. Wang, M. Zhang, D. S. Tu, X. H. Mao, and Y. B. Liao, "Long-period grating relative humidity sensor with hydrogel coating," *Ieee Photonics Technology Letters,* vol. 19, pp. 880-882, May-Jun 2007.

[106] S. Korposh, R. Selyanchyn, W. Yasukochi, S. W. Lee, S. W. James, and R. P. Tatam, "Optical fibre long period grating with a nanoporous coating formed from silica nanoparticles for ammonia sensing in water," *Materials Chemistry and Physics,* vol. 133, pp. 784-792, Apr 16 2012.

[107] S. Korposh, S. W. Lee, S. W. James, and R. P. Tatam, "Refractive index sensitivity of fibre-optic long period gratings coated with SiO2 nanoparticle mesoporous thin films," *Measurement Science & Technology,* vol. 22, Jul 2011.

[108] S. A. Slattery, D. N. Nikogosyan, and G. Brambilla, "Fiber Bragg grating inscription by high-intensity femtosecond UV laser light: comparison with other existing methods of fabrication," *Journal of the Optical Society of America B-Optical Physics,* vol. 22, pp. 354-361, Feb 2005.

[109] W. Ha, K. Oh, Y. M. Jung, K. K. Jun, W. Shin, I. B. Sohn, *et al.*, "Fabrication and Characterization of a Broadband Long-Period Grating on a Hollow Optical Fiber with Femtosecond Laser Pulses," *Journal of the Korean Physical Society,* vol. 53, pp. 3814-3817, Dec 2008.

[110] A. Couairon and A. Mysyrowicz, "Femtosecond filamentation in transparent media," *Physics Reports-Review Section of Physics Letters,* vol. 441, pp. 47-189, Mar 2007.

[111] A. Saliminia, R. Vallee, and S. L. Chin, "Waveguide writing in silica glass with femtosecond pulses from an optical parametric amplifier at 1.5 mu m," *Optics Communications,* vol. 256, pp. 422-427, Dec 15 2005.

[112] V. P. Kandidov, S. A. Shlenov, and O. G. Kosareva, "Filamentation of high-power femtosecond laser radiation," *Quantum Electronics,* vol. 39, pp. 205-228, Mar 2009.

[113] P. J. Lemaire, "Reliability of Optical Fibers Exposed to Hydrogen - Prediction of Long-Term Loss Increases," *Optical Engineering,* vol. 30, pp. 780-789, Jun 1991.

[114] H. Itoh, Y. Ohmori, and M. Nakahara, "Loss Increases Due to Chemical-Reactions of Hydrogen in Silica Glass Optical Fibers," *Journal of Lightwave Technology,* vol. 3, pp. 1100-1104, 1985.

[115] A. Cusano, A. Iadicicco, P. Pilla, A. Cutolo, M. Giordano, and S. Campopiano, "Sensitivity characteristics in nanosized coated long period gratings," *Applied Physics Letters,* vol. 89, Nov 13 2006.

[116] E. Ciaramella, E. Riccardi, and M. Schiano, "System penalties due to polarisation mode dispersion of chirped gratings," in *Optical Communication, 1998. 24th European Conference on,* 1998, pp. 515-516 vol.1.

[117] A. M. Vengsarkar, Q. Zhong, D. Inniss, W. A. Reed, P. J. Lemaire, and S. G. Kosinski, "Birefringence reduction in side-written photoinduced fiber devices by a dual-exposure method," *Opt Lett,* vol. 19, pp. 1260-2, Aug 15 1994.

[118] Y. Ishii, S. Okude, K. Nishide, A. Wada, and K. Shima, "PDL reduction of long-period fiber grating by rotating exposure method," in *Optical Communication, 2001. ECOC '01. 27th European Conference on,* 2001, pp. 354-355 vol.3.

[119] C. D. Poole, C. D. Townsend, and K. T. Nelson, "Helical-Grating 2-Mode Fiber Spatial-Mode Coupler," *Journal of Lightwave Technology,* vol. 9, pp. 598-604, May 1991.
[120] S. T. Oh, K. R. Lee, U. C. Paek, and Y. J. Chung, "Fabrication of helical long-period fiber gratings by use of a CO2 laser," *Optics Letters,* vol. 29, pp. 1464-1466, Jul 1 2004.
[121] J. N. Jang, S. Y. Kim, S. W. Kim, and M. S. Kim, "Temperature insensitive long-period fibre gratings," *Electronics Letters,* vol. 35, pp. 2134-2136, Nov 25 1999.
[122] L. Byeong Ha and P. Un-Chul, "Multislit interpretation of cascaded fiber gratings," *Lightwave Technology, Journal of,* vol. 20, pp. 1750-1761, 2002.
[123] P. S. J. Russell, "Photonic-crystal fibers," *Journal of Lightwave Technology,* vol. 24, pp. 4729-4749, Dec 2006.
[124] J. Villatoro, V. Finazzi, V. P. Minkovich, V. Pruneri, and G. Badenes, "Temperature-insensitive photonic crystal fiber interferometer for absolute strain sensing," *Applied Physics Letters,* vol. 91, Aug 27 2007.
[125] J. Villatoro, V. Finazzi, G. Badenes, and V. Pruneri, "Highly Sensitive Sensors Based on Photonic Crystal Fiber Modal Interferometers," *Journal of Sensors,* vol. 2009, p. 11, 2009.
[126] C. Li, S. J. Qiu, Y. Chen, F. Xu, and Y. Q. Lu, "Ultra-Sensitive Refractive Index Sensor With Slightly Tapered Photonic Crystal Fiber," *Ieee Photonics Technology Letters,* vol. 24, pp. 1771-1774, Oct 1 2012.
[127] S. J. Qiu, Y. Chen, J. L. Kou, F. Xu, and Y. Q. Lu, "Miniature tapered photonic crystal fiber interferometer with enhanced sensitivity by acid microdroplets etching," *Applied Optics,* vol. 50, pp. 4328-4332, Aug 1 2011.
[128] H. P. Uranus, "Theoretical study on the multimodeness of a commercial endlessly single-mode PCF," *Optics Communications,* vol. 283, pp. 4649-4654, Dec 1 2010.
[129] R. Jha, J. Villatoro, G. Badenes, and V. Pruneri, "Refractometry based on a photonic crystal fiber interferometer," *Optics Letters,* vol. 34, pp. 617-619, Mar 1 2009.
[130] J. L. Kou, J. Feng, Q. J. Wang, F. Xu, and Y. Q. Lu, "Microfiber-probe-based ultrasmall interferometric sensor," *Optics Letters,* vol. 35, pp. 2308-2310, Jul 1 2010.
[131] L. M. Tong, R. R. Gattass, J. B. Ashcom, S. L. He, J. Y. Lou, M. Y. Shen, *et al.*, "Subwavelength-diameter silica wires for low-loss optical wave guiding," *Nature,* vol. 426, pp. 816-819, Dec 18 2003.
[132] G. Brambilla, "Optical fibre nanowires and microwires: a review," *Journal of Optics,* vol. 12, Apr 2010.
[133] S. P. Ugale and V. Mishra, "Modeling and characterization of fiber Bragg grating for maximum reflectivity," *Optik,* vol. 122, pp. 1990-1993, 2011.
[134] I. Riant, "Fiber Bragg gratings for optical telecommunications," *Comptes Rendus Physique,* vol. 4, pp. 41-49, 1// 2003.
[135] E. Udd, "Review of multi-parameter fiber grating sensors - art. no. 677002," *Fiber Optic Sensors and Applications V,* vol. 6770, pp. 77002-77002, 2007.
[136] J. Chen, B. Liu, and H. Zhang, "Review of fiber Bragg grating sensor technology," *Frontiers of Optoelectronics in China,* vol. 4, pp. 204-212, 2011/06/01 2011.

[137] J. Jung, H. Nam, B. Lee, J. O. Byun, and N. S. Kim, "Fiber Bragg grating temperature sensor with controllable sensitivity," *Applied Optics*, vol. 38, pp. 2752-2754, May 1 1999.
[138] K. K. Tian, Y. L. Liu, and Q. M. Wang, "Temperature-independent fiber Bragg grating strain sensor using bimetal cantilever," *Optical Fiber Technology*, vol. 11, pp. 370-377, Oct 2005.
[139] C. Caucheteur, F. Lhomme, K. Chah, M. Blondel, and P. Megret, "Simultaneous strain and temperature sensor based on the numerical reconstruction of polarization maintaining fiber Bragg gratings," *Optics and Lasers in Engineering*, vol. 44, pp. 411-422, May 2006.
[140] C. Fernandez-Valdivielso, I. R. Matias, and F. J. Arregui, "Simultaneous measurement of strain and temperature using a fiber Bragg grating and a thermochromic material," *Sensors and Actuators a-Physical*, vol. 101, pp. 107-116, Sep 30 2002.
[141] M. Sumetsky, Y. Dulashko, and A. Hale, "Fabrication and study of bent and coiled free silica nanowires: Self-coupling microloop optical interferometer," *Optics Express*, vol. 12, pp. 3521-3531, Jul 26 2004.
[142] G. D. Marshall, R. J. Williams, N. Jovanovic, M. J. Steel, and M. J. Withford, "Point-by-point written fiber-Bragg gratings and their application in complex grating designs," *Optics Express*, vol. 18, pp. 19844-19859, Sep 13 2010.
[143] K. M. Zhou, M. Dubov, C. B. Mou, L. Zhang, V. K. Mezentsev, and I. Bennion, "Line-by-Line Fiber Bragg Grating Made by Femtosecond Laser," *Ieee Photonics Technology Letters*, vol. 22, pp. 1190-1192, Aug 15 2010.
[144] R. M. Liu, D. K. Liang, and A. Asundi, "Small diameter fiber Bragg gratings and applications," *Measurement*, vol. 46, pp. 3440-3448, Nov 2013.
[145] A. D. Kersey, M. A. Davis, H. J. Patrick, M. LeBlanc, K. P. Koo, C. G. Askins, *et al.*, "Fiber grating sensors," *Journal of Lightwave Technology*, vol. 15, pp. 1442-1463, Aug 1997.
[146] M. G. Xu, L. Reekie, Y. T. Chow, and J. P. Dakin, "Optical in-Fiber Grating High-Pressure Sensor," *Electronics Letters*, vol. 29, pp. 398-399, Feb 18 1993.
[147] H. J. Sheng, M. Y. Fu, T. C. Chen, W. F. Liu, and S. S. Bor, "A lateral pressure sensor using a fiber Bragg grating," *Ieee Photonics Technology Letters*, vol. 16, pp. 1146-1148, Apr 2004.
[148] G. Meltz and W. W. Morey, "Bragg grating formation and germanosilicate fiber photosensitivity," 1991, pp. 185-199.
[149] A. O. a. K. Kalli, *Fiber Bragg Gratings- Fundamentals and Applications in Telecommunications and Sensing*. Boston: Artech House, 1999.
[150] F. Ahmed and M. B. G. Jun, "Filament-Based Fabrication and Performance Analysis of Fiber Bragg Grating Sensors Using Ultrashort Pulse Laser," *Journal of Micro and Nano-Manufacturing*, vol. 2, pp. 021007-021007, 2014.
[151] S. Ju, P. R. Watekar, and W. T. Han, "Enhanced Sensitivity of the FBG Temperature Sensor Based on the PbO-GeO2-SiO2 Glass Optical Fiber," *Journal of Lightwave Technology*, vol. 28, pp. 2697-2700, Sep 15 2010.
[152] C. Seo and T. Kim, "Temperature sensing with different coated metals on fiber Bragg grating sensors," *Microwave and Optical Technology Letters*, vol. 21, pp. 162-165, May 5 1999.

[153] C. Lupi, F. Felli, L. Ippoliti, M. A. Caponero, M. Ciotti, V. Nardelli, *et al.*, "Metal coating for enhancing the sensitivity of fibre Bragg grating sensors at cryogenic temperature," *Smart Materials & Structures*, vol. 14, pp. N71-N76, Dec 2005.
[154] Y. Feng, H. Zhang, Y. L. Li, and C. F. Rao, "Temperature Sensing of Metal-Coated Fiber Bragg Grating," *Ieee-Asme Transactions on Mechatronics*, vol. 15, pp. 511-519, Aug 2010.
[155] L. Gang-Chih, L. Wang, C. C. Yang, M. C. Shih, and T. J. Chuang, "Thermal performance of metal-clad fiber Bragg grating sensors," *Photonics Technology Letters, IEEE*, vol. 10, pp. 406-408, 1998.
[156] C. S. Park, K. I. Joo, S. W. Kang, and H. R. Kim, "A PDMS-Coated Optical Fiber Bragg Grating Sensor for Enhancing Temperature Sensitivity," *Journal of the Optical Society of Korea*, vol. 15, pp. 329-334, Dec 2011.
[157] L. Jin, W. G. Zhang, H. Zhang, B. Liu, H. Zhao, Q. C. Tu, *et al.*, "An embedded FBG sensor for simultaneous measurement of stress and temperature," *Ieee Photonics Technology Letters*, vol. 18, pp. 154-156, Jan-Feb 2006.
[158] P. Lu, L. Men, and Q. Chen, "Resolving cross sensitivity of fiber Bragg gratings with different polymeric coatings," *Applied Physics Letters*, vol. 92, p. 171112, 2008.
[159] Y. Ran, Y. N. Tan, L. P. Sun, S. A. Gao, J. Li, L. Jin, *et al.*, "193nm excimer laser inscribed Bragg gratings in microfibers for refractive index sensing," *Optics Express*, vol. 19, pp. 18577-18583, Sep 12 2011.
[160] Y. Ran, L. Jin, Y. N. Tan, L. P. Sun, J. Li, and B. O. Guan, "High-Efficiency Ultraviolet Inscription of Bragg Gratings in Microfibers," *Ieee Photonics Journal*, vol. 4, pp. 181-186, Feb 2012.
[161] D. Grobnic, S. J. Mihailov, H. M. Ding, and C. W. Smelser, "Bragg grating evanescent field sensor made in biconical tapered fiber with femtosecond IR radiation," *Ieee Photonics Technology Letters*, vol. 18, pp. 160-162, Jan-Feb 2006.
[162] C. T. Shyu and L. K. Wang, "Sensitive Linear Electric-Current Measurement Using 2 Metal-Coated Single-Mode Optical Fibers," *Journal of Lightwave Technology*, vol. 12, pp. 2040-2048, Nov 1994.
[163] K. T. V. Grattan and T. Sun, "Fiber Optic Sensor Technology: Introduction and Overview," in *Optical Fiber Sensor Technology*, K. T. V. Grattan and B. T. Meggitt, Eds., ed: Springer US, 2000, pp. 1-44.
[164] L. C. Li, L. Xia, Z. H. Xie, L. N. Hao, B. B. Shuai, and D. M. Liu, "In-line fiber Mach-Zehnder interferometer for simultaneous measurement of refractive index and temperature based on thinned fiber," *Sensors and Actuators a-Physical*, vol. 180, pp. 19-24, Jun 2012.
[165] L. C. Li, X. Li, Z. H. Xie, Z. L. Liao, F. Tu, and D. M. Liu, "Simultaneous measurement of refractive index and temperature using thinned fiber based Mach-Zehnder interferometer," *Optics Communications*, vol. 285, pp. 3945-3949, Sep 1 2012.
[166] P. Lu, L. Q. Men, K. Sooley, and Q. Y. Chen, "Tapered fiber Mach-Zehnder interferometer for simultaneous measurement of refractive index and temperature," *Applied Physics Letters*, vol. 94, Mar 30 2009.

[167] H. P. Luo, Q. Z. Sun, Z. L. Xu, D. M. Liu, and L. Zhang, "Simultaneous measurement of refractive index and temperature using multimode microfiber-based dual Mach-Zehnder interferometer," *Optics Letters,* vol. 39, pp. 4049-4052, Jul 1 2014.

[168] Y. Cao, H. Y. Liu, Z. R. Tong, S. Yuan, and J. Su, "Simultaneous measurement of temperature and refractive index based on a Mach-Zehnder interferometer cascaded with a fiber Bragg grating," *Optics Communications,* vol. 342, pp. 180-183, May 1 2015.

[169] Q. Q. Yao, H. Y. Meng, W. Wang, H. C. Xue, R. Xiong, B. Huang, *et al.*, "Simultaneous measurement of refractive index and temperature based on a core-offset Mach-Zehnder interferometer combined with a fiber Bragg grating," *Sensors and Actuators a-Physical,* vol. 209, pp. 73-77, Mar 1 2014.

[170] H. Y. Choi, M. J. Kim, and B. H. Lee, "All-fiber Mach-Zehnder type interferometers formed in photonic crystal fiber," *Optics Express,* vol. 15, pp. 5711-5720, Apr 30 2007.

[171] Y. Wang, M. W. Yang, D. N. Wang, S. J. Liu, and P. X. Lu, "Fiber in-line Mach-Zehnder interferometer fabricated by femtosecond laser micromachining for refractive index measurement with high sensitivity," *Journal of the Optical Society of America B-Optical Physics,* vol. 27, pp. 370-374, Mar 2010.

[172] C. R. Liao, Y. Wang, D. N. Wang, and M. W. Yang, "Fiber In-Line Mach-Zehnder Interferometer Embedded in FBG for Simultaneous Refractive Index and Temperature Measurement," *Ieee Photonics Technology Letters,* vol. 22, pp. 1686-1688, Nov 15 2010.

[173] Y. F. Lu, C. Y. Shen, C. Zhong, D. B. Chen, X. Y. Dong, and J. H. Cai, "Refractive Index and Temperature Sensor Based on Double-Pass M-Z Interferometer With an FBG," *Ieee Photonics Technology Letters,* vol. 26, pp. 1124-1127, Jun 1 2014.

Appendix A - Femtosecond laser machined V-grooves on SMF to measure ambient refractive index

Femtosecond laser fabricated V-grooved fiber-optic sensor and long period grating are presented in this work for ambient refractive index measurement. The grooved sensor is constructed by laser micromachining of V-grooves at 500 µm interval on a pure silica single mode fiber. The tips of grooves partially penetrate the fiber core and thus perturb the light transmission. Variation in intensity of transmission light when the grooves are filled with liquid is used to measure ambient index. A potential application of grooved sensor in liquid level measurement is also demonstrated in this study.

Figure A.1 shows the schematics of the sensors proposed in this work. The RI/ liquid level sensor was fabricated by engraving V-grooves on SMF so that the groove notch partially penetrates the core. Fiber grooved sensor is characterized with ambient refractive index. The sensor works in transmission mode. So the sensor was coupled with a broad band light source (AFC BBS-1550) and an optical spectrum analyzer (OSA) (PHOTONETICS Walics) and tested with liquid and glycerin solutions of variable indices for sensor calibration.

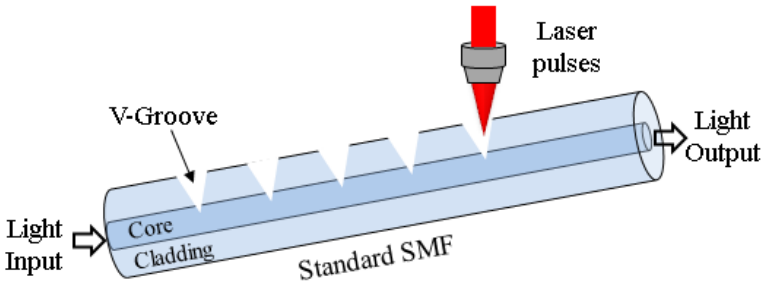

Figure A. 1 Schematic of fiber V-grooved sensor for RI measurement

The V-grooved fiber sensor (for ambient refractive index and liquid level sensing) is constructed by micromachining grooves using femtosecond laser radiation. Fig. A.2 shows a femtosecond laser machined groove. Initially a small pocket is milled out using transverse laser scanning process. Subsequently, a small V-groove is fabricated that penetrates the fiber core as shown in the figure below. The groove cut into the fiber core facilitates perturbation of light with external solutions when comes in contact.

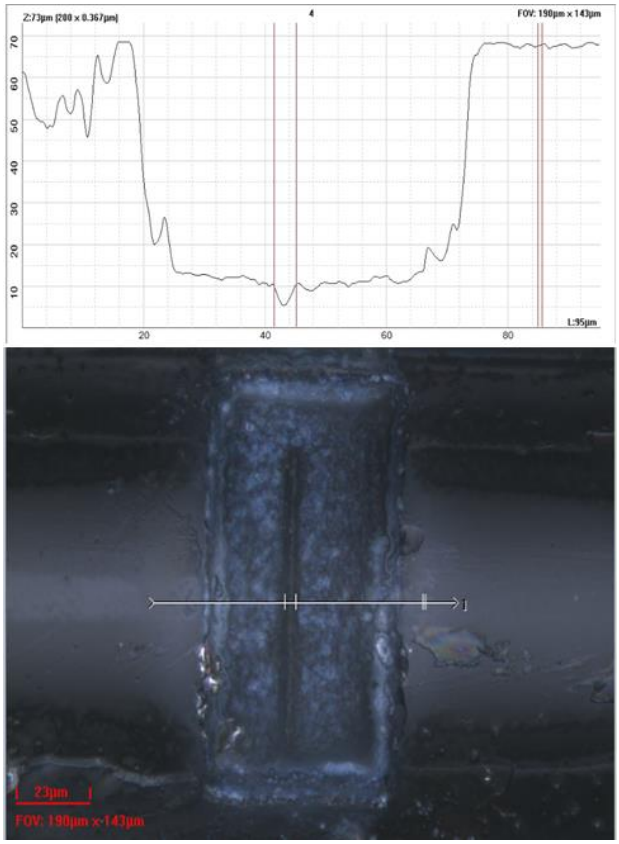

Figure A. 2 Micromachining grooves on optical fiber using femtosecond laser

Figure A.3 shows a cluster of V-grooves fabricated on a standard single mode fiber. Prior to groove inscription, the fiber was fixed on a microscope slide using epoxy glue. As shown in the figure, the fiber is then coupled with a light source and an optical spectrum analyser. The fiber grooves were immersed in different concentration of

glycerin solutions for ambient index measurement. For liquid level sensing, the grooves were successively immersed in water and corresponding transmission intensity was measured for sensor characterization.

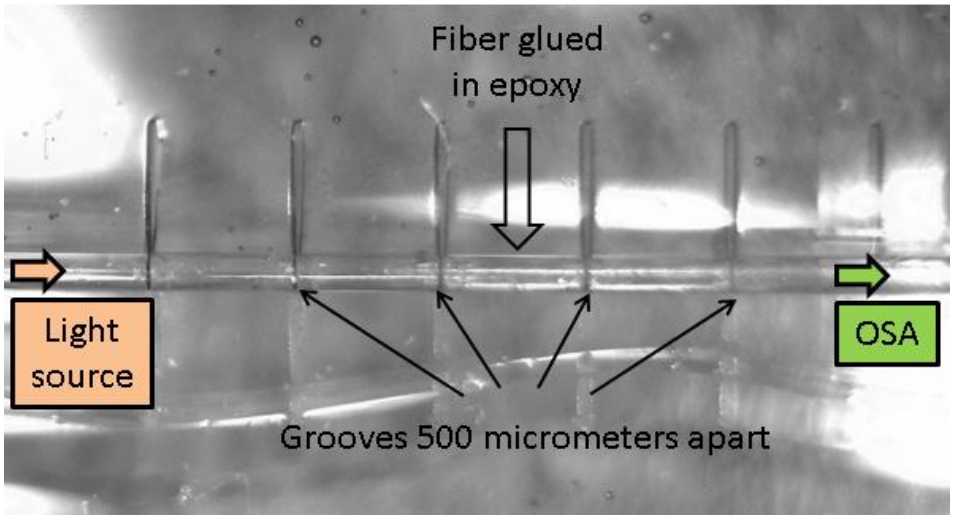

Figure A. 3 Grooves micromachined on standard single mode fiber with femtosecond laser radiation

The refractive index characterization of the fiber grooved sensor is demonstrated in Fig. A.4. To characterize the sensor with ambient refractive index, all the grooves were immersed (at a time) in different concentration of glycerin solutions (RI ranges from 1.3327 to 1.4483). For each ambient RI, the transmission intensity is measured at 1600 nm wavelength. The measured light intensity is then plotted against refractive indices to achieve the characterization plot. As shown in Fig. A.4, for low concentration of glycerin solutions, the fiber remains lossy due to sudden index mismatch and light scattering in the grooves. As the concentration of glycerin solution increases, light that previously was lost in the grooves couples back to the core due to index matching. This explains the gradual increase of transmission intensity with the increase in ambient index in Fig. A.4.

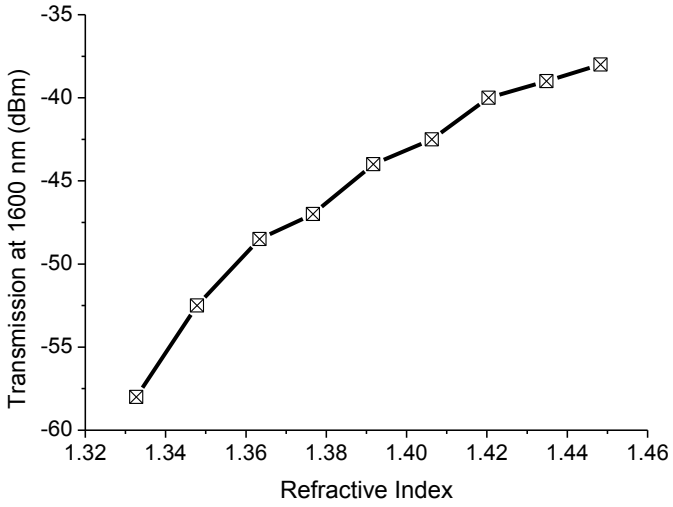

Figure A. 4 RI sensing with grooved fiber sensor

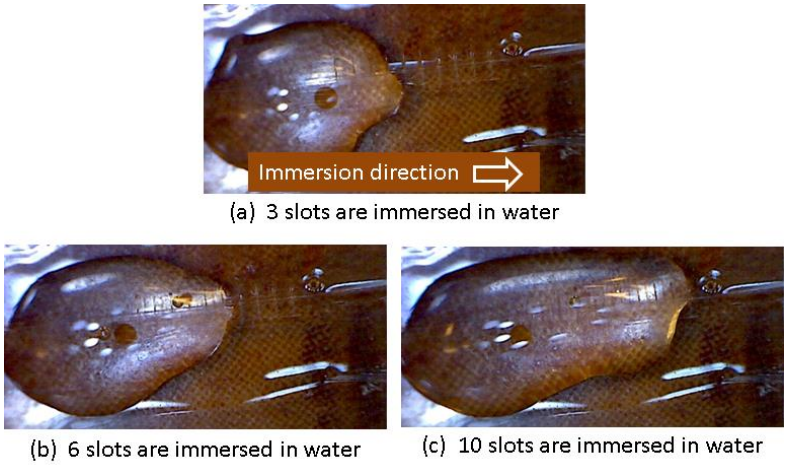

Figure A. 5 Gradual immersion of slots (micromachined with laser) with water

Ambient refractive index dependent potential liquid level sensing using the fiber V-grooved sensor is demonstrated in Figs. A.5 and A.6. The fiber grooves were gradually immersed in water and corresponding transmission intensity was monitored at 1600 nm wavelength. Fig. A.5 shows three scenarios, where 3, 6, and 10 grooves were immersed at a time to observe output light intensity. The results are plotted in Fig. A.6 that shows increase in light intensity with greater number of slots (grooves) immersed in water. This

illustrates the possibility of using the grooved fiber as a liquid level sensor. The resolution of the sensor can be varied simply by adjusting the relative distance between the grooves and changing the penetration depth of the grooves into the fiber core.

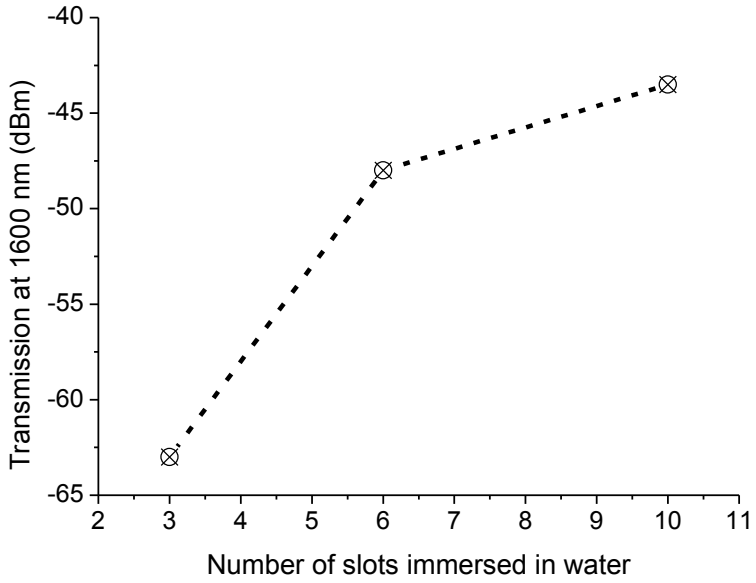

Figure A. 6 Change in transmission intensity at 1600 nm when the fiber slots are gradually immersed in water one after another

In conclusion, this work presents femtosecond laser assisted fabrication of fiber-grooved sensor for ambient refractive measurements. The intensity based V-grooved sensor works according to fiber-optic index matching phenomenon. The sensors show high sensitivity to ambient refractive index. The grooved fiber sensor has the potential to be used for liquid level sensing. Primary data on water level sensing shows potential applications of V-grooved fiber in liquid level sensing.

Appendix B - Simulation of long period grating in single mode fiber to understand their characteristics

B.1 Considered simulation parameters:

Primarily objective of this study is to understand the impact of the grating parameters on its transmission spectrum. As shown in Fig. B. 1, LPG's characteristic behaviors are analyzed by manipulating the following grating parameters:

1. Scanning length in a period
2. Periodic length of the LPG
3. Refractive index modulation

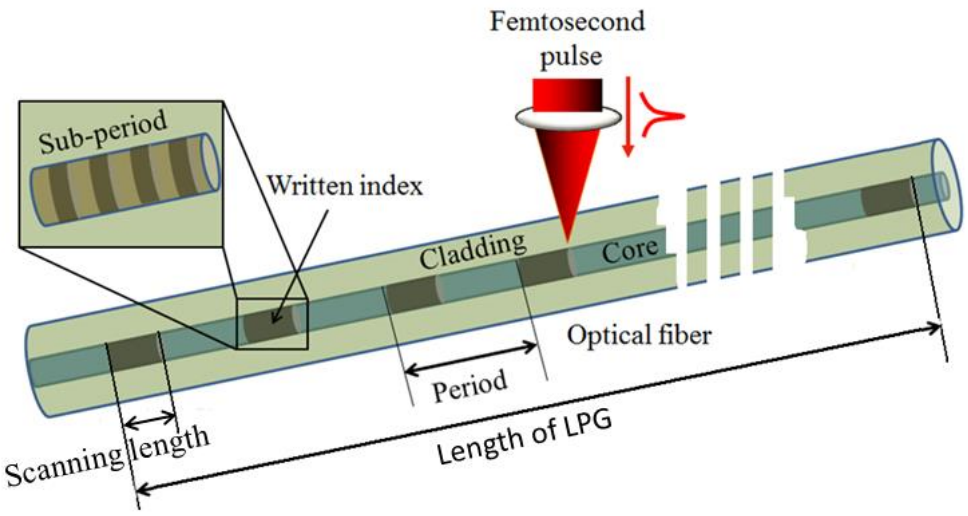

Figure B. 1 Schematic of long period grating index modulation

B.2 Characteristic behavior of LPG's transmission spectrum

Efficient design and fabrication of in-fiber long period grating depends on the accurate spectral allocation of its transmission valleys. Hence, it is critical to understand grating

parameters that govern the characteristics of long period grating's transmission dips. For a fixed index modulation, the writing of long period grating is optimized as a function of the total number of periods. The key parameters such as scanning length, periodic length, and RI modulation are also investigated in this study.

B.2.1 Growth of long period grating

Fig. B.2 shows the growth of transmission spectrum of long period grating. As the number of period gradually increases, the grating's rejection spectrum gets stronger; consequently, a profound dip appears in its transmission spectrum. For an optimum number of periods, the transmission spectrum exhibits strongest attenuation at a certain wavelength. A farther increase in period results in weaker attenuation. Shown in Fig. B.3, the transmission valley is deepest when the grating has 46 periods.

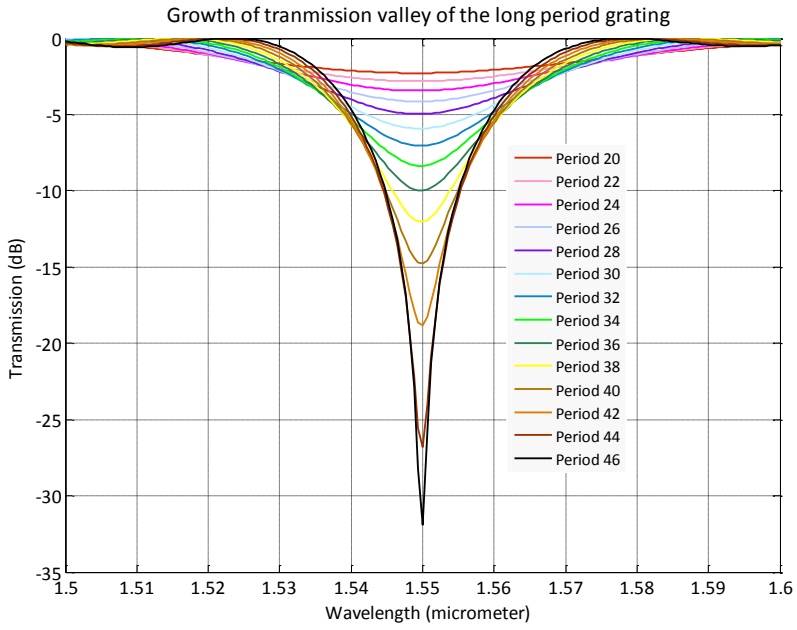

Figure B. 2 Growth of long period grating as a function of total number of periods

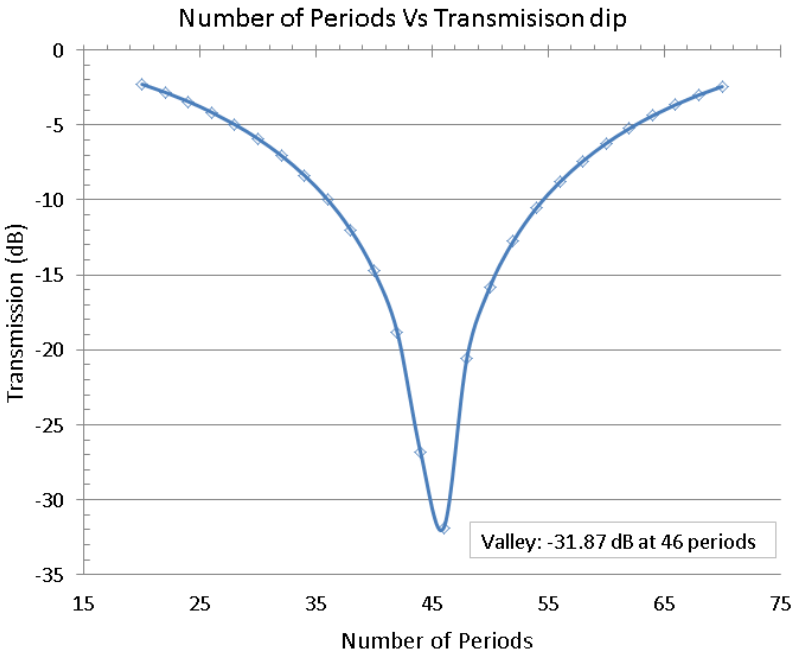

Figure B. 3 LPG's growth optimization for its deepest transmission valley

B.2.2 Scanning length in a period

The scanning length in a period (shown in Fig. B.4) turns out to be a significant parameter that tailors LPG's transmission spectrum. Each mode of a long period grating has characteristic behavior. The attenuation and spectral location of transmission dip varies with scanning length in a period. The higher order modes extend closer to the cladding-ambient interface and more sensitive to ambient RI change, thus, this study focuses primarily on higher order modes as shown in Fig. B.4 (a). For mode 5 and 6, a scanning length of 80 μm provides strongest attenuation of ~22 dB below zero. All cladding modes experience linear spectral red shift with an increase in scanning length. Therefore, to design a long period grating with a significant attenuation dip (transmission spectrum) and desired spectral location, a corresponding scanning length in a period can be picked up from Fig. B.4 (a) and (b).

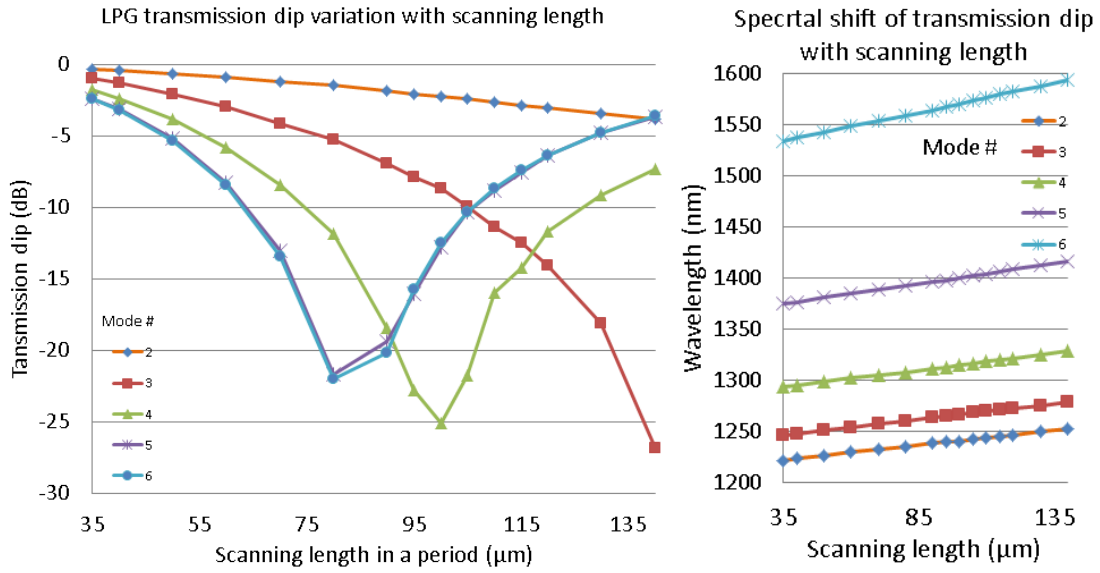

Figure B. 4 Scanning length dependent behaviors of LPG's transmission valleys. Each mode exhibits highest transmission dip for a particular scanning length (a), while all the modes show linear red shift with an increase in scanning length in a period.

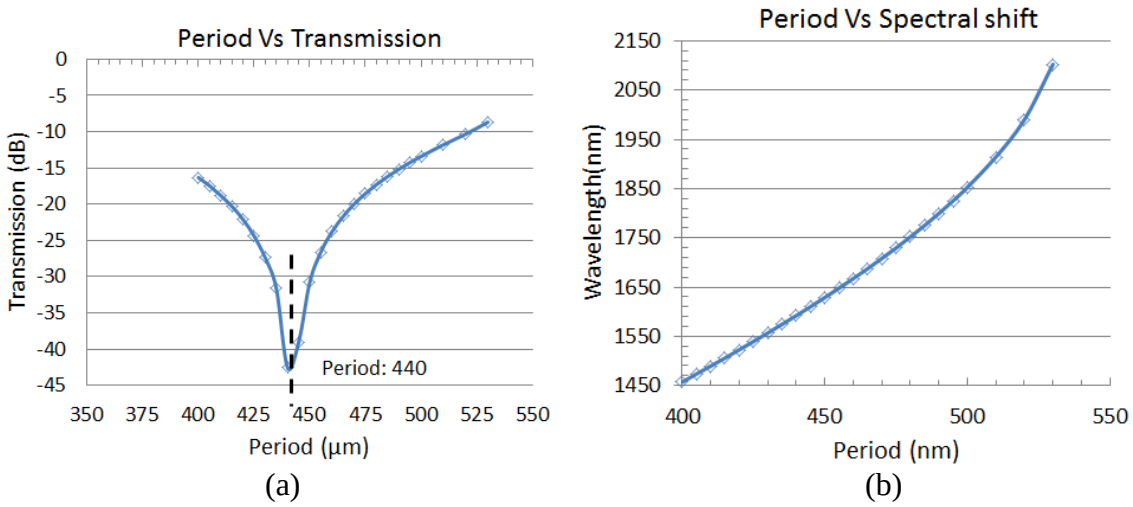

Figure B. 5 Impact of LPG's periodic length on the height and spectral location of attenuation valley in transmission spectrum. Maximum attenuation is observed at period length of 440 µm (a) and the transmission dip shows linear red shift with periodic length (b) for 1450 nm to 1750 nm

B.2.3 Periodic length of the LPG

Similar to scanning length, the periodic length has identical effect on LPG's transmission spectrum. In search of a greatest attenuation valley, the periodic length of 440 µm offers optimum/maximum attenuation as shown in Fig. B.5 (a). Spectral window of interest for fiber optic sensing operation spans between 1500 nm to 1600 nm. The linear spectral red shift (between 1450 nm to 1750 nm) with periodic length is illustrated in Fig. B.5(b).

B.2.4 Effect of period on FWHM of the transmission dip

The FWHM of transmission valley of a long period grating determines the resolution of sensing as the resolution is inversely proportional to FWHM. Fig. B.6 shows how the FWHM of the transmission valley changes with a gradual increase in LPG's periodic length. Simulation results show that the FWHM reaches to its minimum (highest sensing resolution) value when the LPG has a period of 440 µm.

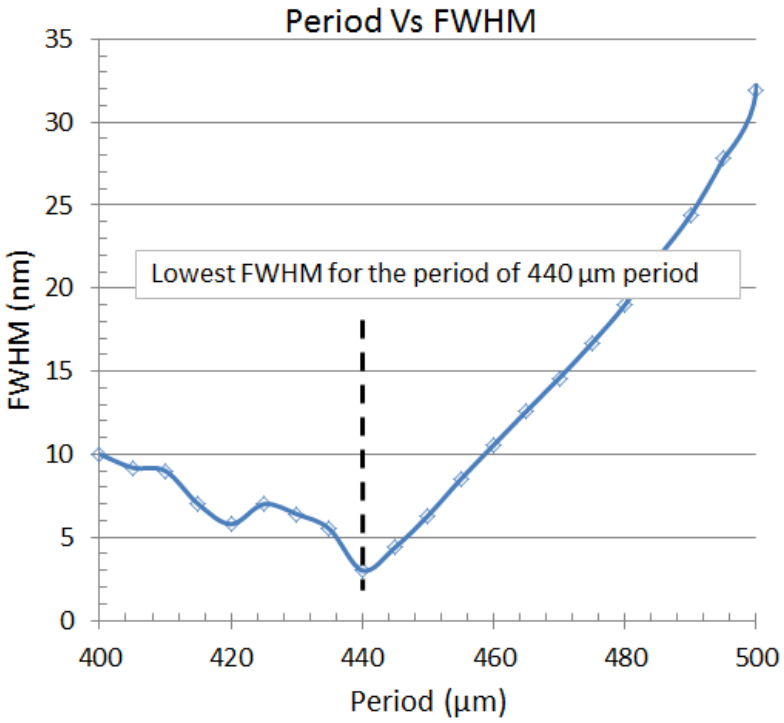

Figure B. 6 Periodic length dependent FWHM of transmission valley

B.2.4 Refractive index modulation Tuning

For the period of 440 µm, Fig. B.7 (a) shows the dependency of amount of transmission loss on index modulation. An index modulation of ~ 0.00039 provides highest attenuation loss for the LPG. Spectral location of the grating shows blue shift with an increase in index modulation as shown in Fig. B.7 (b).

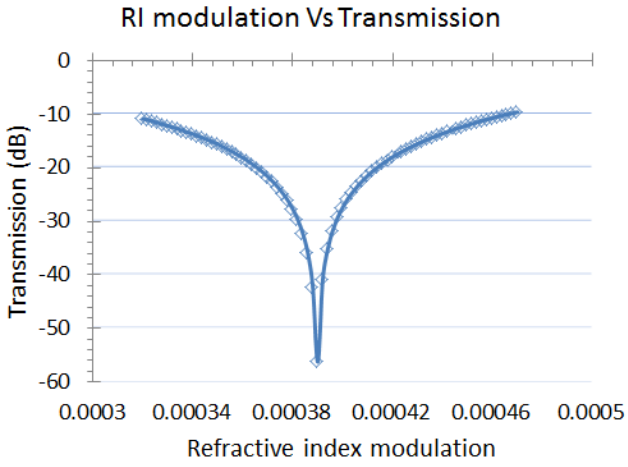

(a)

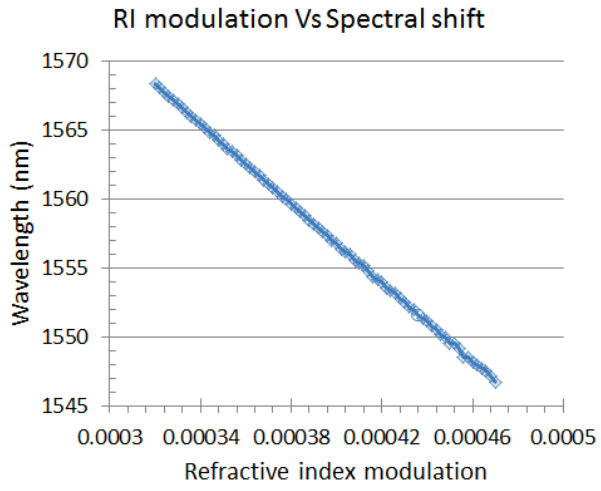

(b)

Figure B. 7 Refractive index modulation dependent transmission (a) and spectral location of transmission dip (b)